

DOTTORATO DI RICERCA IN

Ingegneria Biomedica, Elettrica e dei Sistemi

Ciclo 37

Settore Concorsuale: 09/E2 Electrical Energy Engineering

Settore Scientifico Disciplinare: IIND-08/B (ING-IND/33) Electrical Power Systems

IMPROVED OPERATION OF POWER DISTRIBUTION SYSTEMS BY THE USE OF FLEXIBILITY SERVICES AND ENERGY COMMUNITIES

Presentata da: Tohid Harighi

Coordinatore Dottorato

Prof. Michele Monaci

Supervisore

Prof. Alberto Borghetti

Co-supervisore

Prof. Fabio Napolitano

"The sun rises, the sun sets, and still,
Life's wheel turns; energy never stands still"

Omar Khayyam

(May 18, 1048 – December 4, 1131)

PhD scholarship of the National Operational Programme for Research and Innovation 2014-2020 (CCI 2014IT16M20P005), ESF resources react-eu, Action IV.4 "Doctorates and research contracts on innovation issues" and Action IV.5 "Doctorates on Green topics." with scholarship CUP no. J35F21003140006.

Acknowledgements

This thesis would not have been possible without the support and guidance of many individuals, and I would like to take this opportunity to express my heartfelt gratitude.

To my supervisor, Prof. Alberto Borghetti, thank you for believing in my ideas and challenging me to reach new heights. Your mentorship and patience have been invaluable. To my colleagues and collaborators, your insights and camaraderie made this journey not only fruitful but also enjoyable.

I am deeply thankful to my co-supervisor, Prof. Fabio Napolitano, for his insightful suggestions and constructive critiques, which have greatly enhanced the quality of this thesis.

I am sincerely grateful to Prof. Carlo Alberto Nucci for his valuable insights, constructive feedback, and encouragement throughout this research.

A special thanks to my family, who stood by me during the most challenging moments and celebrated every little victory along the way. To my wife, Leili Golzari, thank you for your unwavering support and love—I could not have done this without you.

Lastly, I am grateful for the funding and resources provided by University of Bologna, and I would like to extend my heartfelt gratitude to my industrial supervisor, Adriano Calzolari, for his exceptional guidance, practical insights, and unwavering support throughout this research. His expertise and industry-oriented perspective have been instrumental in connecting my academic work with real-world challenges.

I am equally grateful to the colleagues at INRETE Distribuzione Energia S.p.A. and HERAtech S.r.l. for their collaboration, encouragement, and valuable discussions during the project. Their technical support and teamwork have provided me with a deeper understanding of industrial applications and have enriched the overall quality of this research.

Abstract:

The thesis presents the results of a research activity on the operation of distribution system with the presence of flexibility service providers and renewable energy communities.

The first part of the thesis focused on flexibility operations in the electric vehicle (EV) parking lots (PLs), i.e. parking lots equipped with several EV charging stations. The operation of the parking lot is affected by significant uncertainties regarding the number and characteristics of the vehicle present in the parking lot. For day-ahead scheduling, a multistage stochastic approach have been developed and adapted to the calculation of the maximum flexibility levels that the parking lot can offer to the distribution system operator (DSO). To reduce the computational time, *k*-medoid clustering procedure is applied. Flexibility is expressed in terms of the PL power-adjustment capacity in response to the DSO request, with the possibility of energy recovery in order to guarantee the fulfilment of the EV charging service. The DSO optimizes the voltage profile of the distribution grid using PL power flexibility and other distributed energy resources (DERs). A multi-objective decentralized formulation was used for the optimization and the results are presented for 24-hour operation of the IEEE 123 node test feeder with four PLs and 15 DERs, whose reactive power output can be varied. The results show the improvement achieved in terms of the voltage profiles compared with the case without any voltage optimization.

The second part of the study includes the analysis of the provision of reactive power services by energy communities (ECs) in medium voltage distribution networks. The reduction of the penalization for low power factor operation is obtained by considering both the exchanges of active and reactive among prosumer participants of the community. The analysis is focused on renewable generation provided by photovoltaic (PV) units, equipped by battery energy storage systems (BESS). The optimization of the voltage profile in the network is also assisted by the presence of transformers equipped with on-load tap changers (OLTC). Different test cases have been considered, including some feeders of the distribution network of the city of Modena connected to the same high voltage-medium voltage substation. The research findings demonstrate that ECs can significantly contribute to the optimization of reactive power services by coordinating the operation of distributed generation. By leveraging the flexibility of these resources, ECs can also provide reactive power support to the grid, reducing the need for the installation of new reactive power compensation devices.

Furthermore, the study explored the impact of multiple ECs operating within the same distribution network. The pricing of the transaction within ECs is a critical aspect investigated in this thesis. The research proposes a methodology for determining fair and efficient prices based on shadow prices of balancing constraints. This approach ensures that the benefits are distributed among community

members. In terms of reducing energy procurement costs, the analysis demonstrates that ECs can offer significant economic advantages to their members. These advantages reduce with the increase of the number of communities in the same network.

Table of Contents

Chapter 1.	Introduction
1.1.	Topics and specific contributions of the thesis
1.1.1.	EVs parking lots flexibility services
1.1.2.	Flexible operation of energy communities
1.1.3.	Structure of the thesis
1.1.4.	Publications 24
Chapter 2.	Flexibility Exploitation: Model of the Parking Lot and Its Use for Voltage
Optimizatio	on26
2.1.	Flexibility modeling for parking lots with multiple EV charging stations
2.1.1.	Chapter content
2.1.2.	EV parking lots as flexibility service providers
2.1.3.	Stochastic parameters and scenario management
2.1.4.	Scenario generation
2.1.5.	Scenario clustering and tree construction
2.1.6.	Characterization of each scenario in the tree
2.1.7.	Intraday decision procedure
2.1.8.	Optimization models to represent EV parking lot flexibility
2.1.9.	Calculation of the reference consumption profiles
2.1.10.	Calculation of the maximum power reduction and increase margins
2.1.11.	Case studies and results
2.2.	Flexible Operation of an EV Parking Lot for Voltage Control of a Distribution
Network	40
2.2.1.	Introduction
2.2.2.	Methodology41
2.2.3.	EV parking lot model
2.2.4.	Voltage optimization of the distribution network
2.2.5.	Model for the representation of the EV parking lot flexibility (Calculation of the
reference co	onsumption profiles
2.2.6.	Calculation of the maximum power reduction and increase margins

2.2.7.	Multi-periods voltage optimization approach	44
2.2.8.	Voltage optimization objective function	45
2.2.9.	Equality constraints	45
2.2.10.	Inequality constraints	46
2.2.11.	Case studies and results	47
2.2.12.	Results	48
2.3.	Conclusion	51
Chapter 3.	Model of the energy communities	53
3.1.	Optimization model for the analysis of multiple energy communities in the s	ame
distribution	network with different providers	53
3.1.1.	Introduction	53
3.1.2.	Optimization Model	54
3.1.3.	Objective function	54
3.1.4.	Branch constraints	55
3.1.5.	Constraints at the branch connections	57
3.1.6.	User constraints	58
3.1.7.	Description of the test cases	59
3.1.8.	Results and comparisons	61
3.2. Distrib	uted Optimization and Application of the Model to a Real Distribution Network	68
3.2.1.	Introduction	68
3.2.2.	Day-ahead Distributed Optimization Procedure	69
3.2.3.	Individual and Collective User Optimization Model	70
3.2.4.	Linearized DSO Model	72
3.2.5.	Multiplier Update	74
3.2.6.	Case study and test results	75
3.3.	Conclusion	79
Chapter 4.	Reactive power services from communities	82
4.1.	Introduction	82
4.2.	Motivations and literature review	82
4.3.	Contributions and chapter organization	83

4.4.	Structure of the chapter	84
4.5.	Structure of the optimization procedures	85
4.6.	Reference optimization model of the distribution network with the presence of	a local
energy com	munity	87
4.7.	Objective function	89
4.8.	Penalization of low power factor operation	89
4.9.	Coupling constraints	91
4.10.	Branch constraints	91
4.11.	Cone constraints	92
4.12.	OLTC and capacitor constraints	92
4.13.	User plant constraints	93
4.14.	Active and reactive power exchanges among the community participants	93
4.15.	Repeated optimization to achieve a feasible solution	94
4.16.	Iterative procedure to obtain a refined solution	95
4.17.	Calculation of the maximum and minimum reactive power deviations	96
4.18.	Maximum increase of reactive power injection or decrease of reactive	power
absorption		96
4.19. Maxii	mum decrease of reactive power injection or increase of reactive power absorbance	rption.
		97
4.20.	Model implementation, test cases description and results	98
A.	Test case A	98
В.	Test case B	104
C.	Test case C	107
4.21.	Conclusions	115
Chapter 5.	Conclusions	117
5.1.	Flexibility exploitation of EV parking lots	117
5.2.	Model and analysis of the energy communities	118
5.3.	Future work	119
References		120

List of figures

Figure 1 Procedure scheme
Figure 2 Procedure scheme. 21
Figure 3 Day-ahead forecast profiles of the number of EVs entering (solid lines) and exiting (dashed
lines) in the three parking lots considered: PLA in black, PLB in blue, PLC in red
Figure 4 Scenario tree for parking lot PLA. The identification numbers of the medoids are shown for each stage of 6 hours, together with, between parenthesis, both the arc probabilities and scenario probabilities π^{ω}
Figure 5 Flexibility margins and corresponding recoveries of scenario 56 of PL A: down flexibility
starting at $t_{\text{flex}} = 29$ (7:15 am) and up flexibility starting at $t_{\text{flex}} = 45$ (11:15 am)39
Figure 6 Initial period of the flexibility intervals with a margin larger than 100 kW for scenario 56 a) PLA, b) PLD. Downward flexibility in green and upward flexibility in red
Figure 7 The 123-bus test feeder with 4 voltage control zones (VCZ) indicated by different colors
The relevant pilot nodes (PN) in green circles, as well as the considered 4 PV systems (PVS) in red
circles and a parking lot (PL) in a blue circle, are also shown in the scheme
Figure 8 Reference and maximum flexibility profiles for: a) t _{flex} equal to 37, i.e., at 9:15 am, (down)
and 41, i.e., at 10:15 am, (up); b) t _{flex} equal to 75, i.e., at 6:45 pm, (down) and 88, i.e. at 10 pm, (up)
Figure 9 The voltage profile of the 123-bus network at the 26 th interval
Figure 10 The voltage profile of the 123-bus network at the 27 th interval
Figure 11 The voltage profile of the 123-bus network at the 28 th interval
Figure 12 The voltage profile of the 123-bus network at the 29 th interval
Figure 13 Scheme of the network for test cases.
Figure 14 Random association of each user to a different provider
Figure 15 Random association of each user to a different community with some nodes excluded from the communities.
Figure 16 Community EC3: prices of the internal transactions π_{EC3} , prices of the transactions with
the external energy provider f1 ($\pi_{\text{sell f1}}$, $\pi_{\text{buy f1}}$) and f2 ($\pi_{\text{sell f2}}$, $\pi_{\text{buy f2}}$)

Figure 17 Community EC3: net power exchanges with provider f1 and with provider f2 (positive
sign indicates power consumed, negative produced)63
Figure 18 Community EC3: power exchanges P_{LEC} inside the community, between the members with provider f1 and those with provider f2 (positive sign indicates power imported, negative exported).
Figure 19 Communities formed by neighboring members
Figure 20 Total daily procurement costs of the communities and of the users in the noEC group, for different number of communities
Figure 21 Average daily costs per user in the communities, in the same communities with PLEC
forbidden, and in the noEC group, for different number of communities
Figure 22 Total procurement costs of all the users in the network, procurement costs of the users in the noEC group and of EC1, EC2 and EC3.
Figure 23 Procurement costs of EC1, EC2, and EC3 and of the users in the noEC group for different sizes of the BES units
Figure 24 The procedure stops when the violations of the network constraints in the DSO problem are less than a predefined tolerance or when there are no more improvements to the solution 70
Figure 25 Generic T-model equivalent circuit
Figure 26 Layout of the real MV test network. The HV/MV substation is indicated by a circle and, the five feeders considered are distinguished by different colors
Figure 27 Percentage reduction of a) energy procurement cost and b) noncompliance penalties, varying the number of communities, with respect to the case in which P_{LEC} and Q_{LEC} transactions are forbidden.
Figure 28 Scheme of the procedure.
Figure 29 Scheme of the model of a generic branch with the connection point of a user
Figure 30 Operating region that complies with the minimum power factor
Figure 31 Profiles of the a) active and b) reactive power exchanges between community participants. Test case A
Figure 32 Bus voltage profiles. Test case A
Figure 33 Prices of the internal transactions, prices of the transactions with the external energy provider, cumulative value of the power exchanged with the energy provider. Test case A

Figure 34 Profiles of the cumulative value of the community reactive power calculated by the
reference, Qup and Qdown procedures for scenarios: a) 2 (like 1 not shown), b) 3, c) 4 (like 0 not
shown). Test case A
Figure 35 Comparison between the prices of the internal transactions and the prices of the
transactions with the external energy provider. Cumulative value of the power exchanged with the
energy provider. Test case B
Figure 36 Profiles of the cumulative value of the reactive powers of the community participants
calculated by the reference, Qup and Qdown procedures for scenarios: a) 1 (like 0 and 2 not shown),
b) 4 (like 3 not shown), c) 6 (like 8 not shown), d) 7 (like 5 not
Figure 37 Comparison between the prices of the internal transactions and the prices of the
transactions with the external energy provider. Cumulative value of the power exchanged with the
energy provider. Test case C
Figure 38 Profiles of the cumulative value of the reactive powers of the community participants
calculated by the reference, Qup and Qdown procedures for scenarios: a) 1 (like 0 and 3 not shown),
b) 2, c) 4. Test case B
Figure 40 Profiles of the cumulative reactive power values of the community members calculated by
the reference, Qup and Qdown procedures for the scenarios: a) 0, b) 1
Figure 41 Comparison of the reactive power reference profiles through the HV/MV transformers at
the substation due to the five feeders in scenario 0 and scenario 2

List of tables

Table 1 Characteristics of the EVs 42
Table 2 Forecasted daily demand, PV generation as percentage of the load, total storage in percentage of PV generation, for each community and for the group outside the communities
Table 3 Daily costs and PF non-compliance penalties for each community and the noEC group considering the two different power providers. 62
Table 4 Daily costs and PF non-compliance penalties for each group of users if direct exchanges P_{LEC} are not allowed. 62
Table 5 Forecasted daily demand, PV generation as percentage of the load, total storage in percentage
of PV generation, for each community of neighboring users
Table 6 weather data76
Table 7 Energy Consumption and Generation Data 76
Table 8 Allocation of the demand, PV generation, and battery storage as percentage of the total three-day values for the communities and the NoEC set
Table 9 Base case: energy costs in thousands of euros for each community considering the three different retailers on winter (W) and summer (S) days
Table 10 Base case energy cost reductions in % with respect to the case where P_{LEC} and Q_{LEC} or only Q_{LEC} exchanges are forbidden
Table 11 Noncompliance costs (in euro) in the base case and when P_{LEC} and Q_{LEC} exchanges are forbidden
Table 12 Summary of the results for the reference optimization of case study A
Table 13 Summary of the results for the Qdown optimization of case study A
Table 14 Summary of the results for the Qup optimization of case study A
Table 15 Summary of the results for case study A Scenario 3 with different values of reactive power penalty and flexibility reward (in parentesis, percentage variations with respect to Tables 1, 2, and 3)
Table 16 Summary of the results for the reference, Qup and Qdown optimizations of case study B. $C_{\rm ep}$ indicates the cost of the exchanges with the energy provider, $P_{\rm NC}$ indicates the noncompliance penalty, R indicates the reward

Table 17 Summary of the results for the reference, Q up and Qdown optimizations of case study B
$C_{ m ep}$ indicates the cost of the exchanges with the energy provider, $P_{ m NC}$ indicates the noncompliance
penalty, R indicates the reward, cpu indicates the total computational time
Table 18 Assumed daily profile of the prices π _{buy} in €/kWh 11
Table 19 Summary of the results for the reference, Qup and Qdown optimizations in the first thre
scenarios. C _{grid} is the cost of the exchanges with the energy provider, P _{NC} is the noncomplianc
penalty, R is the reward11
Table 20 Summary of analogous results of Table 19 for three summer days. 11
Table 21 Summary of the results for the reference, Qup and Qdown optimizations in four variation
of scenario 0

List of Symbols

 Δt : single period duration.

 $E_{\rm EV}$, $P_{\rm EV}$: EV battery size and its maximum charging power.

 $\eta_{\rm ch}$, $\eta_{\rm V2V}$: Efficiency of grid battery charging and of vehicle-to-vehicle (V2V) energy transfer.

 δ : Self-discharge rate of EV batteries.

 ρ_{TOU}^t , ρ_{flex}^t , ρ_{μ} : Time-of-use tariff of energy from the grid, of power flexibility services, and of initial EV energy use.

 t_{flex} , n_{flex}^+ , n_{rec} : First period of the flexibility interval, number of subsequent flexibility periods, and number of recovery periods.

 $N_{\text{park max}}$: Maximum number of EV charging points.

 T_s : periods in stage s.

 $S_{\text{in}}^{\omega,t}$, $S_{\text{out}}^{\omega,t}$: Sets of EVs entering and leaving the car park in period t.

 $\Delta P_{\text{flex}}^{\omega,t}$, $R_{\text{flex}}^{\omega,t}$: Maximum allowed increase or decrease in car park power consumption in period t and corresponding flexibility revenue.

 $C_s^{\omega,t}$: Cost of using the initial EV stored energy.

 $E_{\text{S net}}^{\omega,t}$, $E_{\text{ch,grid}}^{\omega,t}$: Net energy stored in the batteries and charging energy from the grid in period t.

 $E_{\mathrm{ch},j}^{\omega,t}$: Minimum energy profile to properly charge EVs arriving in period j.

 $P_{\text{ref}}^{\omega,t}$: Reference consumption profile of the parking lot.

 $P^{\omega,t}$: Power absorbed by the parking lot from the grid.

 $l_{\text{V2V}}^{\omega,t}$: V2V energy transfer losses in period t.

 π^{ω} : Probability value of scenario ω .

 $N_{\text{EV in}}^{\omega,t}$, $N_{\text{EV out}}^{\omega,t}$, $E_{\text{S-}}^{\omega,t}$; Number of electric vehicles (EVs) arriving and departing in period t, and corresponding cumulative stored energy, respectively.

 $E_{\text{ini}\,j}^{\omega,t}$, $E_{\text{g},j}^{\omega,t}$: Initial energy and energy gain of the EVs arriving in period j and leaving in period t.

 $N_{EV}^{\omega,t}$, $E_{\rm Smax}^{\omega,t}$, $P_{\rm max}^{\omega,t}$: Number of parked EVs at the end of period t, corresponding total battery size, and cumulative maximum charge power.

 $\mu^{\omega,t}$: Utilization fraction of EV energy entering at time t.

Chapter 1. Introduction

Electricity distribution systems are undergoing significant transformations, with new operating methods emerging to boost renewable energy production, mitigate climate change impacts, and support sustainable development. In various regions worldwide, new regulatory frameworks are encouraging greater involvement of end users in electricity markets. Initiatives like energy communities and peer-to-peer electricity trading between neighbors have become valuable opportunities in Europe and beyond. These energy exchanges and communities rely heavily on advanced metering infrastructure, storage systems to balance consumption and renewable energy production, and efficient optimization algorithms. Moreover, energy communities are anticipated to offer grid services, such as active and reactive power balancing, to the distribution and transmission networks they are linked to. Notable regulatory frameworks include the EU Directive on common rules for the internal electricity market (EU 2019/944) and the updated Renewable Energy Directive (2018/2001/EU), both enhancing the role of self-consumers and renewable energy communities. For instance, the Italian Regulatory Authority for Energy, Networks, and Environment (ARERA) has launched a call for projects on local ancillary services (resolution August 3, 2021 352/2021/R/eel), complementing an earlier resolution (May 5, 2017 300/2017/R/eel) on global ancillary services acquired by the transmission system operator within the electricity market regulation (document July 23, 2019 322/2019/R/eel). Local microgrids and renewable energy communities, using qualified generation and storage units, reactive power devices, and demand response techniques, are expected to provide these services. Another example involves communities managing sections of the public network connecting participants, as outlined in the ARERA resolution 120/2022/R/eel, effectively acting as a distribution system operator (DSO) and delivering services to both connected users and the transmission system operator (TSO).

The research activity presented in this thesis relates to the analysis of the flexibility services that can be provided by single users and collectives or communities in order to facilitate the use of renewable resources.

Specifically, the first part of the thesis focuses on flexibility services that can be provided by Electric Vehicle (EV) parking lots that contain a large number of EV charging stations. The calculation of the flexibility margin required for the participation in the local market takes into account the uncertainties associated with the presence of the vehicles in the parking lot, the initial charge in their batteries, and the parking duration. The model is implemented as stochastic optimization.

The second part of the thesis focuses on the provision of active and/or reactive power compensation services by a single or multiple energy communities connected to the same medium voltage distribution network. The aim of the optimization problem is the reduction of both the procurement costs and the penalties due to low power factor operation. Moreover, a procedure for the calculation of the maximum flexibility margins, both upward and downward, has been implemented.

For the optimization calculations, the models are implemented as linear programming (LP), mixed integer linear programing (MILP), or (mixed integer) quadratic constant programing (QCP, MIQCP) depending on the specific purposes.

1.1. Topics and specific contributions of the thesis

As mentioned, the research activity addresses two main topics.

The first topic focuses on the calculation of the flexibility margins of EV parking lots, and their use by the DSO for voltage profile optimization.

The second topic is the analysis of the reactive power compensation in energy communities and the provision of reactive power flexibility services. Moreover, the presence of multiple communities in the same medium voltage distribution network has been analyzed, considering the network constraints.

Here below, there is a summary of the aims, methodologies, and contributions of the thesis. The literature review of each topic is included in the subsequent chapters of the thesis, along with a full description of the developed models, the case studies, the tests, and the obtained results. Part of the case studies refer to real feeders of the medium voltage distribution network of the city of Modena. The data collection, the operational criteria analysis, and the specific application of the developed model have been carried out during the six months research period spent at the offices of INRETE Distribuzione Energia (Hera Group).

1.1.1. EVs parking lots flexibility services

This topic deals with the development of the model that captures the aggregated flexibility potential of parking lots equipped with multiple EV charging stations. The model is incorporated into a stochastic optimization procedure to predict the maximum flexibility margins of the parking lot in advance. The EV aggregator overseeing the charging stations provides intra-day ancillary services to

the grid by defining the range within which power consumption can be adjusted, either increasing or decreasing. These power variations are made in response to requests from the DSO to maintain adequate EV charging levels. The effectiveness of the model is evaluated for parking lots with different numbers of charging stations and different daily profiles of EV arrivals and departures.

In order to reduce the number of scenarios, *k*-medoid clustering based is adopted. The implemented LP stochastic optimization is structured in 4 stages allowing the update of the decisions every 6 hours during the day. The objective function includes both procurement costs and the reward to the vehicle owners for the use of the energy already stored in their vehicles through vehicle-to-vehicle (V2V) exchanges. The upward and downward margin calculation takes into account the energy recovery in the periods following the flexibility provision.

As mentioned, the model for the calculation of the flexibility margins is tested for different parking lots with several charging stations. It considers the flexibility interval of a single 15-min period, 2 periods, and 3 consecutive periods.

Overall, this developed procedure for the stochastic optimization of EV parking lots and flexibility margin calculations ensures that charging requirements are met. The optimization model aggregates EV battery behavior and formulates the problem as a linear one, making it computationally efficient even for large parking lots. It accounts for losses associated with grid charging and vehicle-to-vehicle energy exchanges enabled by bidirectional charging stations. To enhance the flexibility of the EV parking lot, power reductions and increases in consecutive periods are considered while ensuring schedule feasibility, by including a recovery after the interval when flexibility is requested. This approach operates as a day-ahead evaluation with a 4-stage stochastic process, updating the decisions every 6 h to reflect real-time EV data. Numerical tests on parking lots of various sizes demonstrate the effectiveness of the method.

In framework of a collaboration with the power system group at the Univ. of Cassino and of the University of Campania, the activity also results in the development of an optimization model for voltage control in a distribution network, leveraging the flexibility offered by parking lots equipped with multiple EV charging stations.

The optimization method for the use of EV parking lot flexibility for voltage profile optimization includes two major parts: calculation of the EV parking lot flexibility margins by each parking lot operator, and the voltage optimization carried out by the DSO. As shown in Figure 1, at the beginning of each 6-hour stage, the parking lot operator provides the DSO with reference power absorption

profiles and the corresponding up and down flexibility margins. The DSO performs real-time voltage profile optimization and returns power change requests and energy recovery (either up or down) to the PL every 15 minutes.

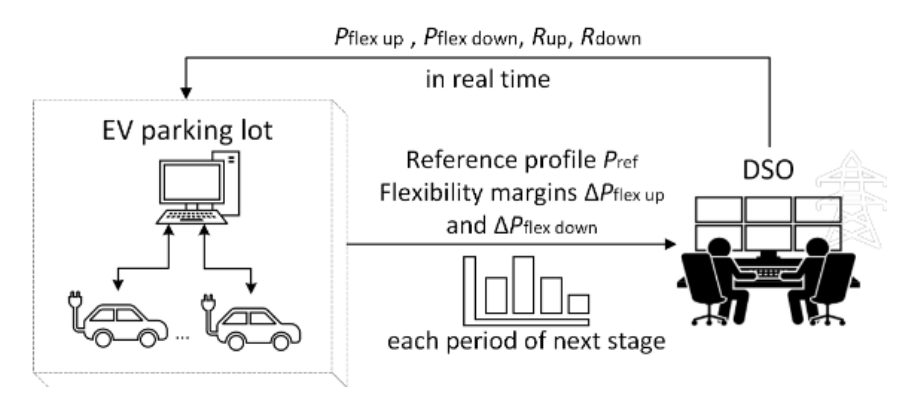


Figure 1 Procedure scheme.

The optimization is achieved by defining an objective function that minimizes the sum of voltage deviations from a reference value, constrained by a linearized set of power flow equations. The approach involves decoupling networks via pilot nodes and employing a linearized power flow model, with optimization based on a rolling horizon approach to accommodate demand recovery. A daily budget constraint is also considered for the cost of active and reactive power flexibility. To deliver ancillary services to the grid, the EV aggregator managing the charging stations can adjust intra-day schedules within defined flexibility margins. This ensures adequate EV charging levels through a stochastic optimization method.

Applying this method to a 123-bus test network demonstrated the effectiveness of these flexibility services in voltage optimization.

1.1.2. Flexible operation of energy communities

In this thesis, the energy community is considered as a framework to allow direct transactions between the participants to the community, without the inclusion of incentives. The members of the community are connected to feeders of the same substation that provide the connection to the transmission network. As, shown in Figure 2 the members can transact both active and reactive power. Active power transactions allow to reduce the costs or increase the revenues with respect to the transactions with the retailer. Reactive power transactions allow to reduce the penalties associate to low power factor operation, considering that the reactive power of each user is partially compensated by the reactive power transaction with other members of the same community connected to feeders fed by the same high voltage-medium voltage transformer. Although Figure 2 shows a single retailer and a

single, in the considered framework, the members of the community may freely have a contract with different retailers, belong to one community or not, and multiple communities can be present in the same distribution network.

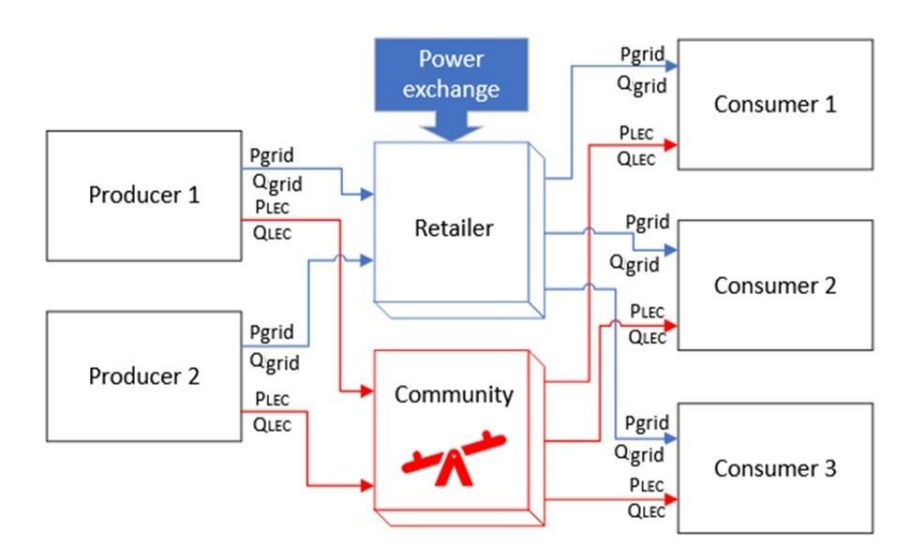


Figure 2 Procedure scheme.

The optimization model considers a day-ahead scheduling problem for energy resources and control means. The optimization horizon is 24 hours (a day) with a 15-minute resolution. The objective function minimizes the electricity procurement costs for the entire community, considering known tariffs for active power exchange with the external reseller and incorporating penalties for participants whose power factor falls below a specified limit. A deterministic day-ahead scheduling problem is considered assuming the forecast of load and photovoltaic production known without uncertainties. The formulation of the optimization problems and the solution computational requirements are suitable for the inclusion in a stochastic approach.

The analysis of the presence of multiple independent communities in the same distribution network (as allowed by regulation) has been carried out by the development of a specific optimization model. Each community minimizes its energy procurement costs through a day-ahead scheduling of internal transactions among its members and available energy resources, including battery energy storage (BES) systems. Members of the same community may be served by different electricity retailers. Each retailer has different contract terms. Internal transactions are priced using the shadow prices of the balancing constraints between the power provided by the electricity retailer and the power received by other community members. The price of the energy transactions between community members are determined as shadow prices of balancing constraints. In addition, there is an

optimization problem for the DSO, which takes into account the network constraints and minimizes the violations of the limits of the branch currents and the bus voltages.

Other than several test cases available in the literature, the main case study used for the application of the approaches is based on the part data of a real distribution network obtained in the framework of the collaboration with INRETE DISTRIBUZIONE as a part of the internship. The network, located in Modena, Italy, includes 5 real MV feeders connected to a 132/15 kV substation. The substation is equipped with a 50 MVA transformer and two 25 MVA transformers, all with onload tap changers, OLTCs. The system includes 134 buses and branches. Three electricity retailers (Pr1, Pr2, and Pr3) with different price profiles are considered. The load and generation profiles are obtained from the DSO records at each 15-minute interval, separately for each MV node, for three days in January and in July 2023.

The day-ahead optimization procedure takes into account the network constraints and provides the prices of the internal transactions as the shadow prices of the power balancing constraints for each user. In addition, the procedure also allows reactive power exchanges between members of the same community other than active power. The results show the effectiveness in reducing both energy procurement costs and noncompliance costs for each community. The sensitivity analysis on the number of communities shows that as the number of communities increases, cost reductions and penalties decrease, approaching the case without internal transactions within communities.

The widespread use of photovoltaic (PV) systems reduces local active power consumption during daylight hours and increases the problem of low power factor operation. The research activity considers the contribution of reactive power exchange among community members to mitigate low power factor penalties, which is a typical issue when using distributed generation, especially PV. The up and down margins of reactive power flexibility with respect to the reference profile are calculated for both users and the community, assuming a fixed reward. The flexibility margins can be used by the DSO for voltage reactive power optimization or offered to the TSO at the DSO-TSO interface.

By enabling reactive power transactions, the implemented procedure not only reduces overall costs, but also allows the community to provide reactive power flexibility services to the grid. The results consistently show that using reactive power compensation resources to offset low power factor penalties and provide flexibility services has a minimal impact on the community's energy procurement costs, making the approach economically favorable. The proposed computational models demonstrate reasonable time efficiency, making them well suited for integration into

stochastic procedures that account for uncertainties in PV production, load consumption profiles, and the probability of DSO/TSO requests for reactive power adjustments throughout the day.

1.1.3. Structure of the thesis

Chapter 2 is devoted to description of the implemented modo for the flexibility exploitation of parking lots equipped with several charging stations. In order to limit the computational effort the batteries of the cars connected to the charging stations are aggregated. However, the model includes the evaluation of the vehicle to vehicle (V2V) energy transfers. Therefore, these transfers can be constrained to zero if bidirectional charging stations are not available and a revenue for the vehicles owner can be included to compensate for the decrease of battery health due to charging-discharging cycles. The chapter also describes the coupling between the EV parking lot flexible operation with of voltage optimization procedure of the distribution network.

Chapter 3 is devoted to model of the energy communities. The chapter describes the assumptions and the regulatory framework. The energy community is represented as an agreement among final users and prosumers that allows direct power exchanges using the public distribution network. The chapter illustrates the relationships with the community members and the relevant resellers, taking into account the freedom for each the end-users to leave or join the community and chose a different reseller than the one of other community members. The analysis does not consider incentives, seen as a temporary support for first establishment of this type of agreements as in the Italian scenario. The chapter also deals with the analysis of the effects of the number of communities sharing the same distribution network and a mechanism is developed to include the management of the network congestions through the definition of a specific DSO optimization model.

Chapter 4 is focuses on the provision of reactive power flexibility services from communities. In this chapter, the effect of providing reactive power on energy costs and penalties is investigated. The chapter describes the details of the model, with specific reference to the calculation of the penalties associated with low power factor operation.

Chapter 5 concludes the thesis by reviewing the main results both relevant to the representation of the flexible operation of parking lots equipped with several charging stations and relevant to the analysis of energy communities, the definition of the internal transaction prices, the provision of reactive power flexibility services, and the influence of the presence of multiple communities sharing the same distribution network. The chapter also lists some topics that may deserve future investigation.

1.1.4. Publications

The results of the research activity have been presented in the following publications that are the basis for this thesis.

Book chapters

- Borghetti, A., Harighi, T., Nucci, C.A., Graditi, G., Di Somma, M. and Caliano, M. (2024). Integration of Multiple Energy Communities: Transaction Prices, Reactive Power Control, and Ancillary Services. In Integrated Local Energy Communities (eds M. Di Somma, C. Papadimitriou, G. Graditi and K. Kok). https://doi.org/10.1002/9783527843282.ch9
- Borghetti, A., Harighi, T., Lilla, S., Napolitano, F., Nucci, C.A., Prevedi, A., Tossani, F., Graditi, G. (2024), Comunità energetiche e nuova gestione della distribuzione dell'energia elettrica. Accademia delle Scienze Annales, Class of Physical Sciences, Volume 2. https://doi.org/10.30682/annalesps2402i

Journal papers

- Tohid Harighi, Alberto Borghetti, Fabio Napolitano, Fabio Tossani, "Provision of reactive power services by energy communities in MV distribution networks", Sustainable Energy, Grids and Networks, Vol. 34, 2023, https://doi.org/10.1016/j.segan.2023.101038 (published)
- T. Harighi, A. Borghetti, F. Napolitano, F. Tossani, "Flexibility Modeling for Parking Lots with Multiple EV Charging Stations" Electric Power Systems Research, Vol. 234, 2024, https://doi.org/10.1016/j.epsr.2024.110732
- De Santis, Michele, Tohid Harighi, Anna Rita Di Fazio, Alberto Borghetti, and Mario Russo. "Enhancing voltage optimization in distribution networks through flexible operation of EV parking lots." Sustainable Energy, Grids and Networks 41 (2025): 101601. https://doi.org/10.1016/j.segan.2024.101601
- Borghetti, A., Graditi, G., Harighi, T., Lilla, S., Napolitano, F., Nucci, C.A., Prevedi, A. and Tossani, F., 2025. How Can Energy Communities Be Part of the Urban Energy Transition?: A Focus on Electrical Perspectives. IEEE Power and Energy Magazine, 23(3), pp.78-88. https://doi.org/10.1109/MPE.2025.3542755

Conference papers

- T. Harighi, S. Lilla, A. Borghetti "Modeling of Independent Energy Communities Sharing the Same Distribution Network" 2024 International Conference on Smart Energy Systems and Technologies (SEST), Torino, Italy, DOI: https://doi.org/10.1109/SEST61601.2024.10694676
- T. Harighi, A. Borghetti, S. Lilla, C. A. Nucci, A. Calzolari, M. Salicini, C. Cercolani "Quantifying Maximum Limits for Reactive Power Flexibility Provision in Energy Communities: A Case Study of A Real Distribution Power Network" International Conference of CIGRE 2024, URL: https://www.e-cigre.org/publications/detail/c6-10393-2024-quantifying-maximum-limits-for-reactive-power-flexibility-provision-in-energy-communities-a-case-study-of-a-real-distribution-power-network.html
- T. Harighi, A. Borghetti, F. Napolitano and F. Tossani, "Optimization Model for the Analysis of Multiple Energy Communities in the Same Distribution Network with Different Providers,"

- 2023 IEEE Belgrade PowerTech, Belgrade, Serbia, 2023, pp. 1-6, doi: https://doi.org/10.1109/PowerTech55446.2023.10202985
- M. De Santis, A. R. Di Fazio, M. Russo, T. Harighi and A. Borghetti, "Voltage Optimization in Distribution Networks using EV Parking Lots and PV systems as flexibility options," 2023 IEEE International Conference on Environment and Electrical Engineering and 2023 IEEE Industrial and Commercial Power Systems Europe (EEEIC / I&CPS Europe), Madrid, Spain, 2023, pp. 1-6, doi: https://doi.org/10.1109/EEEIC/ICPSEurope57605.2023.10194708
- T. Harighi, A. Borghetti, M. De Santis, A. R. Di Fazio and M. Russo, "Flexible Operation of an EV Parking Lot for Voltage Control of a Distribution Network," 2023 International Conference on Smart Energy Systems and Technologies (SEST), Mugla, Turkiye, 2023, pp. 1-6, doi: https://doi.org/10.1109/SEST57387.2023.10257434

Chapter 2. Flexibility Exploitation: Model of the Parking Lot and Its Use for Voltage Optimization

2.1. Flexibility modeling for parking lots with multiple EV charging stations

2.1.1. Chapter content

This chapter focuses on a multi-stage stochastic optimization model or a parking lot with many charging stations. The model is used to calculate the maximum flexibility margins both upward and downward for each period of the day. These flexibility margins can be offered to the DSO in a local market for the provision of ancillary services.

The second part of the chapter deals with the application of the developed flexibility model for voltage optimization in the distribution network. The stochastic optimization model of the parking lot is combined with an optimal power flow procedure with the aim to minimize the voltage variations with respect to the reference value.

2.1.2. EV parking lots as flexibility service providers

Electric vehicle (EV) batteries are expected to play an expanded role in the provision of grid services, as described in [1] and references therein. This chapter presents a multistage stochastic optimization procedure for calculating the flexibility capabilities of an electric vehicle (EV) parking lot equipped with many charging stations. The aggregator of the charging stations offers flexibility services in response to the distribution system operator's (DSO) requests. This study does not address the possibility of concurrent participation in a wholesale flexibility market. The maximum deviations of the parking lot load consumption with respect to a reference profile need to be calculated in advance by the EV aggregator to support the DSO with the information needed to efficiently use the service.

Other than different model-based or data-driven approaches on EV charging power forecasting (e.g., [2] and references therein), the literature includes several studies that explore the impact of optimizing the operation of EV parking lots in addressing network congestions [3] and mitigating the variability of renewable energy sources [4]. Additionally, various models have been proposed to represent the participation of EV aggregators in energy and ancillary services markets, e.g. [5], and within the framework of demand response programs, as in [6].

The flexibility in the load profile of the EV parking lot can be harnessed by the DSO to address voltage or congestion issues, as shown in, for example, [7]. Procuring reserve flexibility should ensure

the energy recovery needed for the provision of the expected charging services to the EVs [8]. Furthermore, the flexibility offered by EV charging stations can also play a significant role in optimizing the design and operation for energy communities and virtual power plants, as shown in, e.g., [9], [10], and [11].

This chapter focuses on the calculation of the maximum flexibility margins, i.e., the maximum up and down feasible variations with respect to the expected reference consumption profile. These margins are offered in advance by the EV parking lot aggregator to the DSO. To improve the dynamic adaptation of the margin calculation to current parking conditions (i.e., to the number and characteristics of the EVs actually connected to the charging stations), a multistage stochastic optimization approach is integrated with an intraday decision procedure. This approach allows the update of the calculated margins at the beginning of each stage in which the daily horizon is divided. In general, this approach produces results, specifically flexibility margins, that are close to those estimated assuming perfect information about the future (deterministic solution) and larger than those obtained by considering the worst-case scenarios (robust solution).

The chapter presents a multistage optimization procedure based on an aggregated representation of the EV parking lot, which takes into account several factors, including power absorbed from the grid, the efficiency of EV battery charging and vehicle-to-vehicle (V2V) exchanges allowed by the use of bidirectional charging stations, self-discharge rates, and the energy levels of EVs upon arrival and departure from the car park.

The procedure begins by generating scenarios based on the forecasted number of EVs entering and leaving the parking lot. These scenarios account for the uncertainty associated with the daily forecast, considering also the EV rated battery size and diffusion, as well as the maximum charging power. Subsequently, a clustering procedure is applied to construct a multistage scenario tree that represents various possibilities of EV charging. The optimization model, which is built upon the approach presented in [12], calculates the reference consumption profile for the representative scenario of each cluster. It achieves this by minimizing the procurement costs for the EV parking lot, which include both those associated with purchasing the energy from the grid and the consumption of the initial energy stored in the vehicles. Additionally, the model determines the maximum power reduction and increase margins to be offered as flexibility services.

The flexibility margins represent the maximum achievable power reduction and increase that ensure the maintenance of appropriate EV charging levels. Following a power change requested by the DSO, the considered regulatory framework allows the EV parking lot to recover its energy level within a predefined subsequent interval, through a constant variation in the absorbed power.

The following subsections of the first part of this chapter are organized as follows. Section 02.1.3 describes the scenario management of the stochastic parameters, which represent the parked EVs, and the construction of the multistage scenario tree. Section 2.1.8 describes the optimization models of the EV parking lot that provide the demand flexibility services. Section 2.1.11 describes the case studies and the results for different sizes of parking lots. Section 2.3 concludes chapter 2.

2.1.3. Stochastic parameters and scenario management

The flexibility margins of the EV parking lot, which determine how much power consumption can be reduced or increased in response to a DSO request while ensuring appropriate EV charging level, are calculated using stochastic optimization, where some parameters and variables are subject to uncertainty or randomness. These uncertainties mainly relate to the characteristics and the number of EVs connected to the charging stations throughout the day. The description of the procedure is divided into two parts. The first part, which is the subject of this Section, defines the stochastic parameters by using scenarios, each representing a different realization of the uncertain parameters, and performs scenario management. This process generates the multistage tree model, which aggregates similar scenarios at various stages of the day-long optimization horizon. Section 2.1.8 deals with the second part of the procedure, which includes the definition of constraints and objectives of the stochastic models. A first optimization model calculates the daily reference consumption profile of the car park without any request for providing flexibility to the DSO. Two additional models allow the calculation of the maximum feasible reduction and increase in power consumption for each period. All these models are formulated as linear programming mathematical problems, without the inclusion of binary variables, ensuring computational efficiency, even when dealing with a large number of EVs and charging stations. This is achieved by adopting an aggregate representation of the charging stations and EV batteries, which preserves the accuracy of the calculation of the power exchanges with the network and of the charge/discharge losses, including those associated with V2V exchanges.

2.1.4. Scenario generation

The procedure starts by generating several scenarios for the next day. The scenario generation procedure assumes the availability of the forecasts of the number of EVs entering ($N_{\rm EV\,in}^t$) and leaving ($N_{\rm EV\,out}^t$) the parking lot in each of the 96 periods of the following day. These forecasts can be obtained by the analysis of the EV entry and exit data from previous or similar days. All the entries and departures of a period are assumed to occur at the end of that period. For each scenario ω , entering $N_{\rm EV\,in}^{\omega,t}$ and leaving $N_{\rm EV\,out}^{\omega,t}$ EV numbers are obtained by multiplying the corresponding forecast

sequences by $1+k_i$, which accounts for the increasing forecast uncertainty throughout the day. Time series k_i is generated by using a normal distribution with the mean value set to zero, and the standard deviation calculated as $\sqrt{1-\psi_t^2}$, where ψ_t is a decreasing function of t. Each value obtained is rounded to the nearest positive integer. Moreover, for each scenario, the order of the numbers of leaving EVs is adjusted so that the number of parked EVs is never negative. To construct an accurate aggregate model of the parking lot, the sequences of arriving and departing EV numbers are associated with specific populations of EVs. Each EV is defined by entry and exit time periods, ensuring that the entire population of EVs reproduces the sequences of arriving and departing EV numbers. To achieve this, a simple 'first in, first out' strategy is implemented. Only those EVs that can connect to an available charger are considered (i.e., they are limited by $N_{\text{park max}}$) and they are assumed to disconnect at their departure time. Furthermore, each EV is characterized by its rated battery size E_{EV} , the maximum power P_{EV} allowed by the charging station, and the initial state of charge. To define the first two characteristics, the procedure uses a predefined categorization of currently available EV models and their market penetration. Specifically, the attributes of each EV are selected based on the prevalence of each category, which represents the probability that a vehicle entering the parking lot belongs to that category. The initial energy of the vehicles entering the car park follows a truncated normal distribution, with the mean and standard deviation values assumed to be 0.3 times the size of the battery. It is assumed that the EVs leaving the parking lot are fully charged or charged to the maximum level allowed by the charging power and parking duration. While it is possible to account for scenarios where some EVs leave the parking lot with lower energy levels by introducing a penalty into the objective functions, this aspect is not addressed here for the sake of simplicity. The results of this chapter have been obtained assuming the same rated power for all charging stations, but the procedure can be adapted to the case where different types of charging stations are present.

2.1.5. Scenario clustering and tree construction

The procedure has been implemented as a day-ahead evaluation considering a 4-stage stochastic approach (one day-ahead stage and three intraday stages), where the day-ahead evaluation is updated every 6 hours during the day to use information on the actual number and characteristics of the EVs in the parking lot. We assume that the EV parking lot aggregator provides the reference consumption profile and the down and up flexibility margins at the beginning of each intraday stage for each of the relevant 15-minute time periods.

For each stage s, similar scenarios are grouped into a scenario tree. For this purpose, the k-medoid clustering procedure is applied. Starting from a single cluster in the first (day-ahead) stage, each cluster can originate different clusters in the next stage. The clustering procedure provides both the medoid for each cluster and stage (i.e., one of the initial scenarios that minimizes the dissimilarity measure with respect to the other scenarios in the cluster) and probabilities π^{ω} . Compared to the k-means algorithm, which calculates centroids by averaging data points within clusters, the k-medoid approach avoids non-integer numbers of entering, leaving, and parked EVs. This ensures the preservation of scenario feasibility after clustering. Here is a detailed description of the procedure. The clustering is based on the number of parked EVs (assuming that they are all connected to a charging station), $N_{EV}^{\omega,i}$. Alternatively, the clustering can use the sum of the battery sizes of the parked EVs. Even a combination of the two parameters can be considered, normalizing them based on their minimum and maximum values at each time period, as described in [13]. For each stage, the dissimilarity measure d, based on the Euclidean distance $\|\cdot\|_2$ between two scenarios $N_{EV}^{\omega,i}$ and $N_{EV}^{\omega,i}$ is

$$d\left(N_{EV}^{\omega_{1},t},N_{EV}^{\omega_{2},t}\right) = \sum_{t \in T_{s}} \left\|N_{EV}^{\omega_{1},t} - N_{EV}^{\omega_{2},t}\right\|$$
(2.1)

where T_s is the subset of periods in stage s. Regarding the clustering procedure, different distance definitions can be used to assess the dissimilarities between scenarios, such as the Manhattan distance, as shown in [14].

At stage s=1, a scenario ω_i is chosen as medoid $C_1^{s=1}$ such that the average dissimilarity between $N_{EV}^{\omega_i,t}$ and every other scenario $N_{EV}^{\omega_j,t}$ in the set of generated scenarios is minimized. At stage s=2 and subsequent stages, the set of scenarios aggregated in the previous stage is divided into K clusters. The steps of the clustering routine applied in stage s=2 and subsequent stages are the following.

A. Selection of initial medoids: the first medoid is randomly chosen, and the remaining K-1 initial medoids are selected as the most distant K-1 scenarios by using (2.1). Various methods for selecting initial medoids are detailed in [15].

B. Selection of the closest medoid: each scenario ω is grouped to the medoid for which the distance given (2.1) is minimal. This results in the creation of K clusters denoted as C_1^s to C_K^s for stage s.

- C. Update of the medoids: within each cluster, the scenario that minimizes the average distance to every other scenario in the same cluster is chosen as the new medoid.
- D. Iteration and medoid update: after updating the medoids, the procedure is repeated starting from step 2. This iterative process continues until either the scenarios chosen as medoids do not change in consecutive iterations, or the maximum allowed number of iterations is reached.
- E. Cluster merging check: the distance between each pair of medoids and the average distance among the scenarios grouped in the relevant clusters is compared, and if the former is lower than the latter, the two clusters are merged.
- F. Scenario replacement: when stable medoids are obtained, all the scenarios of each cluster are replaced by the corresponding medoid, namely, the sequences of $N_{\rm EV\,in}^{\omega,t}$ and $N_{\rm EV\,out}^{\omega,t}$ for t in T_s . To ensure feasibility during the transition between stages, this replacement is performed at the level of each individual EV within the population, preserving all EV characteristics, including the rated battery size, maximum charging power, and initial charging level.
- G. Subsequent stages: the clustering routine is independently carried out for each cluster of the previous stage.
- H. Scenario tree construction: the described procedure results in the formation of a scenario tree composed of nodes (namely, the medoids) at each stage, connected by arcs. The probability associated with each node in the tree corresponds to the summation of the probabilities of each scenario assigned to the corresponding cluster.

The maximum number of clusters K is chosen to preserve the tractability of the problem by limiting the final number of scenarios in the tree while ensuring an adequate representation of the stochastic processes during the day. The scenario generation technique allows for the inclusion of specific metrics that assess the selection of the maximum value of K, such as the elbow method or the silhouette coefficient, using the obtained objective function values. Other metrics, like the value of stochastic solution and the expected value of perfect information, can also be considered. In this chapter, the results are obtained for a maximum K equal to 3.

2.1.6. Characterization of each scenario in the tree

As a result of the scenario tree construction, sets $S_{\rm in}^{\omega,t}$ and $S_{\rm out}^{\omega,t}$ of entering and leaving EVs are defined, for each scenario ω and period t. The aggregated storage size $E_{\rm Smax}^{\omega,t}$ of the parking lot and the maximum charging power $P_{\rm max}^{\omega,t}$ are derived by summing the corresponding data of the individual

arriving and departing vehicles, i.e. $E_{\rm EV}$, $P_{\rm EV}$. Moreover, the increase of stored energy due to the initial energy in the incoming EVs, $E_{\rm S+}^{\omega,t}$, and the energy decrease due to the charged outgoing EVs, $E_{\rm S-}^{\omega,t}$, are obtained as

$$E_{S+}^{\omega,t} = \sum_{i \in S_{in}^{\omega,t}} E_i^0 \tag{2.2}$$

$$E_{S^{-}}^{\omega,t} = \sum_{i \in S^{\omega,t}} E_i^{-} \tag{2.3}$$

where E_i^0 and E_i^- are the energy of the *i*-th EV when entering and leaving the parking lot, respectively. The difference between E_i^- and E_i^0 represents the final charge gain during the parking time, for the *i*-th EV.

Each set of EVs that enter and leave in the same periods is grouped by means of two matrices, the rows of which indicate the entry periods and the columns the exit periods. Specifically, in order to retain the information on the period of entry and exit of the energy initially stored in the batteries, matrix $E_{\text{ini},j}^{\omega,t}$ is formed as the sum of E_i^0 for the EVs that enter in period j and exist in period t. Similarly, for the charge gain, matrix $E_{g,j}^{\omega,t}$ is constructed as the summation of $E_i^- - E_i^0$ for the EVs entering a period j and leaving at period t.

2.1.7. Intraday decision procedure

The solution provided by the recourse model, which is based on the scenario tree constructed using the day-ahead forecasts of the number of arriving and departing EVs, generates multiple potential decisions at each stage beyond the first one (i.e., during the day). Consequently, a decision making procedure is implemented to determine the most suitable decision for each stage among those identified by the stochastic problem solution. This selection takes into account the current number of parked EVs.

More precisely, at the beginning of each of the considered three stages after the first, the intraday procedure selects the scenario from the tree that offers the best match with the real number of parked EVs compared to those associated with the nodes/medoids of the scenario tree.

2.1.8. Optimization models to represent EV parking lot flexibility

Once the scenario tree is defined, the procedure uses the optimization models described in this Section. The models are formulated as linear programming problems and calculate, for each stage and node of the tree, non-negative variables $P_{\text{ref}}^{\omega,t}$, $\Delta P_{\text{flex down}}^{\omega,t}$ and $\Delta P_{\text{flex up}}^{\omega,t}$, through repeated stochastic optimizations. Due to the aggregated structure of the EV parking lot model and its linearity, each optimization is computationally efficient, requiring only tens of milliseconds regardless of the number of EVs and charging stations. The assumptions made include an agreement between the EV parking lot aggregator and the DSO that allows the parking lot to recover the power change during a predefined interval following the flexibility provision interval. Therefore, each flexibility margin is associated with a maximum recovery of opposite sign within the recovery interval. The actual recovery is assumed to be proportional to the effective reduction requested by the DSO. It is also assumed that the DSO does not request any further reductions or increases during the recovery period and that the power variation is constant over time. The model calculates the flexibility margins assuming that the DSO request is limited to a single 15-min period, denoted as of $t_{\rm flex}$. Furthermore, the calculation is repeated assuming that the DSO requires flexibility provision in additional consecutive 15-min periods after t_{flex} , denoted as n_{flex}^+ . These calculations are performed with the constraint that the flexibility margin remains the same throughout the entire flexibility interval, i.e., from t_{flex} to $t_{\text{flex}} + n_{\text{flex}}^+$. The values of $P_{\text{ref}}^{\omega,t}$ and $\Delta P_{\text{flex}}^{\omega,t}$, along with their associated recovery profiles, are provided to the DSO at the beginning of each stage.

2.1.9. Calculation of the reference consumption profiles

The objective function for the day-ahead calculation of the parking lot consumption profile $P^{\omega,t}$ is to minimize the procurement costs, considering probability π^{ω} of each scenario ω :

$$\min \sum_{\omega} \pi^{\omega} \sum_{t} \left(\rho_{TOU}^{t} P^{\omega, t} \Delta t + C_{S}^{\omega, t} \right)$$
 (2.4)

The model considers the presence of bidirectional charging stations, used for V2V energy exchanges but not to inject power into the external grid. These exchanges help ensure that EVs depart with the maximum charge allowed by the parking duration, $E_{S-}^{\omega,t}$, using the energy stored in EVs expected to have prolonged parking times. The energy balance equation for the parking lot is:

$$E_{\text{S net}}^{\omega,t} = (1 - \delta)E_{\text{S net}}^{\omega,(t-1)} + E_{\text{ch,grid}}^{\omega,t} - E_{\text{S-}}^{\omega,t} + \mu^{\omega,t}E_{\text{S+}}^{\omega,t} - l_{\text{V2V}}^{\omega,t} + \sum_{i=1}^{t} (1 - \mu^{\omega,i})E_{\text{ini},j}^{\omega,t}$$
(2.5)

that represents the aggregate energy stored in the parked EVs in scenario ω at the end of period t. $E_{\rm S\,net}^{\omega,t}$ takes into account not only the energy supplied by the grid $E_{\rm ch,grid}^{\omega,t}=\eta_{\rm ch}\,P^{\omega,t}\Delta t$ but also the possibility to use for V2V a part of the initial energy $E_{\rm S+}^{\omega,t}$ of the EVs that entered the parking lot in

period t (namely, $\mu^{\omega,t}E_{S+}^{\omega,t}$). The fraction of the initial energy used is represented by non-negative variable $\mu^{\omega,t}$, which is subject to upper bound $\mu_{\max}^{\omega,t}$ that ensures a minimum energy margin e_{\min}) maintained in the EV batteries. The associated cost of using the initial energy of the EVs is represented by $C_S^{\omega,t} = \rho_\mu \mu^{\omega,t} E_{S+}^{\omega,t}$ in (2.4), which can be interpreted as the remuneration of the vehicles providing the service. In the context of V2V energy exchanges, constraint (2.5) accounts for the associated energy losses through non-negative variable $l_{V2V}^{\omega,t}$ given by

$$l_{\text{V2V}}^{\omega,t} \ge \left(1 - \eta_{\text{V2V}}\right) \left(E_{\text{ch,grid}}^{\omega,t} - \sum_{j=1}^{t-1} E_{\text{ch}j}^{\omega,t} + \mu^{\omega,t} E_{\text{S}+}^{\omega,t}\right)$$
(2.6)

where η_{V2V} represents the efficiency of the V2V energy exchanges, taking into account the losses in the power electronic converters and in the batteries. The long-term reduction in efficiency due to aging and demanding operation is not considered. $E_{\text{ch}\,j}^{\omega,t}$ for t>j is the profile that ensures that the EVs parked in the interval $\left[j,\tau\right]$ receive $E_{\text{g},j}^{\omega,\tau}$, i.e., their final charge gain, before leaving the parking lot. $E_{\text{ch}\,j}^{\omega,t}$ is zero for $t\leq j$. The sum of $E_{\text{ch}\,j}^{\omega,t}$ is equal to the total net charge increase at the departure period τ of the last EVs among those entered in period j, while it is larger before that period. The constraints representing $E_{\text{ch}\,j}^{\omega,t}$ are

$$\sum_{t=j+1}^{i} E_{\text{ch},j}^{\omega,t} - \sum_{t=j+1}^{i} E_{\text{g},j}^{\omega,t} \ge 0 \quad \text{for all } i < \tau$$

$$\sum_{t=1}^{j} E_{\text{ch},j}^{\omega,t} = 0$$

$$\sum_{t=j+1}^{\tau} E_{\text{ch},j}^{\omega,t} - \sum_{t=j+1}^{\tau} E_{\text{g},j}^{\omega,t} = 0$$
(2.7)

where τ is the departure period of the last EV among those entered in period j. In the presence of V2V energy exchanges, some EVs receive more energy from the grid than they need to cover their final charge gain during their parking time. In (2.6), the term $E_{\rm ch,grid}^{\omega,t} - \sum_{j=1}^{t} E_{\rm ch\,j}^{\omega,t} + \mu^{\omega,t} E_{\rm S+}^{\omega,t}$ represents the energy from the grid that is used for V2V exchanges. According to (2.6), $l_{\rm V2V}^{\omega,t}$ losses are calculated when the excess energy is stored, not when the V2V exchange is performed. This does not affect the final result since $\eta_{\rm V2V}$ is assumed to be constant. If the chargers are not bidirectional, both μ and $l_{\rm V2V}$ are set to zero. The V2V energy can also be used to add a cost in the objective function (2.4)

associated with the remuneration of vehicles providing the V2V service. Non-negative variable $E_{\text{S net}}^{\omega,t}$ is constrained as

$$E_{\text{S net}}^{\omega,t} \le E_{\text{Smax}}^{\omega,t} - \sum_{j=1}^{t} (1 - \mu^{\omega,j}) E_{\text{ini},j}^{\omega,t}$$
 (2.8)

Assuming that the connection of the parking lot with the external grid is limited by $P_{\text{max,grid}}$ then

$$P^{\omega,t} \le \min\left(P_{\text{max,grid}}, P_{\text{max}}^{\omega,t}\right) \tag{2.9}$$

The solution of problem (2.4)-(2.8) provides reference profile $P_{\text{ref}}^{\omega,t} = P^{\omega,t}$ for all scenarios ω .

2.1.10. Calculation of the maximum power reduction and increase margins

The calculation of the maximum power reduction and increase margins is performed for each period. It considers cases where flexibility is requested in a single period t_{flex} and cases where flexibility is also requested in additional consecutive periods n_{flex}^+ , limited to $n_{\text{max,flex}}^+$.

The objective function is:

$$\min \sum_{\omega} \pi^{\omega} \sum_{t} \left(\rho_{TOU}^{t} P^{\omega, t} \Delta t + C_{S}^{\omega, t} - R_{flex}^{\omega, t} \right)$$
 (2.10)

where non-negative $R_{\rm flex}^{\omega,t}$ is the revenue associated with the provision of the maximum flexibility in $t_{\rm flex}$:

$$R_{\text{flex}}^{\omega,t} = \begin{cases} \rho_{\text{flex}}^{t} \Delta P_{\text{flex}}^{\omega,t} \Delta t & \text{if } t_{\text{flex}} \leq t \leq t_{\text{flex}} + n_{\text{flex}}^{+} \\ 0 & \text{otherwise} \end{cases}$$
(2.11)

Predefined tariff ρ_{flex}^t is the compensation rate that the DSO pays to the flexibility provider for achieving a non-negative power change $\Delta P_{\text{flex}}^{\omega,t}$ in period t_{flex} compared to reference power level $P_{\text{ref}}^{\omega,t}$. $\Delta P_{\text{flex}}^{\omega,t}$ is defined as:

$$\Delta P_{\text{flex}}^{\omega,t} = P_{\text{ref}}^{\omega,t} - P^{\omega,t} \text{ for down margin}$$

$$\Delta P_{\text{flex}}^{\omega,t} = P^{\omega,t} - P_{\text{ref}}^{\omega,t} \text{ for up margin}$$

$$\text{for } t_{\text{flex}} \le t \le t_{\text{flex}} + n_{\text{flex}}^+$$
(2.12)

The model includes the possibility for the EV parking lot to recover the power change with respect to $P_{\text{ref}}^{\omega,t_{\text{flex}}}$ that occurred at t_{flex} in a predefined number of periods n_{rec} after $t_{\text{flex}} + n_{\text{flex}}^+$ (with a value of $n_{\text{rec}} = 3$ in the tests). $\Delta P_{\text{flex}}^{\omega,t}$ is constrained to be uniform in the recovery interval by:

$$\Delta P_{\text{flex}}^{\omega,t} \ge -\sum_{j=t_{\text{flex}}}^{t_{\text{flex}}} \frac{\Delta P_{\text{flex}}^{\omega,j}}{n_{\text{rec}}}$$

$$\text{for } t_{\text{flex}} + n_{\text{flex}}^+ < t \le t_{\text{flex}} + n_{\text{flex}}^+ + n_{\text{rec}}$$

$$\Delta P_{\text{flex}}^{\omega,t} = 0 \text{ for } t < t_{\text{flex}} \text{ and } t > t_{\text{flex}} + n_{\text{flex}}^+ + n_{\text{rec}}$$

$$(2.13)$$

The inequality of the previous constraint becomes an equality for the flex-up scenario to prevent the use of incremental losses (such as unnecessary V2V exchanges) to enhance the flexibility margin. In the case of multiple consecutive periods of flexibility, the maximum margin is constrained to be the same in all the periods:

$$\Delta P_{\text{flex}}^{\omega,t} = \Delta P_{\text{flex}}^{\omega,t_{\text{flex}}} \quad \text{for } t_{\text{flex}} < t \le t_{\text{flex}} + n_{\text{flex}}^+. \tag{2.14}$$

All the models are completed with nonanticipativity constraints, typical in stochastic optimization, which ensure that decisions made at different stages depend only on currently available information and not on future outcomes or information that will be revealed later.

2.1.11. Case studies and results

The case studies include three parking lots, denoted as PLA, B, and C, each with a maximum power import capacity of 3 MW. The number of available charging stations for these parking lots is 70 for PLA and PLB, and 45 for PLC. In all scenarios, the parking lots are empty at the beginning of the day, and all EVs leave before the end of the day. Figure 3 shows the different day-ahead forecasts for the number of EVs entering and leaving each parking lot in $\Delta t = 15$ min time periods. These forecasts are used to generate a total of 60 different daily scenarios. The ψ_t function is assumed to decrease linearly from 0.9999 in the first period to 0.99 in the last period. Similar scenarios are grouped together using the k-medoid method, resulting in a 4-stage tree composed of nodes representing the scenarios that are the medoids obtained. The profiles of scenarios with common nodes in the tree are bounded at each stage based on the tree structure. Figure 4 illustrates the tree corresponding to parking lot PLA with 24 medoids in the last stage.

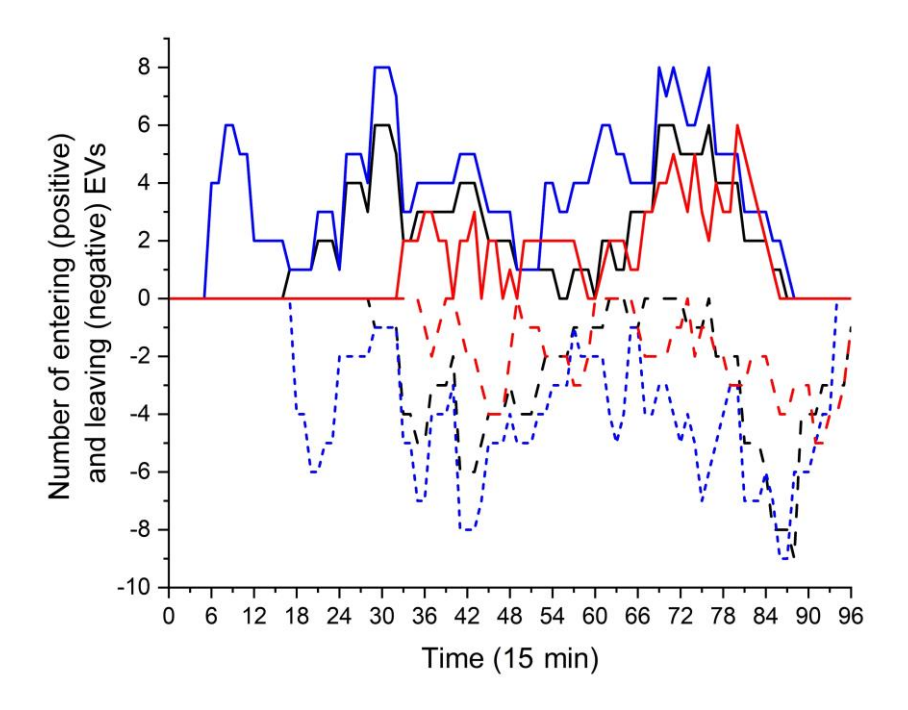


Figure 3 Day-ahead forecast profiles of the number of EVs entering (solid lines) and exiting (dashed lines) in the three parking lots considered: PL A in black, PL B in blue, PL C in red

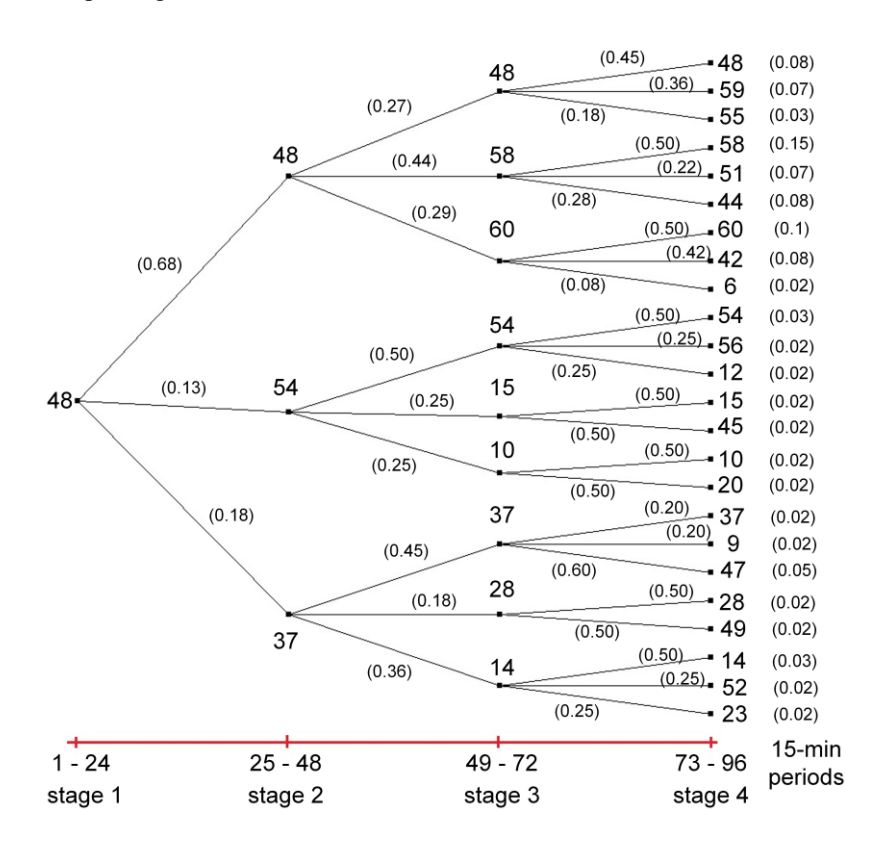


Figure 4 Scenario tree for parking lot PL A. The identification numbers of the medoids are shown for each stage of 6 hours, together with, between parenthesis, both the arc probabilities and scenario probabilities π^{ω}

In the tests, the types of EVs are classified into 4 categories based on their battery capacities and market penetration rates: 1) $E_{\text{EV}} = 25 \text{ kWh}$ with 15% penetration, 2) $E_{\text{EV}} = 45 \text{ kWh}$ with 45%

penetration, 3) $E_{\rm EV}=70$ kWh with 25% penetration, 4) $E_{\rm EV}=100$ kWh with 15% penetration. These values are derived from data available from various Internet sources. While they may be appropriate for the current situation in certain countries, it is essential to adapt them to the actual usage-specific conditions. A maximum charging power of 40 kW is assumed for each charging station, which is representative of typical ac charging stations installed in parking lots where EVs remain connected for extended periods of time. For the EV batteries, δ is assumed to be zero. The charging and V2V energy transfer efficiencies, $\eta_{\rm ch}$ and $\eta_{\rm V2V}$, are set to 0.96 and 0.92, respectively. Time of use price $\rho_{\rm TOU}^{\prime}$ is equal to 72.39 €/MWh from 7 am to 11 pm and to 51.62 €/MWh at other times. If $\mu_{\rm max}^{\omega,t}$ is set greater than 0, the price for using the initial EV energy is $\rho_{\mu}=50$ €/MWh, which is lower than the grid price. In each period, minimum initial energy $e_{\rm min}$ is set to 20% of the sum of the rated capacity of the batteries of the entering EVs. For both downward and upward power flexibility provided by the parking lot, predefined tariff $\rho_{\rm flex}^{\prime}$ is set to 100 €/MWh, significantly higher than the grid prices. For all the cases, the recovery interval is $n_{\rm rec}=3$ periods after the end of the flexibility interval.

AIMMS Developer was used to implement the optimization procedures. The adopted LP solver is Gurobi V10 on 4.7-GHz processors with 32 GB of RAM, running 64-bit Windows.

The objective function values of the stochastic optimizations for the three parking lots are: \in 438 for PL A, \in 568 for PL B, and \in 242 for PL C. The average and maximum objective function reductions with single flexibility are: 1.32 % and 8.63 % for PL A, 1.08 % and 12.11 % for PL B, 1.37 % and 18.71 % for PL C, respectively. These reductions depend on the difference between ρ_{flex}^t and ρ_{TOU}^t . As an illustrative example of the upward and downward flexibility margin evaluations and of the subsequent recovery periods, Figure 5 shows the down and up margins in power variations at t_{flex} =29 and t_{flex} =45, respectively, relative to the reference profile for scenario 56 of PL A included in the stochastic tree of Figure 4. The figure shows the results considering the flexibility interval given by a single period or 2 or 3 consecutive 15-min periods. While both up and down margins can generally be computed for the same interval, the figure separates the up and down flexibilities into distinct t_{flex} for clarity.

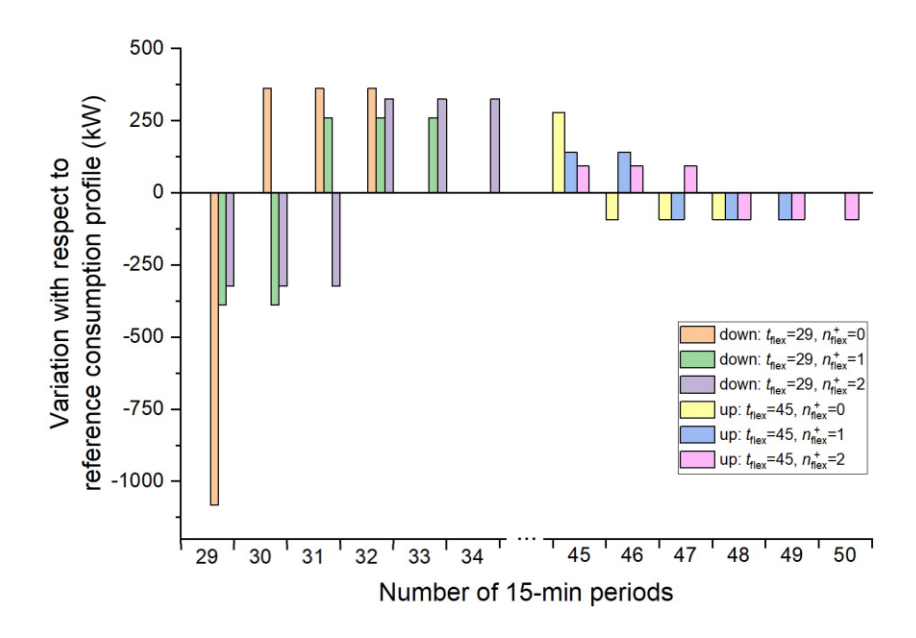


Figure 5 Flexibility margins and corresponding recoveries of scenario 56 of PLA: down flexibility starting at $t_{\text{flex}} = 29$ (7:15 am) and up flexibility starting at $t_{\text{flex}} = 45$ (11:15 am)

Figure 6 shows the periods when the maximum up and down flexibility margins exceed 100 kW for scenario 56 in PL A. It considers the flexibility interval of a single 15-min period, 2 periods, and 3 consecutive periods (only the first period is shown in the figure). In period 46, the parking lot can provide both up and down flexibility for n_{flex}^+ =0. In several cases, when single period flexibility cannot be provided, a two- or three-period flexibility is allowed as the different recovery interval is more suitable.

Figure 6 also shows the results obtained by tripling both the size (i.e., increasing the number of charging stations to 210) and the number of EVs entering and exiting with respect to PL A. This expanded scenario is referred to as PL D. As a result of the changes introduced, the operating conditions of the corresponding scenarios differ between the two parking lots. Nevertheless, the figure shows that the flexibility widens as the size of the parking lot increases, as expected. In scenario 56, for PL A, the maximum up flexibility is 54.0 kW with an average equal to 12.2 kW, and the maximum down flexibility is 70.8 kW with an average equal to 13.1 kW; for PL D, the maximum up flexibility is 101.0 kW with an average equal to 24.3 kW, and the maximum down flexibility is 129.2 kW with average equal to 38.6 kW. In time period 53, the PL D can provide both up and down flexibility for $n_{\text{flex}}^+=0$. The computation time for the cases considered in the chapter is always less than a few minutes.

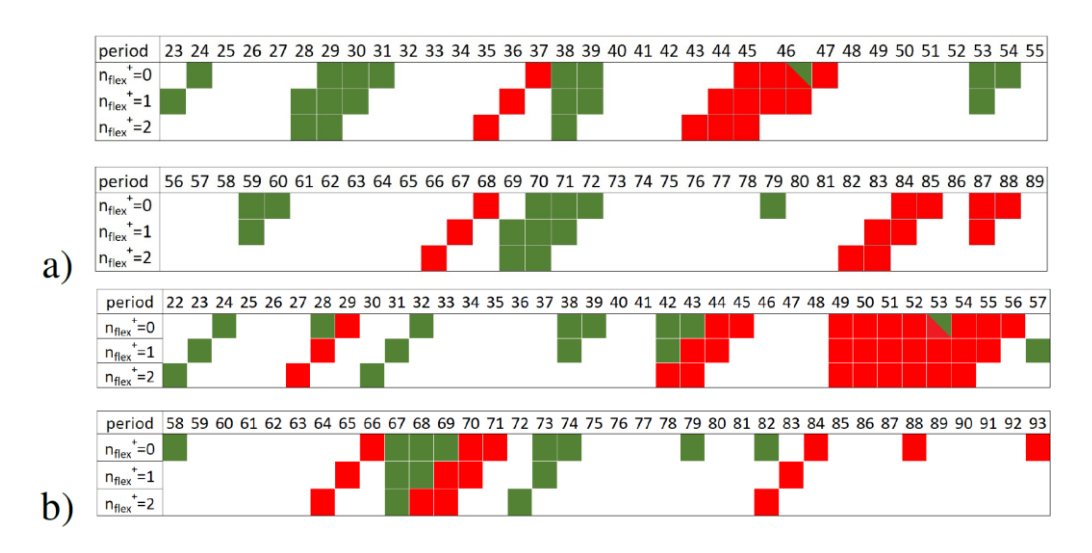


Figure 6 Initial period of the flexibility intervals with a margin larger than 100 kW for scenario 56: a) PL A, b) PL D. Downward flexibility in green and upward flexibility in red.

2.2. Flexible Operation of an EV Parking Lot for Voltage Control of a Distribution Network

2.2.1. Introduction

In recent years, distributed energy resources (DERs) are starting to be seen more as a resource rather than an obstacle for the operation of the network, especially in the paradigm of the future smart grids [16]. The use of various flexibility options can help system operators to cope with the imbalances in generation and demand, due to the unpredictable nature of some renewable power generation sources, and the uncertainties of load consumption and network contingencies. Flexibility services can be offered by single providers (e.g., passive end-users joined to demand response programs, active end-users with renewable distributed generators and/or storage), energy communities, and electric vehicles (EV) aggregators, which are available to vary the injected/absorbed powers in response to a request of the distribution system operator (DSO) and transmission system operator (TSO).

One of the main technical issues in the operation of distribution networks is the voltage control. Optimizing the voltage profile of the network, maximizing the margins with respect to the limits, results in an improved operation from a technical and an economic point of view.

Some flexibilities services with specific reference to active power balancing and alleviation of voltage drops problems are foreseen also by the EVs aggregators, in order to reduce the impact of simultaneous charging of EVs on the operation of the distribution network, particularly if equipped with bidirectional charges (e.g., [17], [9] and references therein). The functions of aggregating the operation of the charging stations of a parking lot may also be incorporated in the energy community

framework [18], [10]. Swappable batteries, i.e., interchangeable power storage units for electric vehicles, may be also included, offering advantages such as quick battery exchange, reduced charging time, and potential scalability of charging infrastructure.

In this chapter, a multi-stage stochastic optimization procedure is used for the calculation of the flexibility margins of a parking lot equipped with several EV charging stations that considers the uncertainty associated with variability of the number and type of cars. The flexibility margins are exploited in a procedure for the optimal control of the voltage profile in the network. The procedure is based on the solution of a voltage optimization problem, which incorporates a recently proposed approximate linear power flow method, and the decomposition of the network in voltage control zone (VCZs), each of ones characterized by a pilot node (PN) (i.e., the most representative node of the operating conditions of the VCZ) [19], [20].

The structure of the chapter follows. Section 2.2.2 describes the general methodology, including the model of the EV parking lot that provides the demand flexibility services, and the voltage profile optimization procedure of the distribution network. Section 2.2.5 describes the multistage stochastic optimization approach used to obtain the reference consumption profile of the EV parking lot, and the optimization model repeatedly applied to obtain the down and up flexibility margins. Section 2.2.7 is devoted to the formulation of the multi-period rolling voltage optimization problem considering the EV parking lot flexibility. Section 2.2.11 describes the case studies based on the IEEE-123 node Test Feeder and presents the results. Section 2.3 concludes the chapter 2.

2.2.2. Methodology

The procedure is divided into two parts. The first part focuses on the calculation of the flexibility margin of the EV parking lot, i.e., how much the power consumption can be reduced or increased, following a DSO request, still guaranteeing the appropriate EV charging level. As the characteristics and the number of cars connected to the charging stations during the day are uncertain [21], the procedure applies a multistage stochastic optimization approach. The second part deals with the centralized optimization approach for the voltage control in the distribution network, which exploits the flexibility margin of the EV parking lots.

2.2.3. EV parking lot model

Following the model described in Subsection 2.1, the procedure has been implemented as a day-ahead evaluation considering a 4-stages stochastic approach (one day-ahead stage and three intra-day

stages), in which the day-ahead evaluation is updated every 6 hours during the day, in order to use information on the actual number and characteristics of the EVs in the parking lot. We assume that the EV parking lot aggregator needs to provide the indication of the reference consumption profile and the down and up flexibility margins at the beginning of each interval for each 15-minute time period (Δt). The reference value of the profile is obtained for each stage s by grouping similar scenarios in a scenario tree by using the k-medoid procedure described in subsection 2.1.4. In the tests, the type of cars is classified in 4 categories, as shown in Table 1, chosen by summarizing data available from various internet sources. While they seem appropriate for the current situation in certain countries, it is essential to tailor them to the specific conditions of the procedure actual use. A maximum charging power of 40 kW is assumed for each charging station, representing typical ac charging stations installed in parking lots where EVs remain connected for extended durations.

Table 1 Characteristics of the EVs

Type of EV	Rated size of the EV storage	Diffusion
1	25 kWh	15 %
2	45 kWh	45 %
3	70 kWh	25 %
4	100 kWh	15 %

With the scenario tree obtained by the application of the k-medoid algorithm, the procedure implements the optimization model, whose linear programming formulation is described in the next section 2.2.5. For each stage and aggregated scenario in the tree, the model calculates $P_{\text{ref}}^{\omega,t}$, $\Delta P_{\text{flex down}}^{\omega,t}$ and $\Delta P_{\text{flex up}}^{\omega,t}$, in each t_{flex} , obtained by the solution of repeated stochastic optimizations. Due to the aggregated structure of the EV parking lot model and its linear characteristic, each optimization requires a short computer time (few seconds), independent of the number of cars and charging stations. This makes the approach feasible from the computational point of view. We assume that the agreement between the EV parking lot aggregator and the DSO allows that the parking lot recovers the power change in period t_{flex} during n_{rec} . Therefore, each flexibility margin is associated to a recovery of opposite sign in the allowed interval after t_{flex} . The actual recovering is assumed to be proportional to the effective reduction requested by the DSO. It is assumed that the DSO does not ask for a further reduction during n_{rec} . The recovery is constrained to follow a uniform pattern during n_{rec} . $P_{\text{ref}}^{\omega,t}$ and the values of $\Delta P_{\text{flex}}^{\omega,t}$ together with the associated recovery profiles are provided to the voltage control procedure as flexibility margins at the beginning of each stage. An intra-day procedure

selects the scenario of the tree that minimizes the deviation with the number of vehicles actually present in the parking lot.

2.2.4. Voltage optimization of the distribution network

The voltage optimization procedure (VOP) starts from the linearization of the DistFlow equations applied to the considered voltage distribution network [19]. The modeling of the distribution system includes π -model for lines, ZIP model for uncontrolled loads, both P-Q and P-V control for distributed energy resources (e.g., PV units and EV parking lots). The Distflow equations are linearized with respect to an initial operating point of the network so as to provide the sensitivity coefficients relating the variations of some network variables (e.g., ΔV^2) to the variations of ΔP^{PV} , ΔQ^{PV} and ΔP^{PL} . The initial operating condition is obtained by solving a single load-flow problem in a base-case.

By exploiting the concept of electrical distance and applying hierarchical clustering methods, such sensitivities are firstly used to cluster the network in VCZs with PNs. Then, this simplified network representation is used from the DSO to optimize the voltage profiles of the PNs, subject to linearized DistFlow equations, nodal voltage limits, and the available DSO budget for local flexibility services, by acting on flexibility offered by PV systems and EV parking lots. The optimization process is performed through the definition of an objective function given by the sum of deviations of node voltages with respect to the reference value. The voltage optimization problem is solved according to a centralized approach based on the zoning methodology, as in [7]. In this chapter, such an approach is extended to take into account the inter-temporal relationships associated to the provision of active power flexibility services provided by EV parking lots. The maximum flexibility of the parking-lot station with respect to the scheduled power profile is available each 1-hour time or lower (e.g., 15 min) within the 24 hours of the day, together with the recovery profile.

2.2.5. Model for the representation of the EV parking lot flexibility (Calculation of the reference consumption profiles

The objective function includes the minimization of the procurement costs considering probability and scenarios as described in 2.1.9 in equation (2.15).

Considering that the net energy entering in the batteries from the grid is $E_{\text{ch,grid}}^{\omega,t} = \eta_{\text{ch}} P^{\omega,t} \Delta t$, the balancing equation of the parking lot is represented by (2.16).

Assuming the presence of bidirectional charging stations, following [12], (2.17) includes the possibility to use the initial energy in the vehicles that enter the parking lot $E_{\rm S+}^{\omega,t}$ at time t, for a fraction given by nonnegative variable $\mu^{\omega,t}$ constrained to be lower than a maximum value that allows a minimum stored energy margin in the vehicles. The associated cost in (2.18) is $C_{\rm S}^{\omega,t} = \rho_u \mu^{\omega,t} E_{\rm S+}^{\omega,t}$. The efficiency of the vehicle-to-vehicle energy exchange is $\eta_{\rm V2V}$.

Moreover, constraint (2.19) includes $l_{\text{V2V}}^{\omega,t}$. Nonnegative $l_{\text{V2V}}^{\omega,t}$ is given by (using indicator constraints in Gurobi, when needed) as illustrated in equations (2.20) and (2.21).

If the charging stations are not bidirectional, μ and l_{v2v} are constrained to be null.

Nonnegative variable $E_{S \text{ net}}^{\omega,t}$ is constrained as in section 2.1.9 in equation (2.22).

The solution of problem (2.23)-(2.24) provides reference profile $P_{\text{ref}}^{\omega,t} = P^{\omega,t}$ for all scenarios ω .

2.2.6. Calculation of the maximum power reduction and increase margins

The calculation of the maximum margins is repeated for each period t_{flex} , both for reduction and increase flexibilities. The objective function of the maximum margins illustrated in section 2.1.10 in equation (2.25).

where nonnegative $R_{\text{flex}}^{\omega,t}$ is the revenue associated with the provision of the maximum flexibility in t_{flex} as illustrated in section 2.1.10 in equation (2.26).

Predefined tariff ρ_{flex}^t is recognized by the DSO to the flexibility provider for a nonnegative power change in period t_{flex} with respect to reference $P_{\text{ref}}^{\omega,t}$. In the maximum power reduction (down) and increase (up) margin calculations, $\Delta P_{\text{flex}}^{\omega,t}$ is illustrated in section 2.1.10 in equation (2.27) for down/up margins.

The model includes the possibility for the EV parking lot to recover the change with respect to $P_{\rm ref}^{\omega,t_{\rm flex}}$ at $t_{\rm flex}$ in a predefined number of periods $n_{\rm rec}$ after $t_{\rm flex}+n_{\rm flex}^+$ ($n_{\rm rec}=3$ in the tests). Denoting the set of these recovering periods as $n_{\rm rec}$, $\Delta P_{\rm flex}^{\omega,t}$ is constrained in section 2.1.10 in equation (2.28).

2.2.7. Multi-periods voltage optimization approach

The proposed optimization considers the same approach presented in [7]. Such an approach is extended in this chapter to perform a multi-periods voltage optimization. At first, it is evaluated

whether to use the parking lot flexibility in the interval immediately after the present one or if it is preferable to use it in one of the subsequent n_{rec} intervals. After the most favorable time interval has chosen, the parking lot limits its flexibility in the following n_{rec} intervals to recover the energy made available to the DSO in the first interval. The DSO also takes advantage of the PV flexibility, which does not impose constraints on subsequent intervals.

In the following, the voltage optimization problem is directly written in variation form with respect to an initial operating point $(\cdot)_0$. It is illustrated for a distribution network with one main feeder composed of N nodes and N-1 branches (e.g., transformer or line) and including PV systems, EV parking lots and uncontrolled loads.

Assuming $n_{\text{rec}} = 3$, at time t the flexibilities, that the PV systems and the EV parking lots can offer in the next time interval t+1, are evaluated by considering the variations of the electrical variables in the following four time intervals t+1, t+2, t+3 and t+4. Four different voltage optimizations are performed (i.e., one for each time interval t+1, t+2, t+3 and t+4, respectively).

2.2.8. Voltage optimization objective function

At each time interval, the voltage optimization solves the overall objective function for the four quarter-of-hours, as follows:

$$\frac{1}{N} \sum_{i=1}^{4} \left(\Delta \mathbf{x}_{t+i}^{T} \mathbf{\Gamma}^{T} \mathbf{\Gamma} \Delta \mathbf{x}_{t+i} - 2\Delta \mathbf{V}_{\text{ref}}^{T} \mathbf{\Gamma} \Delta \mathbf{x}_{t+i} + \Delta \mathbf{V}_{\text{ref}}^{T} \Delta \mathbf{V}_{\text{ref}} \right)$$
(2.29)

where $\Delta \mathbf{x}_t^T = [\Delta \mathbf{x}_t^{PVT} \quad \Delta \mathbf{x}_t^{PLT} \quad \Delta \mathbf{x}_t^{L,forT}]$ is the vector of the variations of the active and reactive powers injected/absorbed by PV systems, EV parking lots and uncontrolled loads at time interval t; $\Gamma = [\Gamma_{V_{pn,PQ}} \quad \Gamma_{V_{pn,PQ}} \quad \Gamma_{V_{pn,PQ}}]$ is a sensitivity matrix containing the sensitivity coefficients of the squared voltage amplitudes of the PN's to the powers injected/absorbed by PV systems, EV parking lots and uncontrolled loads; and $\Delta \mathbf{V}_{ref} \triangleq \mathbf{V}_{ref}^2 - (\mathbf{V}^2)_0$ is defined as the vector of the variations of the squared voltage reference values with respect to the initial operating point.

2.2.9. Equality constraints

For the first interval t+1, the following five equality constraints are considered (e.g. $\Delta \mathbf{x}_{res}$ is related to a result of a previously calculated variation):

$$\Delta \mathbf{x}_{t+1}^{PL} = \Delta \mathbf{x}_{t+1}^{PL,u} - \Delta \mathbf{x}_{t+1}^{PL,d}$$

$$\Delta \mathbf{x}_{t+1}^{PL} = \mathbf{x}_{t+1}^{PL,schd} - \mathbf{x}_{t}^{PL,schd} + \Delta \mathbf{x}_{t+1}^{PL,u} - \Delta \mathbf{x}_{t+1}^{PL,d} - \frac{1}{3} (\Delta \mathbf{x}_{res,t}^{PL,u} - \Delta \mathbf{x}_{res,t}^{PL,d})$$

$$-\frac{1}{3} (\Delta \mathbf{x}_{res,t-1}^{PL,u} - \Delta \mathbf{x}_{res,t-1}^{PL,d}) - \frac{1}{3} (\Delta \mathbf{x}_{res,t-2}^{PL,u} \Delta \mathbf{x}_{res,t-2}^{PL,d})$$

$$\Delta \mathbf{x}_{t+2}^{PL} = \mathbf{x}_{t+2}^{PL,schd} - \mathbf{x}_{t}^{PL,schd} - \frac{1}{3} (\Delta \mathbf{x}_{res,t-1}^{PL,u} - \Delta \mathbf{x}_{t+1}^{PL,d})$$

$$-\frac{1}{3} (\Delta \mathbf{x}_{res,t}^{PL,u} - \Delta \mathbf{x}_{res,t}^{PL,d}) - \frac{1}{3} (\Delta \mathbf{x}_{res,t-1}^{PL,u} - \Delta \mathbf{x}_{res,t-1}^{PL,d})$$

$$\Delta \mathbf{x}_{t+3}^{PL} = \mathbf{x}_{t+3}^{PL,schd} - \mathbf{x}_{t}^{PL,schd} - \frac{1}{3} (\Delta \mathbf{x}_{t+1}^{PL,u} - \Delta \mathbf{x}_{t+1}^{PL,d}) - \frac{1}{3} (\Delta \mathbf{x}_{res,t}^{PL,u} - \Delta \mathbf{x}_{res,t}^{PL,d})$$

$$\Delta \mathbf{x}_{t+4}^{PL} = \mathbf{x}_{t+4}^{PL,schd} - \mathbf{x}_{t}^{PL,schd} - \frac{1}{3} (\Delta \mathbf{x}_{t+1}^{PL,u} - \Delta \mathbf{x}_{t+1}^{PL,d})$$

$$(2.30)$$

The inequality constraints for the parking lot flexibility at time t+1 can be expressed as (the relationship is reported only for the upward flexibility, $\Delta \mathbf{x}^{PL,u}$, the same can be written for the downward one, $\Delta \mathbf{x}^{PL,d}$):

$$0 \le \Delta \mathbf{x}_{t+1}^{PL} \leqslant \begin{cases} 0, \text{if } \exists \Delta x_{\text{res},t}^{PL,u}, \Delta x_{\text{res},t-1}^{PL,u}, \Delta x_{\text{res},t-2}^{PL,u} \neq 0\\ \Delta x_{\max,t+1}^{PL,u} \text{ otherwise} \end{cases}$$

$$(2.31)$$

2.2.10. Inequality constraints

The voltage optimization at time interval t+1 is subject also to voltage, PV flexibility and DSO constraints as reported in the following:

Voltage constraints

$$\Delta \mathbf{V}_{\min,t+1}^2 \le \Gamma \Delta \mathbf{x}_{t+1} \le \Delta \mathbf{V}_{\max,t+1}^2 \tag{2.32}$$

• PV flexibilities

$$\Delta \mathbf{x}_{\min,t+1}^{PV} \le \Delta \mathbf{x}_{t+1}^{PV} \le \Delta \mathbf{x}_{\max,t+1}^{PV}$$
(2.33)

DSO constraint

$$c^{PV} \mathbf{1}^{T} (-\Delta \mathbf{x}_{t+1}^{PV}) + c^{PL} \mathbf{1}^{T} (\Delta \mathbf{x}_{t+1}^{PL,u}) + c^{PL} \mathbf{1}^{T} (\Delta \mathbf{x}_{t+1}^{PL,d}) \leq b^{DSO}$$

$$\operatorname{diag}(\Delta \mathbf{x}_{t+1}^{PL,u}) (\Delta \mathbf{x}_{t+1}^{PL,d}) \leq 0 \quad \Delta \mathbf{x}_{t+1}^{PL,u} \geq 0 \quad \Delta \mathbf{x}_{t+1}^{PL,d} \geq 0$$
(2.34)

Similar optimizations must be solved for the subsequent interval times t+2, t+3 and t+4. The four objective functions are evaluated in the four intervals and if the best objective function turns out

to be that of the interval t+1, then the flexibility is used in this interval, otherwise it is not used and in the following interval the procedure is repeated.

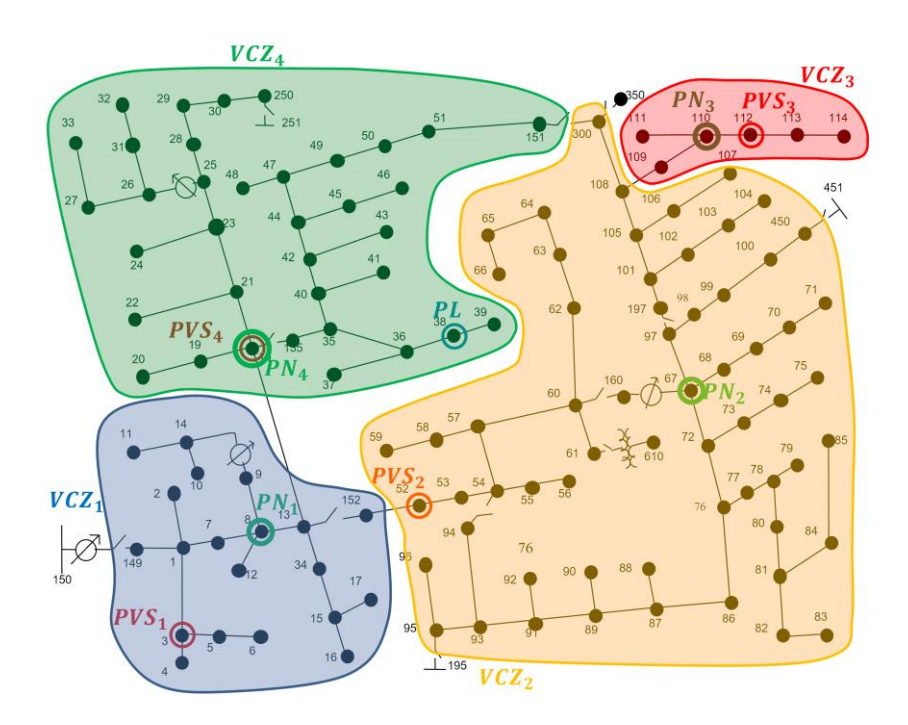


Figure 7 The 123-bus test feeder with 4 voltage control zones (VCZ) indicated by different colors. The relevant pilot nodes (PN) in green circles, as well as the considered 4 PV systems (PVS) in red circles and a parking lot (PL) in a blue circle, are also shown in the scheme.

2.2.11. Case studies and results

The case studies refer to the medium voltage (MV) IEEE-123 node Test Feeder in Figure 7 [22], which has been converted into a three-phase balanced system [23], to apply the proposed approach. The MV feeder is supplied from the HV busbar (slack bus) by a 115-/4.16-kV substation. All parameters of the IEEE-123 test feeder used in this case study are available in [24]. For the sake of simplicity, the action of the voltage regulators has been disabled, that is, constant ratios have been fixed, and the status of the switches has been assumed in the basic configuration. Furthermore, no capacitor banks are present along the feeder. Four PVs, each one of 1.5 MW peak active power, are connected to the grid at nodes 3, 18, 52, 112. The selected parking lot has a rated power equal to 3 MW and is connected at nodes 38. Concerning flexibility, the active and reactive powers of each PV can be reduced up to 10% and in the range ±50% of its momentary production, respectively. The parking lot can offer a reduction of absorbed power with respect to its scheduled value at that time interval. The voltage optimization is performed by applying the zoning methodology to obtain a

simplified representation of the distribution network suitable for voltage control. The network is partitioned in four VCZs with PN_1 , PN_2 , PN_3 , PN_4 at node 8, 67, 110, 18, respectively. The operating conditions of the network refer to 96 quarter-of-hour during the day; in each time interval the power absorption and the flexibility of the parking lot can vary, as well as the power produced by PVs and the consumption by non-flexible loads. During the day, the total balanced load connected to the network can vary between 20% and 100% of their rated value, that is equal to about $P_{tot}^{L,for} = 3.49$ MW and $Q_{tot}^{L,for} = 1.17$ MVAR, following a typical electricity consumption profile of a domestic customer; the power productions by the four PVs follow a standard daily profile. The costs of the flexibility provided by PV units and parking lot (c^{PV} and c^{PL}) are considered equal to 100 €/MWh and the DSO's budget (b^{DSO}) is four times greater (equal to a maximum of 400 €/h).

2.2.12. Results

As an example, Figure 8 shows the power consumption reference profile of one of the scenarios included in the stochastic tree of the considered parking lot with a maximum number of 45 charging stations, together with the down and up maximum flexibility and recovering profiles in the first and second part of the day.

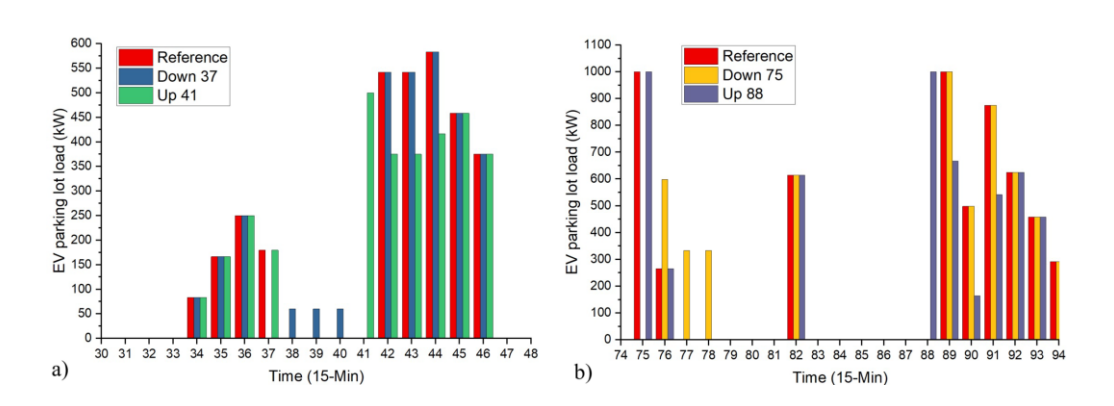


Figure 8 Reference and maximum flexibility profiles for: a) t_{flex} equal to 37, i.e., at 9:15 am, (down) and 41, i.e., at 10:15 am, (up); b) t_{flex} equal to 75, i.e., at 6:45 pm, (down) and 88, i.e. at 10 pm, (up).

The voltage optimization is performed during the day and the parking lot provides variable flexibility for four consecutive intervals from the 26th to the 29th interval, roughly between 7 and 8 in the morning. The voltage profile obtained by the VOP, which leverages both parking lot and PV flexibilities, is compared to the voltage profile obtained from classical power flow solutions (referred to as PF) for the 26th quarter-of-hour. This comparison is illustrated in Figure 9. CPU time for the considered cases was around a couple of seconds. The VOP takes advantage of the downward

flexibility offered by the parking lot, reducing up to 600 kW its absorption, and the PV ones absorbs reactive power. The same is not the case for the PF solution where the voltage drop is evident around node 56, where the parking lot is located according to Figure 9, and the voltage rise around node 24 in proximity of PV_3 . In this interval the load absorption is at 20% of the nominal value and the PVs produce a power of approximately 230 kW, due to the early morning time. Since the parking lot flexibility is used in this first-time interval, in the following three intervals the parking lot is no longer available to provide further flexibility. However, the VOP can still exploit the flexibility of the PVs and take into account the recovery of the parking lot. Figure 10, Figure 11, and Figure 12 show the voltage profiles of the VOP and PF solutions for the 27^{th} , 28^{th} and 29^{th} intervals, respectively. The improvements in voltage regulation introduced by the VOP compared to the PF are evident from the reported profiles, also for the next three-time intervals.

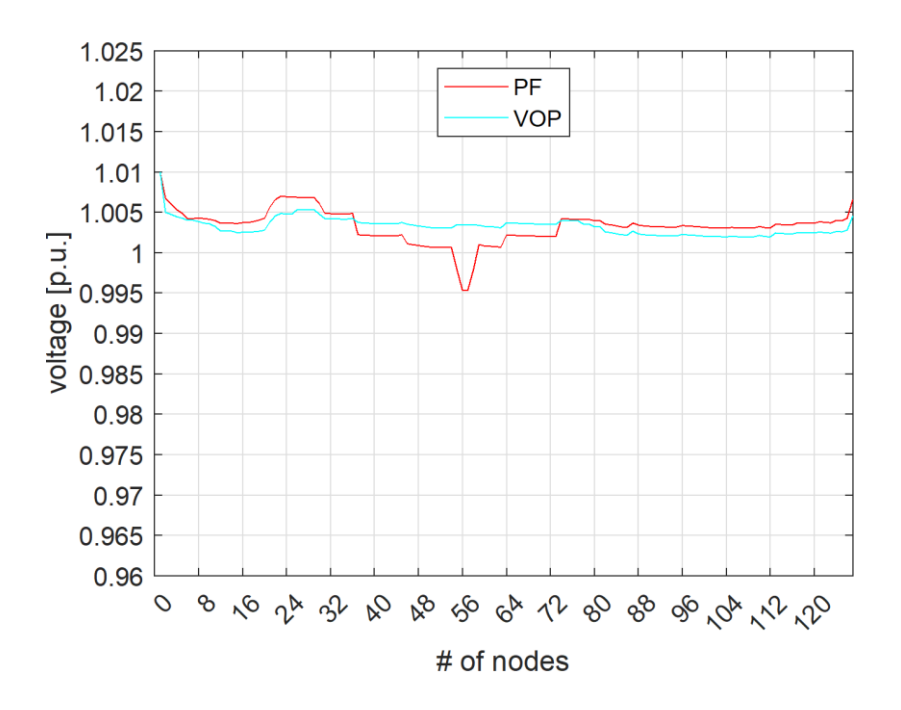


Figure 9 The voltage profile of the 123-bus network at the 26th interval

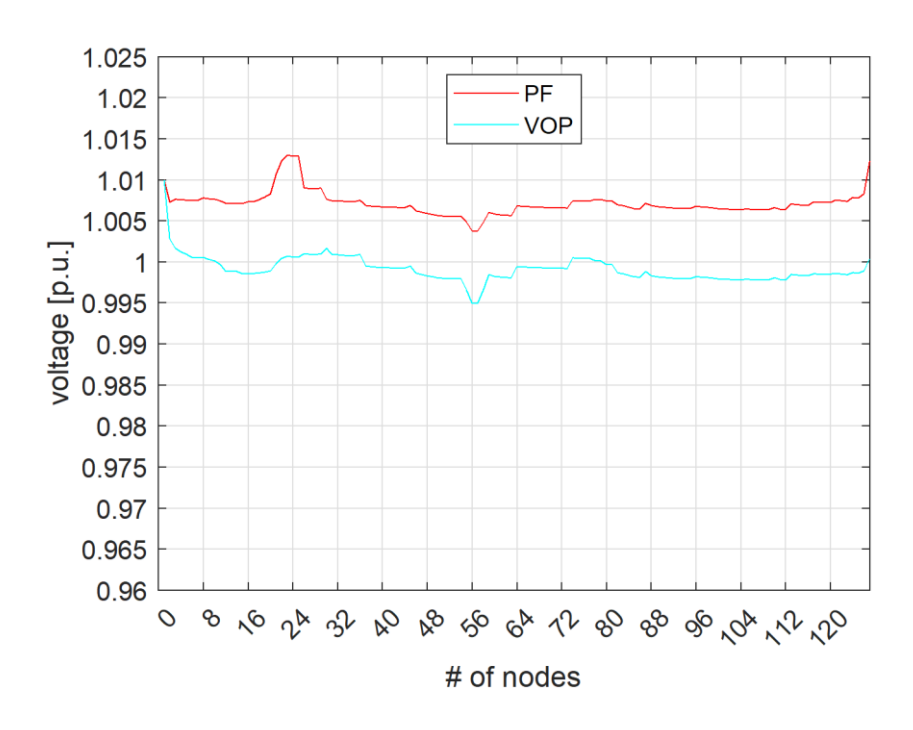


Figure 10 The voltage profile of the 123-bus network at the 27th interval

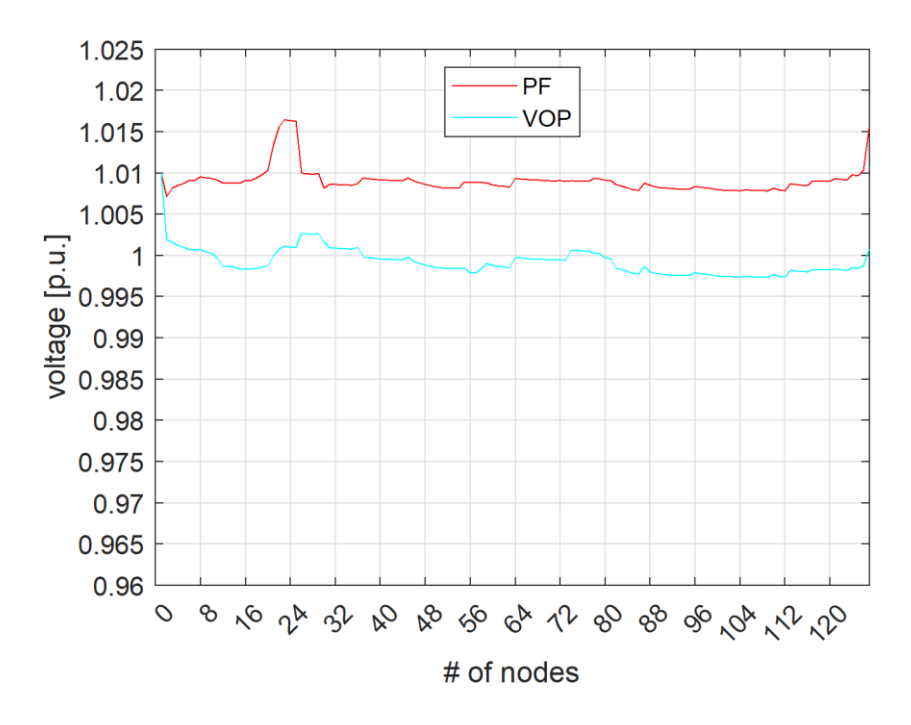


Figure 11 The voltage profile of the 123-bus network at the 28th interval

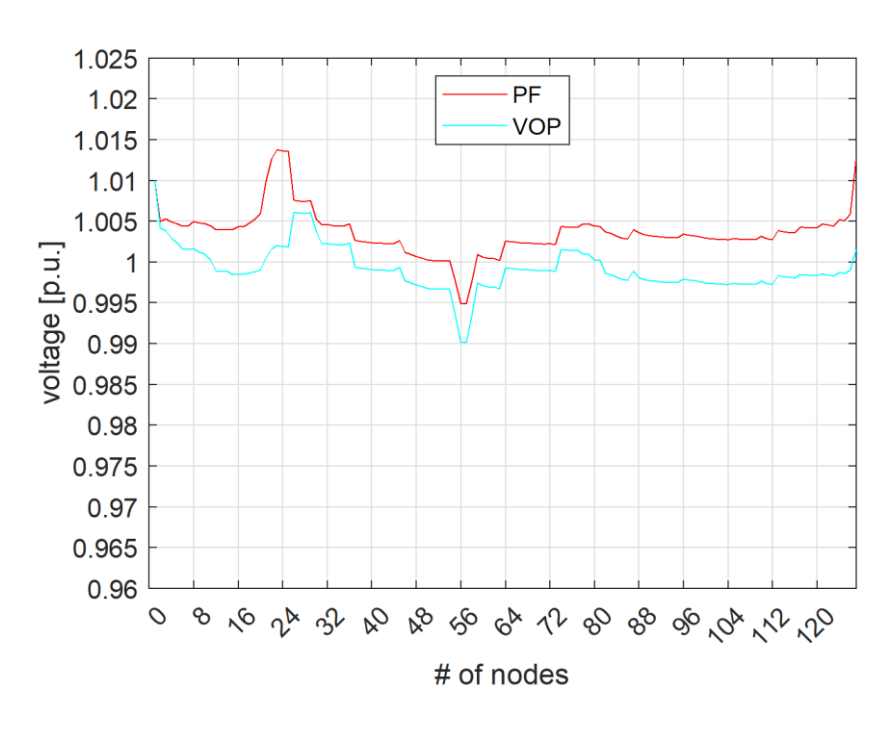


Figure 12 The voltage profile of the 123-bus network at the 29th interval

2.3. Conclusion

This chapter introduces a method to characterize the flexibility offered by parking lots equipped with EV charging stations, which can be used by the distribution system operator to address challenges such as voltage and congestion problems. Key aspects of the method include computing the reference demand profile and flexibility margins for each period of the following day, considering predefined incentives for load changes. The approach uses a multistage stochastic procedure that adapts to realtime conditions and vehicle connections to the charging stations throughout the day. Scenarios for stochastic optimization are created based on forecasts of EV arrivals and departures, accounting for factors like battery size, diffusion, and maximum charging power. Clustering of similar scenarios using the k-medoid method reduces computational complexity while maintaining scenario feasibility. The optimization model aggregates EV battery behavior and formulates the problem as a linear one, making it computationally efficient even for large parking lots. It accounts for losses associated with grid charging and vehicle-to-vehicle energy exchanges enabled by bidirectional charging stations. To enhance the flexibility of the EV parking lot, power reductions and increases in consecutive periods are considered while ensuring schedule feasibility, by including a recovery after the interval when the flexibility is requested. This approach operates as a day-ahead evaluation with a 4-stage stochastic process, updating the decisions every 6 hours to reflect real-time EV data. Numerical tests on parking lots of various sizes demonstrate the effectiveness of the method. Overall, this procedure ensures that charging requirements are met and serves as a valuable tool for the EV

aggregator offering flexibility services to improve the operation of the power distribution network and mitigate the impacts of electromobility. The typical main barriers to practical implementation are related to the lack of an appropriate regulatory framework for the local market and an efficient communication infrastructure.

The second part of the chapter presents a method to characterize and use the flexibility provided by parking lots equipped with EV charging stations for the optimization of the voltage profile in distribution networks. Assuming a predefined reward per kW of up and down load change, the EV charging station aggregator calculates both the reference demand profile and the flexibility margins in advance. For this purpose, a multistage stochastic procedure is implemented allowing a recovering after the period when the flexibility is requested. The flexibility margins calculated by the EV charging stations aggregators are incorporated as a control resource in the voltage optimization procedure of the distribution system operator. The procedure decouples the networks by using pilot nodes and applies a linearized model of the power flow equations. To consider the demand recovering in the period after the provision of the flexibility service, the optimization is carried out for a moving time horizon. A specific daily budget constraint for the expenses related to active and reactive power flexibility procurement is included. The procedure is applied to the 123-bus test feeder, including a parking lot with several charging stations. The results show the effectiveness of the flexibility services for the optimization of the voltage profile. To enhance the flexibility of the EV parking lot, power reductions and increases in consecutive periods can be enabled while ensuring schedule feasibility. This requires adapting the calculation of relevant margins and their utilization in the optimization procedure.

3.1. Optimization model for the analysis of multiple energy communities in the same distribution network with different providers

This chapter focuses on model of the energy communities. In the first part, multiple energy communities in IEEE-123 feeder case study with more than one provider has been analyzed, beside procurement costs and community effects on them. In the second part of this chapter, considers the presence of multiple communities in the same distribution network. The chapter analyzes the electricity procurement costs of both community members and non-members. The results show the effectiveness in reducing both energy procurement costs and noncompliance costs for each community.

3.1.1. Introduction

Energy communities are established to increase the local balance between production and consumption, allowing direct transactions between final users, who can behave as consumers or producers thanks to distributed generation (DG). The current regulatory framework, e.g., in Europe the EU 2019/944 electricity market directive and the 2018/2001/EU revised renewable energy directive [25], [26], allows the presence of more than one community in the same distribution network. Moreover, the users are free to take part in a community or not. They are also free to choose an energy provider different from those selected by the other community members. The presence of various energy providers characterized by specific tariffs (as well as DG power production costs, as shown in e.g., [27] for the case of a biogas unit) are expected to have an impact on the prices of the transactions among the community participants. The literature on the modeling of energy communities and peer-to-peer trading is becoming significant, e.g. [28], [29] and references therein.

This chapter presents a day-ahead scheduling model for the analysis of the presence of more than one community in the same distribution network, including users who choose not to join any community. The model considers the freedom of all users to select their preferred energy provider. Compared with other studies on the subject, i.e. [30], energy sharing between different communities is not allowed. The model provides the value of the fair prices of the transactions among the community members as shadows prices of the relevant balancing constraints. Considering renewable distributed generation and storage, the model is used to analyze the impact of the number of communities and of their characteristics (closeness of the users, size of the generating and storage units) for the IEEE 123-bus test feeder. The results of the day-ahead scheduling with the presence of communities are compared with those obtained when direct transactions among the users are forbidden. Moreover, two different

energy providers are considered and the impact on the prices of the transactions inside each community is shown.

The structure of the chapter follows. Section 3.1.2 describes the day-ahead optimization model of the energy resources available in the distribution network. Section 3.1.7 describes the case studies. Section 3.1.8 shows and compares the results. Section 3.3 concludes the chapter 3

3.1.2. Optimization Model

The power flow model adopts the convex relaxation approach described in e.g.,[31] [32], based on the DistFlow method [33], assuming the three-phase network is radial and balanced. Each branch is represented by a T model, with series impedance of the two branches equal to $0.5(r_i + jx_i)$ and admittance of the central shunt branch equal to jb_i . The square of the current rms values at the two terminals (arbitrarily indicated as in and out) are denoted as $u_{in i,t}$ and $u_{out i,t}$. The model is deterministic, but can be included in a scenario-based stochastic approach able to cope with uncertainties, as described in e.g., [34].

Following the approach presented in [35], the exchanges between participant i and any other member of the same local energy community (LEC) k in time t are represented by variables $P_{LEC\,k,i,t}$ and the exchanges with the external energy provider are described by variables $P_{grid\,i,t}$.

3.1.3. Objective function

The objective of the day-ahead scheduling of the available energy resources and of the transactions among the participants to the same community is the minimization of the function

$$OF = \sum_{i \in \Omega} \sum_{t \in T} \begin{pmatrix} C_{\text{grid } i, t} + \mu_{\text{loss } i, t} \ell_{i, t} + \\ \mu_{\text{BES } i, t} \ell_{\text{BES } i, t} + \mu_{\text{LEC}} \hat{P}_{\text{LEC } k, i, t} \end{pmatrix} \Delta t$$
(3.1)

where $C_{\text{grid }i,t}$ are the cost/revenues of user i relevant to the energy bought from or sold to its energy provider during period t (including all users in the summation, both those belonging to one of the communities and those who have not joined any of them). The day-long time horizon is divided into 96 periods of 15 minutes. $C_{\text{grid }i,t}$ is represented by

$$C_{\operatorname{grid} i,t} \ge \pi_{\operatorname{buy} i,t} P_{\operatorname{grid} i,t} \quad \text{and} \quad C_{\operatorname{grid} i,t} \ge \pi_{\operatorname{sell},i,t} P_{\operatorname{grid} i,t}$$

$$\pi_{\operatorname{buy} i,t} \ge \pi_{\operatorname{sell} i,t} \tag{3.2}$$

where $\pi_{\text{buy }i,t}$ and $\pi_{\text{sell }i,t}$ are the buying and selling tariffs (with $\pi_{\text{buy }i,t} > \pi_{\text{sell }i,t}$). $P_{\text{grid }i,t}$ is positive when bought and negative otherwise.

In (3.1), μ_{loss} , μ_{BES} , μ_{LEC} are the penalization coefficients of the branch power loss, of charge and discharge battery energy storage (BES) losses, of the exchanges inside the LEC to avoid the reselling of the power bought from the provider to the other participants and vice versa. The values of μ_{loss} , μ_{BES} and μ_{LEC} are chosen small enough so that their contribution to the objective function is negligible with respect to C_{grid} . OF does not include generation costs since we assume that all the local generation is provided by photovoltaic (PV) units.

Joule power loss $\ell_{i,t}$ in each branch is

$$\ell_{i,t} = 0.5 \, r_i \, u_{\text{in } i,t} + 0.5 \, r_i \, u_{\text{out } i,t} \tag{3.3}$$

Power losses associated with BES discharging and charging (corresponding to exchanged power P_{BES} positive and negative, respectively) are

$$\ell_{\text{BES } i,t} \ge \begin{cases} (1 - \eta_{\text{dicharge } i}) P_{\text{BES } i,t} \\ (1 - 1/\eta_{\text{charge } i}) P_{\text{BES } i,t} \end{cases}$$
(3.4)

where $\eta_{\text{dicharge }i}$ and $\eta_{\text{charge }i}$ are efficiency factors lower than one. P_{BES} is constrained by the maximum power limit of the battery system.

Nonnegative variable \hat{P}_{LEC} is defined by

$$\hat{P}_{LEC \, k, i, t} \ge \begin{cases} P_{LEC \, k, i, t} \\ -P_{LEC \, k, i, t} \end{cases} \text{ if , 0 otherwise}$$
(3.5)

where Ω_k is the set of members of community k.

3.1.4. Branch constraints

According to the DistFlow method, for each branch i and time interval t, the relationships that link the square rms value of voltages at the terminals, $v_{\rm in}$ and $v_{\rm out}$, and in the central node mp of the T model, $v_{\rm mp}$, with the active and reactive power flows that enters in terminal in $(P_{\rm in}, Q_{\rm in})$ and leaves from terminal out $(P_{\rm out}, Q_{\rm out})$ are:

$$v_{\text{mp}\,i,t} = v_{\text{in}\,i,t} - r_i P_{\text{in}\,i,t} - x_i Q_{\text{in}\,i,t} + 0.25(r_i^2 + x_i^2) u_{\text{in}\,i,t}$$

$$v_{\text{in}\,i,t} - v_{\text{out}\,i,t} = 2r_i P_{\text{in}\,i,t} + 2x_i Q_{\text{in}\,i,t} - 0.75(r_i^2 + x_i^2) u_{\text{in}\,i,t} - 0.25(r_i^2 + x_i^2) u_{\text{out}\,i,t} + x_i b_i v_{\text{mp}\,i,t} (3.6)^1$$

where:

$$P_{\text{in } i,t} = P'_{\text{out } i,t} + 0.5 r_i u_{\text{in } i,t} + 0.5 r_i u_{\text{out } i,t}$$

$$Q_{\text{in } i,t} = Q'_{\text{out } i,t} - b_i v_{\text{mp } i,t} + 0.5 x_i u_{\text{in } i,t} + 0.5 x_i u_{\text{out } i,t}$$

$$P'_{\text{out } i,t} = P_{\text{out } i,t} + P_{\text{user } i,t}$$

$$Q'_{\text{out } i,t} = Q_{\text{out } i,t} + Q_{\text{user } i,t} - Q_{\text{cap } i,t}$$
(3.7)

being Q_{cap} the reactive power injection of the utility capacitor bank if present and Q_{user} is the reactive power absorbed by the user both connected at terminal out (denoted as bus i).

The flows in the network due to direct transactions among the members of community k are represented by

$$P_{LEC_{k,i,t}} = P_{LEC_{in} k,i,t} - P_{LEC_{out} k,i,t}$$
(3.8)

where $P_{LEC \, k,i,t}$ (not null if i is a member of community k).

Nonnegative variable $u_{\text{in }i,t}$, $u_{\text{out }i,t}$ are constrained to be lower than the square of the maximum branch current limit ($I_{\text{max }i}^2$) and nonnegative variables $v_{\text{in }i,t}$, $v_{\text{out }i,t}$ are constrained between the square of the minimum and maximum bus voltage limits ($V_{\text{min }i}^2$, $V_{\text{max }i}^2$).

As usually done, the DistFlow model is incorporated in the quadratically constraint problem by the relaxation of the apparent power equalities, namely

$$\begin{split} P_{\text{in } i,t}^{2} + Q_{\text{in } i,t}^{2} &\leq v_{\text{in } i,t} \ u_{\text{in } i,t} \\ P_{\text{mp } i,t}^{2} + Q_{\text{mp } i,t}^{'2} &\leq v_{\text{mp } i,t} \ u_{\text{in } i,t} \\ P_{\text{mp } i,t}^{2} + Q_{\text{mp } i,t}^{2} &\leq v_{\text{mp } i,t} \ u_{\text{out } i,t} \\ P_{\text{out } i,t}^{'2} + Q_{\text{out } i,t}^{'2} &\leq v_{\text{out } i,t} \ u_{\text{out } i,t} \end{split}$$

$$(3.9)$$

where:

As complex power is equal to voltage and conjugate current product, the sum of the squares of the real and imaginary parts gives $v_{\text{in }i,t} - v_{\text{mp }i,t} = r_i P_{\text{in }i,t} + x_i Q_{\text{in }i,t} - 0.25 (r_i^2 + x_i^2) u_{\text{in }i,t}$ at node in and $v_{\text{mp }i,t} - v'_{\text{out }i,t} = r_i P_{\text{mp }i,t} + x_i Q_{\text{mp }i,t} - 0.25 (r_i^2 + x_i^2) u_{\text{out }i,t}$ at node mp of Figure 29, where $P_{\text{mp }i,t} = P_{\text{in }i,t} - 0.5 r_i u_{\text{in }i,t}$ and $Q_{\text{mp }i,t} = Q_{\text{in }i,t} + b_i v_{\text{mp }i,t} - 0.5 x_i u_{\text{in }i,t}$

$$P_{\text{mp }i,t} = P'_{\text{out }i,t} + 0.5 r_i u_{\text{out }i,t}$$

$$Q_{\text{mp }i,t} = Q'_{\text{out }i,t} + 0.5 x_i u_{\text{out }i,t}$$

$$Q'_{\text{mp }i,t} = Q_{\text{mp }i,t} - b_i v_{\text{mp }i,t}$$
(3.10)

In a feasible solution, all (3.9) should be verified as equalities, as well as one of (3.4). A specific check is automatically performed in the procedure and if the mismatch is greater than a predefined small tolerance the optimization is repeated with the inclusion of two additional nonnegative penalizations in (3.1): one greater than the difference between $\ell_{\rm BES}$ and the maximum of the right side terms of (3.4) calculated by using the $P_{\rm BES}$ i, value provided by the previous solution, the other greater than the difference between $u_{\rm in}$, $u_{\rm out}$ and the maximum values of $\left(P_{\rm in}^2 + Q_{\rm in}^2\right)/v_{\rm in}$, $\left(P_{\rm mp}^2 + Q_{\rm mp}^{\prime 2}\right)/v_{\rm mp}$ and $\left(P_{\rm mp}^2 + Q_{\rm mp}^2\right)/v_{\rm mp}$, $\left(P_{\rm out}^{\prime 2} + Q_{\rm out}^{\prime 2}\right)/v_{\rm out}$, respectively, evaluated according to the previous solution. These additional penalization terms become null when a feasible solution is obtained.

3.1.5. Constraints at the branch connections

Square rms values of voltage $v_{\text{out}i,t}$, total power flows $P_{\text{out}i,t}$ and $P_{\text{LEC_out}\,k,i,t}$ at the sending end should be equal to the corresponding values of $v_{\text{in}\,i+1,t}$, $P_{\text{in}\,i+1,t}$, $P_{\text{LEC_in}\,k,i+1,t}$ at receiving end of the following connected branch (being i as the upstream branch and i+1 the downstream one). Generalizing to the case of multiple branches terminating and originating from the same bus:

$$v_{\text{out } i \in \Omega_j^r, t} = v_{\text{in } i \in \Omega_j^s, t} = v_{j, t}$$

$$(3.11)$$

$$\sum_{i \in \Omega_j^r} P_{\text{out } i,t} = \sum_{i \in \Omega_j^s} P_{\text{in } i,t}$$
(3.12)

$$\sum_{i \in \Omega_j^r} P_{\text{LEC_out } k, i, t} = \sum_{i \in \Omega_j^s} P_{\text{LEC_in } k, i, t}$$
(3.13)

where Ω_j^s and Ω_j^r denote the sets of branches connected to bus j as the sending and receiving end, respectively.

The squared voltage V_0^2 at the connection point to the transmission network (slack bus 0) is assumed to be known and constant during the day. Direct transactions among community members do not cause any power flow exchange with the transmission network, i.e.,

$$\sum_{k \in \Omega_0} P_{\text{LEC_in } k,t} = 0 \tag{3.14}$$

3.1.6. User constraints

The net power for each user is given by:

$$P_{\text{user } i,t} = P_{\text{L} i,t} - P_{\text{G} i,t} - P_{\text{BES } i,t} + \ell_{\text{BES } i,t}$$

$$Q_{\text{user } i,t} = Q_{\text{L} i,t} - Q_{\text{G} i,t} - Q_{\text{BES } i,t} - Q_{\text{C} i,t}$$
(3.15)

where $P_{\rm L}$, $P_{\rm G}$, $P_{\rm BES}$ are the active power requested by the local load, provided by the generating unity and at the output of the BES system, respectively; $Q_{\rm L}$, $Q_{\rm G}$, $Q_{\rm BES}$ are the corresponding values of the reactive power; $Q_{\rm C}$ is the reactive power provided by a capacitor bank inside the user, if present.

The adopted model of the BES unit is given by the following equations:

$$E_{i,t} = E_{i,t-1} - P_{\text{BES } i,t} \ \Delta t$$
 for $1 < t < 96$
 $E_{i,1} = E_{\text{max } i} - P_{\text{BES } i,t} \ \Delta t$ and $E_{i,96} = E_{\text{max } i}$ (3.16)

where $E_{i,t}$ is the energy content constrained by the minimum and maximum energy limits $E_{\min i}$, $E_{\max i}$ respectively. In the numerical tests, $E_{i,t}$ is assumed equal to $E_{\max i}$ at beginning and the end of the optimization horizon (t = 1 and t = 96, respectively).

The linearized ZIP model of the load (in pu) is:

$$P_{Li,t} = P_{Zi,t} \ v_{\text{out}\,i,t} + \left(P_{Ii,t} + \Delta P_{Ii,t}\right) + P_{Pi,t}$$

$$Q_{Li,t} = Q_{Zi,t} \ v_{\text{out}\,i,t} + \left(Q_{Ii,t} + \Delta Q_{ii,t}\right) + Q_{Pi,t}$$
(3.17)

where P_Z and Q_Z , P_I and Q_I , P_P and Q_P are the known active and reactive power consumptions at the rated voltage of the constant impedance, constant current, and constant power components, respectively. ΔP_I and ΔQ_i (different from zero only when the $P_{Ii,i}$ and $Q_{Ii,i}$ are not null) represent the linearized voltage dependence of the constant current component consumption ²:

$$2\left(\Delta P_{\text{I}i,t} \ P_{\text{I}i,t} + \Delta Q_{i\,i,t} \ Q_{\text{I}i,t}\right) = (v_{\text{out}\,i,t} - 1)(P_{\text{I}i,t}^2 + Q_{\text{I}i,t}^2)$$

$$Q_{\text{I}i,t} \ \Delta Q_{i\,i,t} - P_{\text{I}i,t} \ \Delta P_{\text{I}i,t} = 0$$
(3.18)

The total net consumption (positive) or production (negative) of user i should balance the sum of the power exchanges with the energy provider and with the other members of the same community k:

² The first of Eq. (3.18) comes from $\left(P_{1i,t} + \Delta P_{1i,t}\right)^2 + \left(Q_{1i,t} + \Delta Q_{ii,t}\right)^2 = v_{\text{out }i,t}(P_{1i,t}^2 + Q_{1i,t}^2)$ by neglecting $\Delta P_{1i,t}^2$ and $\Delta Q_{1i,t}^2$ and assuming the square of the voltage reference value equal to 1 pu.

$$P_{\text{user } i,t} = P_{\text{grid } i,t} + P_{LEC k,i,t}$$
(3.19)

3.1.7. Description of the test cases

Test network

The test cases are based on 123-bus IEEE feeder [22] shown in Figure 13. The MV side of the substation has rated voltage equal to 4.16 kV, bus 119 rated voltage is 480 V. All the lines are assumed balanced with positive sequence parameters obtained by averaging self and mutual impedances and admittances given in [22]. The loads are assumed balanced too, by averaging the single-phase loads. 49 PV units are added at load buses, with peak power taken equal to the peak load multiplied by a random number uniformly generated between 0 and 2 if the resulting generation/load ratio is greater than 0.9. The rated power of the PV inverters is increased by 10% respect to the PV rated powers. Moreover, 7 battery units are added at different buses as shown in Figure 13.

The substation transformer and the voltage regulators feeding buses 14, 26, and 67 are equipped with an on-load tap changer (OLTC) that controls the voltage equal to 1 pu at the secondary side. Variable capacitor banks are connected to buses 83, 88, 90, 92 (with maximum power equal to the average values indicated in [22] for the three phases) assumed to belong to the utility.

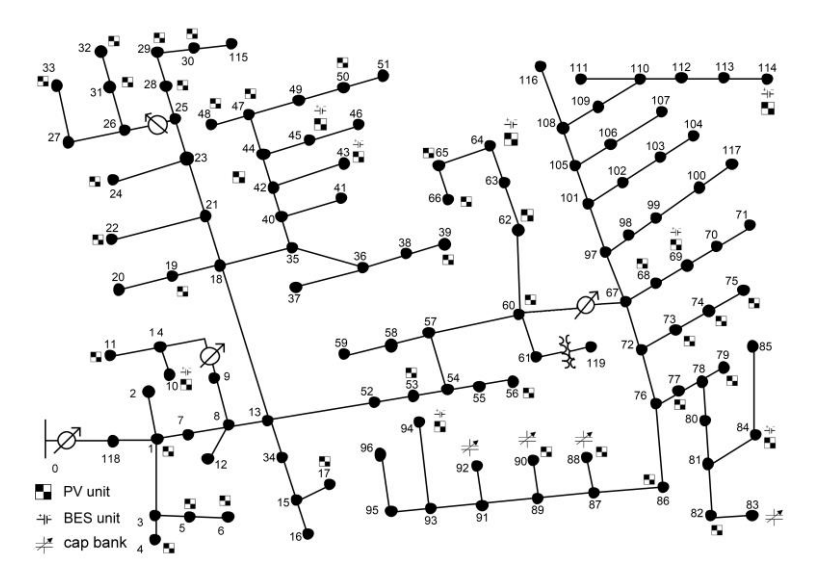


Figure 13 Scheme of the network for test cases.

The test cases refer to a deterministic day-ahead optimization. The data of the test case are in the Excel file available at https://doi.org/10.17632/4npyd68rw8.1. The file contains the per unit load profiles used in all the test cases obtained by the CREST tool [36] using various numbers of dwellings, the

profiles of π_{buy} and π_{sell} for the two different power providers, and the profile of the ratio between power output and panel surface assumed the same for all PV units.

• Assignment of each user to a provider and definition of the communities

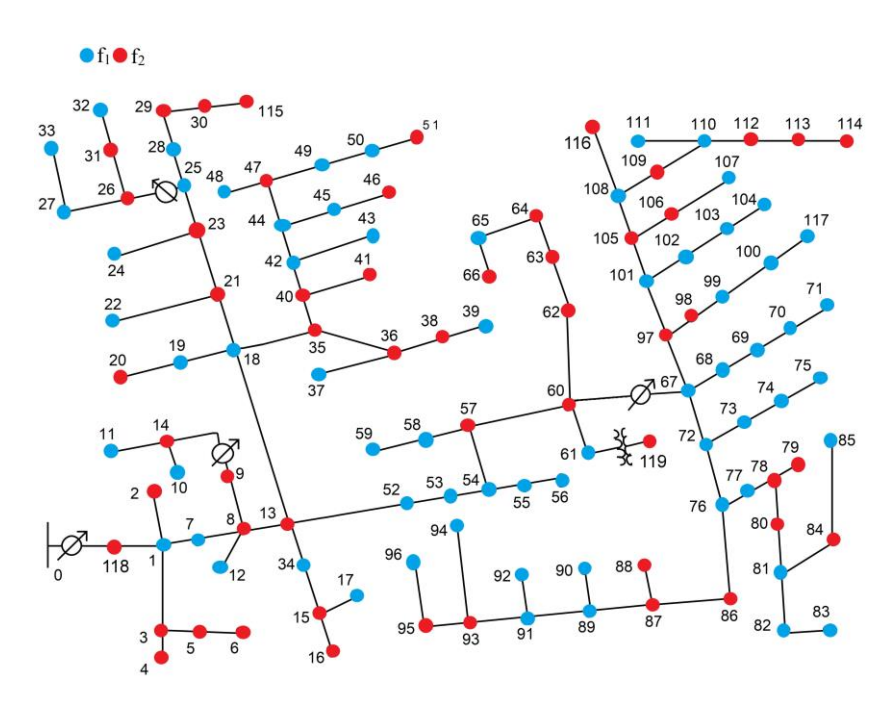


Figure 14 Random association of each user to a different provider.

In the base case, we consider two providers (f_1 and f_2) with different daily price profiles. Each user is randomly associated to one of the two providers as shown in Figure 14.

Analogously, the users are randomly grouped in three communities and the users at some nodes are not included in any community (so they can transact only with their own provider), considering an equal probability for each node to be assigned to community EC1, to EC2, to EC3 or to be not part to any community (group noEC). Figure 15 shows the obtained association and Table 2 shows the forecasted total energy demand during the day, the PV energy generation as percentage of the load, the total storage capacity installed in percentage of the daily PV generation, for each of the 4 groups.

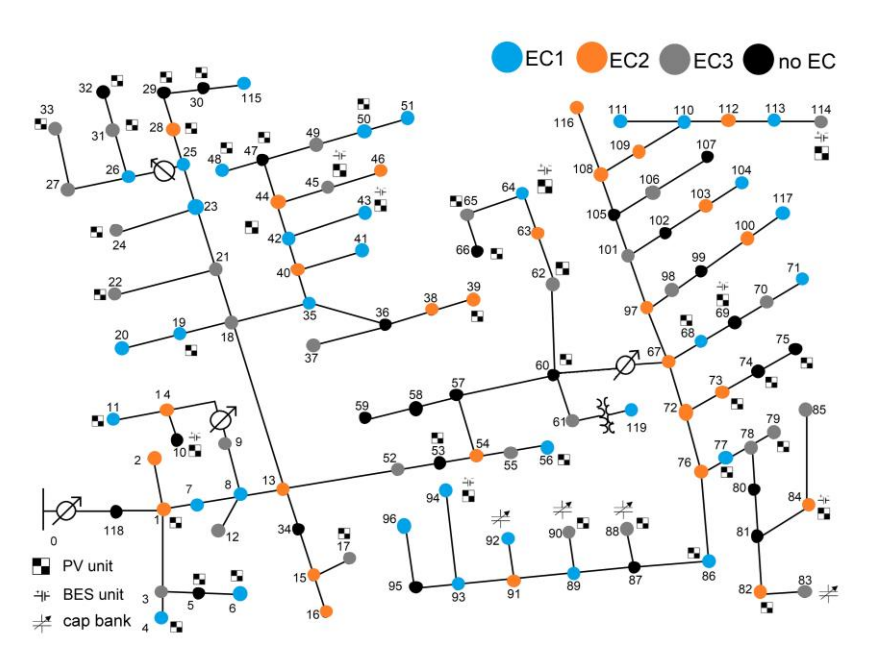


Figure 15 Random association of each user to a different community with some nodes excluded from the communities.

Table 2 Forecasted daily demand, PV generation as percentage of the load, total storage in percentage of PV generation, for each community and for the group outside the communities.

Group	Demand (MWh)	PV generation (%)	Installed BES (%)
EC1	3.76	69.2	0.54
EC2	2.75	27.7	0.79
EC3	3.56	61.5	0.37
NoEC	2.95	59.7	0.85

3.1.8. Results and comparisons

The procedure has been implemented in the AIMMS Developer modelling environment [37]. The results have been obtained by using the Gurobi 9.5 QCP solver and a computer equipped with an Intel-i7 and 32 GB of RAM, running 64-bit Windows 10. The computational time for the cases considered cases is around 100 s, increasing with the number and sizes of BES units.

3.1.8.1. Base case

For the three communities and the set of users who do not belong to any community, Table 3 shows the procurement costs due to the exchanges with the two power providers (indicated as P_{grid} cost) and the costs or revenues due to the sum of direct power exchanges P_{LEC} between the members of the same community owing a contract with a different provider. Comparing these results with those of Table 4, which refers to the case in which P_{LEC} are not allowed, each group of users has an advantage in participating in a community (i.e., the sum of P_{grid} cost and P_{LEC} cost/revenues in Table 3 is lower than the P_{grid} cost in Table 4).

Table 3 and Table 4 show similar non-compliance penalties due to users who consume with a power factor (PF) lower than 0.9 (calculated assuming a 5 kvarh \in forfeit). For community EC3, Figure 16 compares the price daily profiles of the P_{LEC} transactions among the community participants, calculated as the shadow prices of constraint (3.8), with the π_{buy} and π_{sell} tariff profiles of providers f1 and f2. The prices are not shown in the periods when there are no transactions among participants.

Table 3 Daily costs and PF non-compliance penalties for each community and the noEC group considering the two different power providers.

	Provi	ider 1	Provi	der 2	
Group	$P_{\mathrm{grid}} \cos t (\epsilon)$	<i>P</i> _{LEC} cost / revenue (€)	P _{grid} cost (€)	<i>P</i> _{LEC} cost / revenue (€)	Non-compliance Penalty (€)
EC1	419	-73	156	73	458
EC2	595	-103	219	103	1376
EC3	504	-16	94	16	864
noEC	319	0	304	0	269

Table 4 Daily costs and PF non-compliance penalties for each group of users if direct exchanges P_{LEC} are not allowed.

Group	Provider 1 cost (€)	Provider 2 cost (€)	non-compliance penalty (€)
EC1	382 (10.5%)	341 (48.6%)	464
EC2	586 (19.2%)	358 (11.3%)	1377
EC3	582 (19.5%)	161 (45.4%)	864
noEC	319	304	269

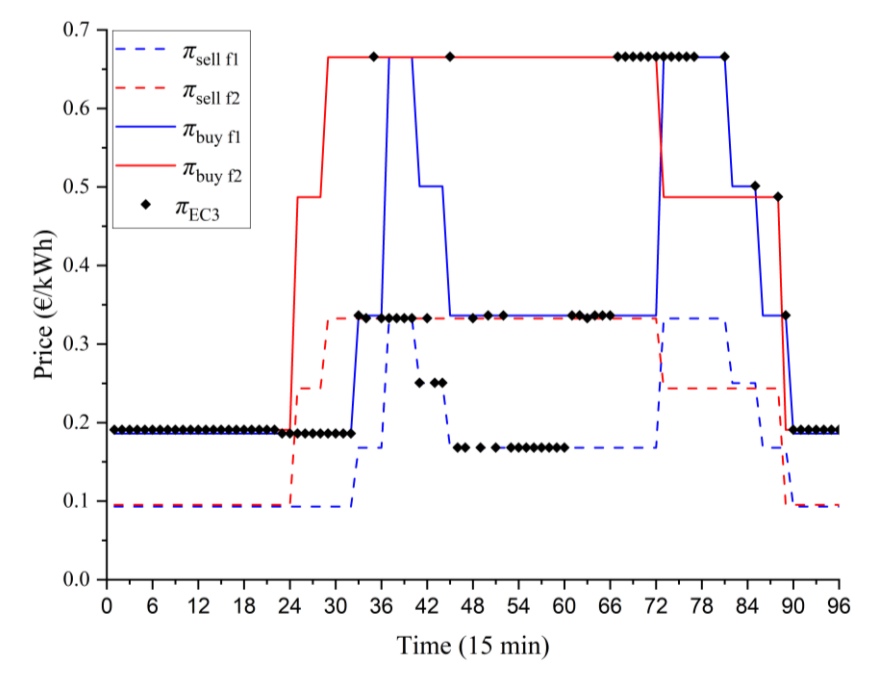


Figure 16 Community EC3: prices of the internal transactions π_{EC3} , prices of the transactions with the external energy provider f1 ($\pi_{sell f1}$, $\pi_{buy f1}$) and f2 ($\pi_{sell f2}$, $\pi_{buy f2}$).

By comparing Figure 16 with Figure 17 (which shows the net power exchanged with f1 and f2) and Figure 18 (which shows the net power exchanges between the prosumers who have a contract with f1 and those who have a contract with f2), the internal transaction prices are close to $\pi_{\text{buy} \text{f1}}$ or $\pi_{\text{buy} \text{f2}}$ when the community as a whole imports power: close to $\pi_{\text{buy} \text{f1}}$ if the marginal consumer (the one with highest buy tariff) has a contract with f1 (periods 23-33, 50, 52, 61, 62, 64-66, 73-77, 81, 85, 89) and to $\pi_{\text{buy} \text{f2}}$ if the marginal consumer has a contract with f2 (periods 1-22, 35, 45, 67-72, 88, 90-96). Analogously, the internal transaction prices are close to $\pi_{\text{sell} \text{f1}}$ or $\pi_{\text{sell} \text{f2}}$ when the community as a whole exports power, depending on whether the marginal producer (the one with the lowest selling rate) has a contract with f1 (periods 37-41, 43, 44, 46, 47, 53-60) or f2 (periods 34, 36-40, 42, 48, 63). The presence of battery may cause deviations from this general rule because the BES energy may be stored and used in periods with different tariffs.

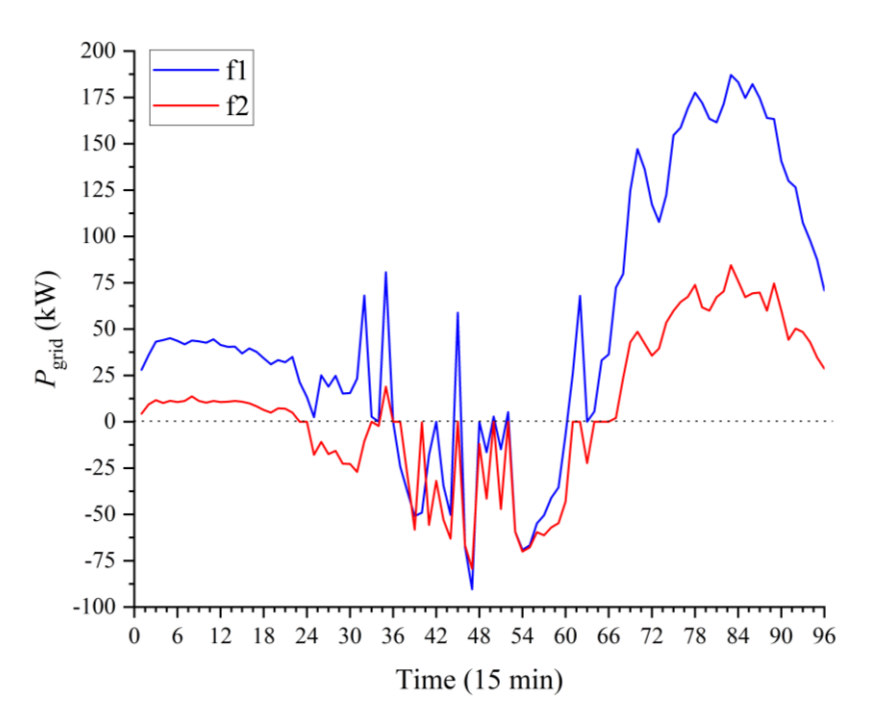


Figure 17 Community EC3: net power exchanges with provider f1 and with provider f2 (positive sign indicates power consumed, negative produced).

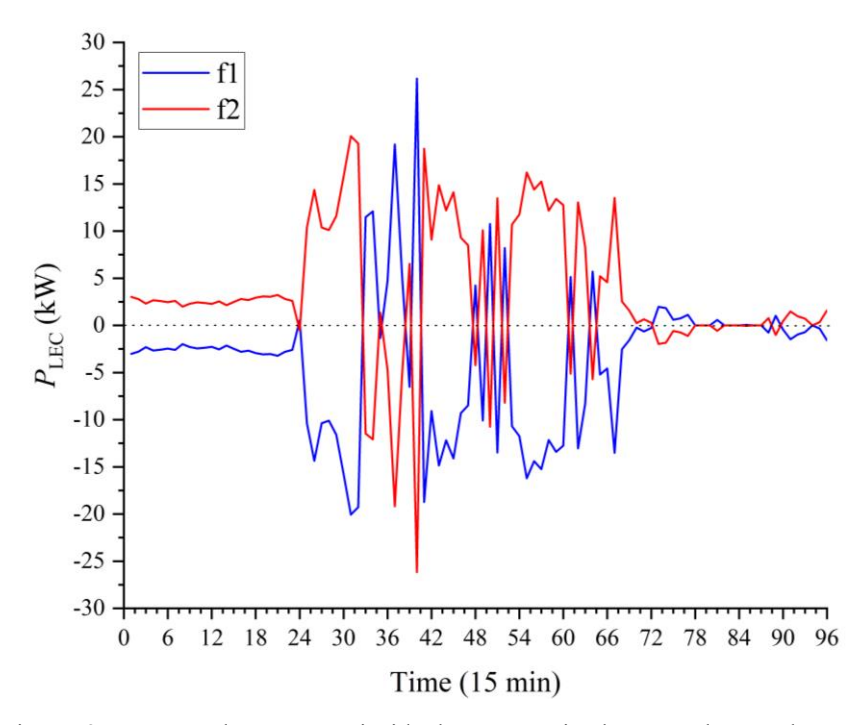


Figure 18 Community EC3: power exchanges P_{LEC} inside the community, between the members with provider f1 and those with provider f2 (positive sign indicates power imported, negative exported).

Similar results are obtained for the other communities EC1 and EC2.

3.1.8.2. Communities of neighboring users

Figure 19 shows a different composition of the three communities, obtained by grouping neighboring users in the same community so that the obtained values of daily demand, PV generation and installed BES percentages, shown in Table 5, are similar to those of Table 2. The noEC group is the same as in the base case.

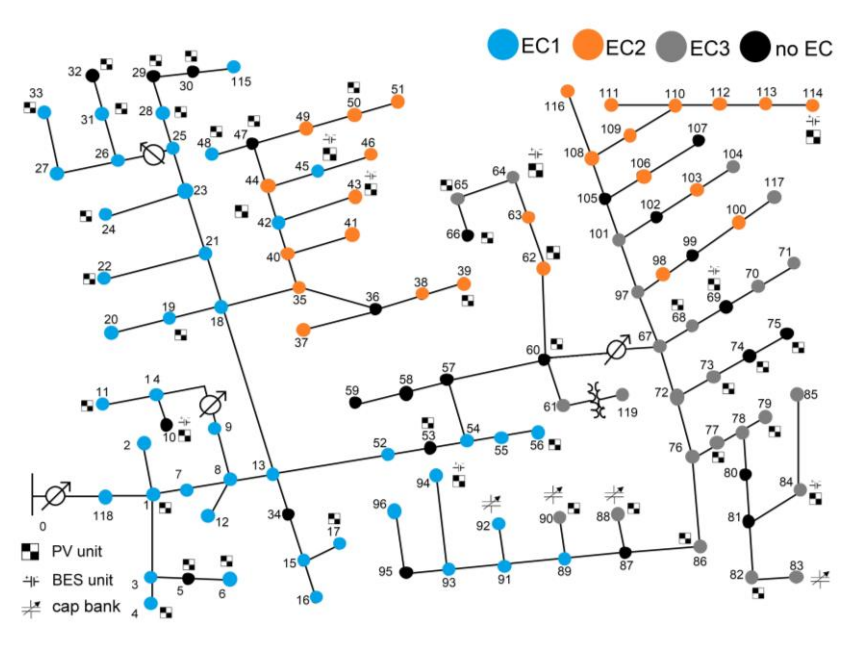


Figure 19 Communities formed by neighboring members.

The daily electricity provision costs in € of community EC1, EC2, and EC3 are 609, 833, 574, respectively, corresponding to variations of 6%, 2.4%, -4% of the base case results. These variations are attributed to differences in the specific characteristics of users belonging to communities rather than to their proximity.

Table 5 Forecasted daily demand, PV generation as percentage of the load, total storage in percentage of PV generation, for each community of neighboring users.

Group	Demand (MWh)	PV generation (%)	Installed BES (%)
EC1	3.76	67.2	0.51
EC2	2.79	28.7	1.12
EV3	3.52	63.4	0.27

3.1.8.3. Different number of communities

The calculation is repeated for different number of communities (from 1 to 18). Each user is randomly associated with a specific community or excluded from the communities, considering a uniform probability. Figure 20 shows the values of the sum of procurement costs (including both providers f1 and f2) for all the communities and the values of the procurement costs of the users outside the communities. Figure 21 shows the average costs per user in the communities allowing exchanges P_{LEC} , in the same communities with P_{LEC} forbidden, and in the noEC group.

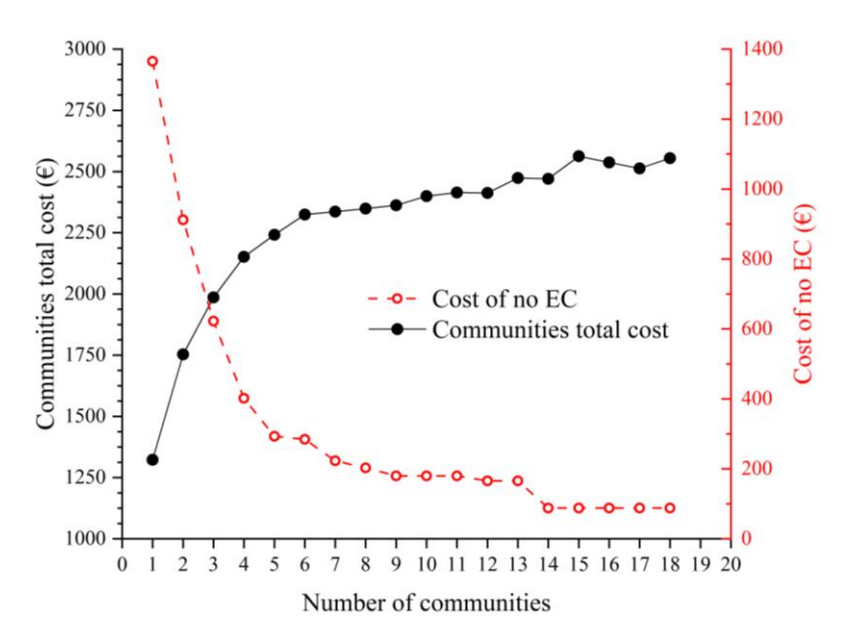


Figure 20 Total daily procurement costs of the communities and of the users in the noEC group, for different number of communities.

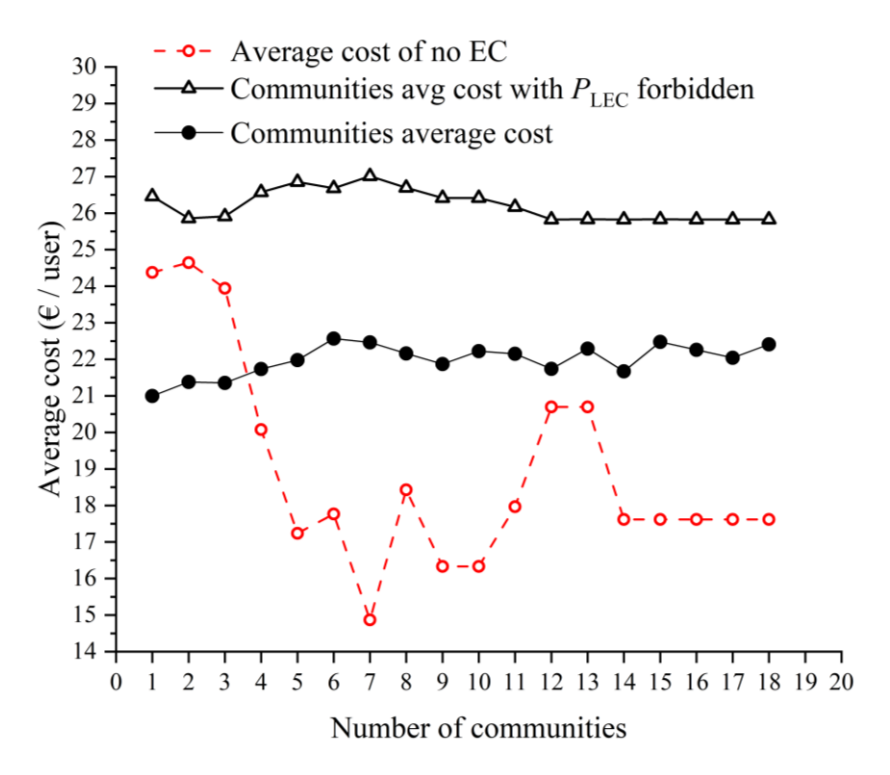


Figure 21 Average daily costs per user in the communities, in the same communities with P_{LEC} forbidden, and in the noEC group, for different number of communities.

By increasing the number of communities, due to the uniform allocation criteria, the number of users not associated to any community decreases. Therefore, the costs of the noEC group tend to decrease, while the total cost of the communities increases. Moreover, when the number of communities

increases, each community becomes smaller. In small communities the procurement costs increase, as it is small the number of users free to transact with other participants. This is confirmed by Figure 21, which shows that the larger the number the communities the lower the advantage of the participation in the community (i.e., the lower the difference between the two black curves).

3.1.8.4. Increase of the PV generation and of the BES units

Figure 22 and Figure 23 show the reduction of the daily energy procurement costs due to the uniform increase of the PV units and of the BES units, multiplying the base case values by coefficients k_{PV} and k_{BES} , respectively. Figure 23 also shows the costs for the case without storage units ($k_{BES} = 0$).

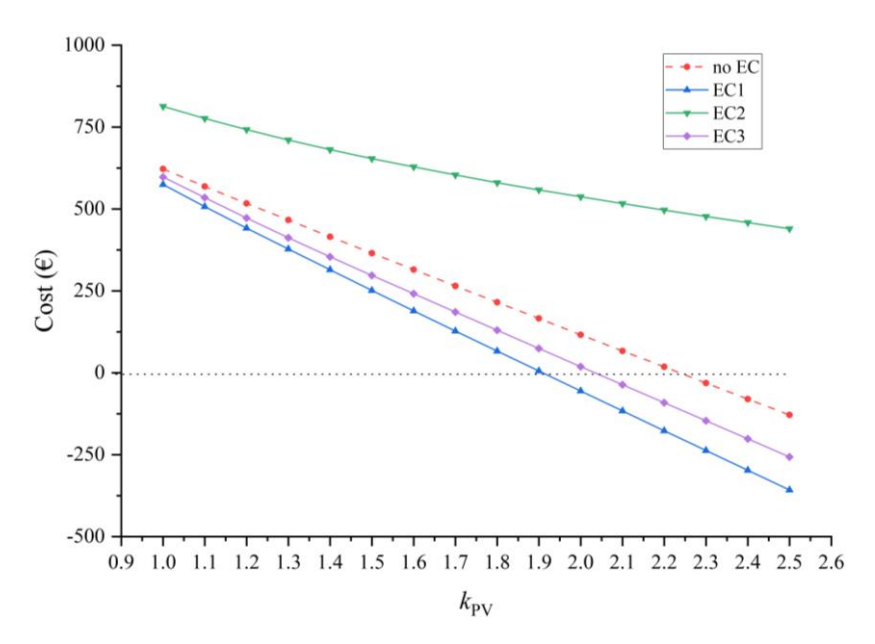


Figure 22 Total procurement costs of all the users in the network, procurement costs of the users in the noEC group and of EC1, EC2 and EC3.

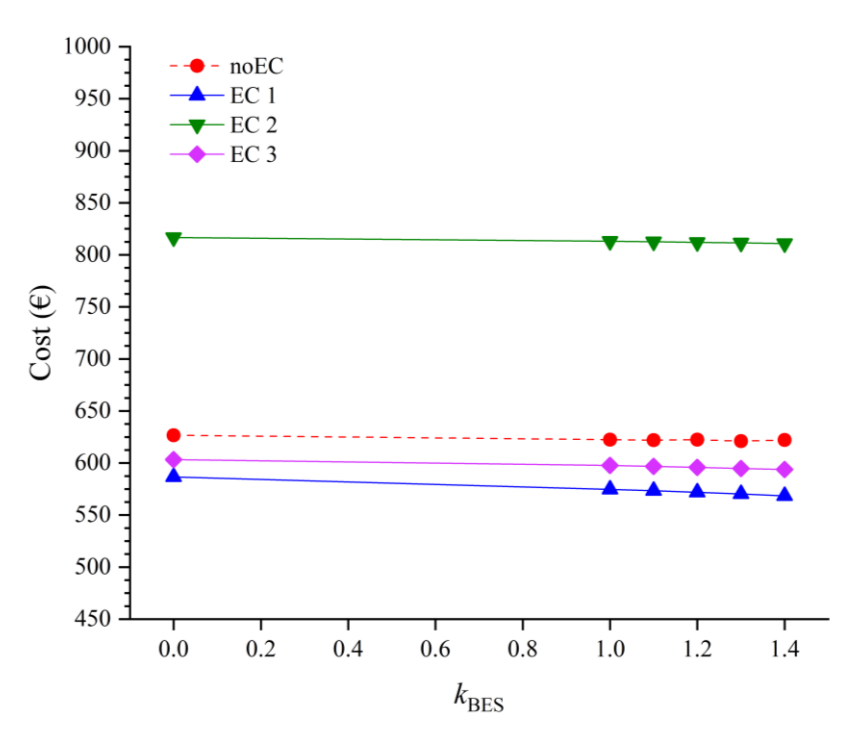


Figure 23 Procurement costs of EC1, EC2, and EC3 and of the users in the noEC group for different sizes of the BES units.

3.2. Distributed Optimization and Application of the Model to a Real Distribution Network

3.2.1. Introduction

The development of Energy Communities (ECs) of prosumers, facilitated by the evolving regulatory framework, e.g., in Europe [38], is expected to further promote the integration of renewable energy sources and the installation of energy storage systems in distribution networks [39]. There is a growing literature on modeling of energy communities and optimal scheduling of the exchanges among their members, taking explicitly into account the limits due to the technical characteristics of the power distribution network. Local market structures are described, for example, in [40], [41] and references therein. Specifically, the model proposed in [40] takes into account the network constraints by including three factors in the market mechanism: voltage sensitivity coefficients, power transfer distribution factors, loss sensitivity factors. In [42], the proposed peer-to-peer (P2P) platform is based on the use of locational marginal prices to calculate network usage charges. In [43] an approach is proposed consisting of three layers: the market layer sending price signals to the EC controller layer, the controller layer for managing the energy flow, and the grid layer for studying the impact on the distribution grid. A Stackelberg-game framework is adopted in [44] to set prices by the distribution system operator (DSO). The focus is the optimal operation of distribution networks that incorporate ECs, by adopting a bi-level optimization scheme. The pricing scheme proposed in [45] addresses the challenges of energy trading in a local electricity market through a decision-making process that includes look-ahead energy storage scheduling. The hosting capacity of a distribution network in presence of ECs is analyzed in [41] by using Monte Carlo simulations for the entire year in order to represent different EC configurations and the effects on energy losses, bus voltage deviations, and thermal loading of branches. The impact on the medium voltage (MV) network is reduced when the EC is operated to minimize the power exchange between the EC and the external grid for each individual time stamp. Compared to earlier studies, this chapter focuses on the analysis of the presence of multiple ECs, with members served by different electricity retailers, in the MV power distribution network. The analysis is carried out by a specifically developed procedure that provides the daily optimization of the communities that consider direct transactions of both active and reactive power between their members and helps in solving network congestions. On the modeling aspects of multiple ECs sharing the same medium voltage (MV) distribution network. Consumption profiles with 15-min resolution for several days in both winter and summer are used to optimize transactions within each energy community. Each user is a member of one of the communities or can remain outside of all communities.

In this approach, each community minimizes its energy procurement costs through a day-ahead scheduling of internal transactions among its members and available energy resources, including battery energy storage (BES) systems. Members of the same community may be served by different electricity retailers. Each retailer has different contract terms. Internal transactions are priced using the shadow prices of the balancing constraints between the power provided by the electricity retailer and the power received by other community members. Preliminary results using the IEEE 123-bus feeder test system and a centralized optimization approach have been presented in [46]. This paper extends the model by representing the use of reactive energy exchanges among members of each EC to limit the penalties due to minimum power factor (PF) operations and by adopting an iterative distributed optimization procedure based on the augmented Lagrangian method [47] to take into account violations of network constraints. Specifically, the objective function of the optimization of each EC is augmented by the penalization coefficients updated at each iteration to minimize the violations of both bus voltage and branch current limits, using a typical sensitivity estimation [48]. The chapter presents the results for different numbers and configurations of communities, price profiles of electricity retailers, and network operating constraints. The chapter also shows the computational feasibility of the proposed approach.

3.2.2. Day-ahead Distributed Optimization Procedure

The procedure focuses on the day-ahead optimization for the next 24 hours, divided into 96 periods of 15 minutes each. The optimization independently performed for each community and the set of users outside the communities, called noEC, with the goal of minimizing the corresponding energy supply costs. In addition, there is an optimization problem for the DSO, which takes into account the

network constraints and minimizes the violations of the limits of the branch currents and the bus voltages. The procedure is iterative and stops when the violations of the network constraints in the DSO problem are less than a predefined tolerance or when there are no more improvements to the solution, as illustrated in Figure 24.

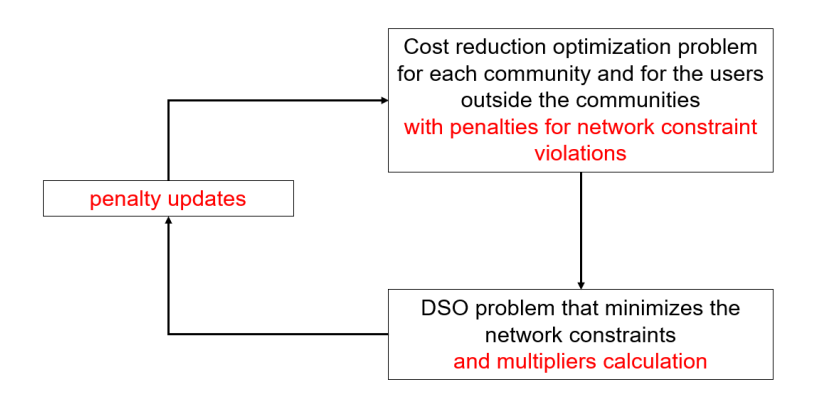


Figure 24 The procedure stops when the violations of the network constraints in the DSO problem are less than a predefined tolerance or when there are no more improvements to the solution.

The next two subsections describe in detail the models implemented for the communities, the noEC set of users, and the DSO problem.

3.2.3. Individual and Collective User Optimization Model

The model is a mixed-integer linear programming problem. To obtain the day-ahead scheduling of the available energy resources and of the transactions between the members of the same community, the following objective function is minimized:

$$OF^{c} = \sum_{t \in T} \left\{ \sum_{i \in \Omega_{c}} \left(C_{\text{fossil}i,t} + C_{\text{grid}i,t} + \mu_{\text{PF}} Q_{\text{PF}i,t} \right) \Delta t + \sum_{k=1}^{N} \left[\left(\lambda_{k,t}^{\text{uP}} + \lambda_{k,t}^{\text{vP}} \right) P_{k,t}^{c} + \left(\lambda_{k,t}^{\text{uQ}} + \lambda_{k,t}^{\text{vQ}} \right) Q_{k,t}^{c} \right] \right\}$$
(3.20)

which includes the operating costs, the penalization for the low PF operation and the additional terms useful to limit the network constraint violations. Multipliers λ are provided by the DSO model at each iteration. The noncompliance amount $Q_{\text{PF}i,t}$ is the excess reactive power with respect pf_{\min} . The value of μ_{PF} is assumed to be known, i.e. set by the regulator or utility.

 $C_{\text{grid}i,t}$ is constrained by equation (3.21)

where $P_{\text{grid}i,t}$ is positive when bought and negative otherwise. Contributions $P_{k,t}^c$ and $Q_{k,t}^c$ to the power at node k of the network are:

$$P_{k,t}^{c} = \sum_{i \in \Omega_{c}^{k}} P_{\text{user}i,t} \quad Q_{k,t}^{c} = \sum_{i \in \Omega_{c}^{k}} Q_{\text{user}i,t}$$

$$(3.21)$$

Following the approach presented in [46], the total net consumption (positive) or production (negative) of user i should balance the sum of the exchanges with the retailer and with the other members of the same community c as shown in equation (3.19).

Constraint (3.19) is associated with the condition that the sign of $P_{\text{useri,t}}$ $P_{\text{gridi,t}}$ and $P_{\text{LECi,t}}$ is the same (dealt with the inclusion of binary variables associated with the sign of $P_{\text{useri,t}}$). The prices of the P_{LEC} transactions between the community members are calculated as the shadow prices of constraint (3.19)

As $Q_{\text{grid }i,t}$ is typically constrained to be nonnegative:

$$Q_{\text{useri,t}} = \begin{cases} Q_{\text{gridi,t}} + Q_{\text{LEC}i,t} & \text{if } Q_{\text{useri,t}} \ge 0, \\ Q_{\text{LEC}i,t} & \text{if } Q_{\text{useri,t}} < 0 \end{cases}$$
(3.22)

The condition on the sign of $Q_{\mathrm{user}i,t}$ (positive if consumed) is dealt with through specific binary variables. For the users of set noEC, the only difference with respect to the community model is that the exchange between users is prohibited, i.e. $P_{\mathrm{LEC}i,t}=0$ and $Q_{\mathrm{LEC}i,t}=0$ if i in noEC. The exchange between the members of each community Ω_k is balanced and the reactive power exchange is limited to the members of the community that are served by the same HV/MV transformer:

$$\sum_{i \in \Omega_c} P_{\text{LEC}i,t} = 0 \sum_{i \in \Theta_k} Q_{\text{LEC}i,t} = 0$$
(3.23)

The net power for each user is given by:

$$P_{\text{useri,t}} = P_{\text{L}i,t} - P_{\text{Gi,t}} - P_{\text{BESi,t}} + \ell_{\text{BESi,t}}$$

$$Q_{\text{useri,t}} = Q_{\text{L}i,t} - Q_{\text{Gi,t}} - Q_{\text{BESi,t}} - Q_{\text{Ci,t}}$$
(3.24)

 Q_G , $Q_{\rm BES}$ are limited by the minimum PF of the local generator and the BES. $Q_{\rm C}$ is fixed or limited by the maximum power of the switchable capacitor bank (discrete switching is not represented for simplicity). $P_{\rm BES}$ is positive when the battery is discharged and is constrained by the maximum power limit of the battery system.

BES power losses $\ell_{\text{BESi,t}}$ are:

$$\ell_{\text{BESi,t}} = \begin{cases} (1 - \eta_{\text{dischargei}}) P_{\text{BESi,t}} & \text{if } P_{\text{BESi,t}} \ge 0\\ (1 - 1/\eta_{\text{chargei}}) P_{\text{BESi,t}} & \text{if } P_{\text{BESi,t}} < 0 \end{cases}$$
(3.25)

where the condition on the sign of $P_{\text{BES}i,t}$ is treated with a specific binary variable. The model of the BES unit is given by:

$$E_{i,t} = E_{i,t-1} - P_{\text{BESi},t} \Delta t \text{ for } 1 < t < 96$$

 $E_{i,1} = E_{\text{maxi}} - P_{\text{BESi},1} \Delta t \text{ and } E_{i,96} = E_{\text{maxi}}$ (3.26)

By defining $\hat{Q}_{i,t} = Q_{Gi,t} + Q_{Ci,t} + Q_{BESi,t} + Q_{LECi,t}$, if the operating condition is not satisfying pf_{min} , a penalty is applied in (3.20) ,proportional to the amount of reactive power excess, denoted as $Q_{PFi,t}$:

$$Q_{\text{PF}i,t} \ge \begin{cases} \operatorname{sgn}(P_{\text{useri,t}}) \left(Q_{\text{lim1}i,t} - \hat{Q}_{i,t} \right) \\ \operatorname{sgn}(P_{\text{useri,t}}) \left(\hat{Q}_{i,t} - Q_{\text{lim2}i,t} \right) \end{cases}$$
(3.27)

Where:

$$Q_{\lim l_{i,t}} = Q_{L_{i,t}} - \tan\left(\arccos p f_{\min}\right) P_{\text{user}_{i,t}}$$

$$Q_{\lim 2i,t} = Q_{L_{i,t}} + \tan\left(\arccos p f_{\min}\right) P_{\text{user}_{i,t}}$$
(3.28)

3.2.4. Linearized DSO Model

The DSO problem minimizes the violations of the network constraints in both bus voltages and branch currents. The configuration of the MV network is radial, so excluding the slack bus, which is the substation HV bus, the number of nodes is equal to the number of buses. A common index k is used to denote both a branch and the corresponding end. The model of the network represents each branch with a balanced T-model, composed of two impedances (called in and out) each equal to half the longitudinal impedance of the branch and a shunt admittance in the middle Figure 25.

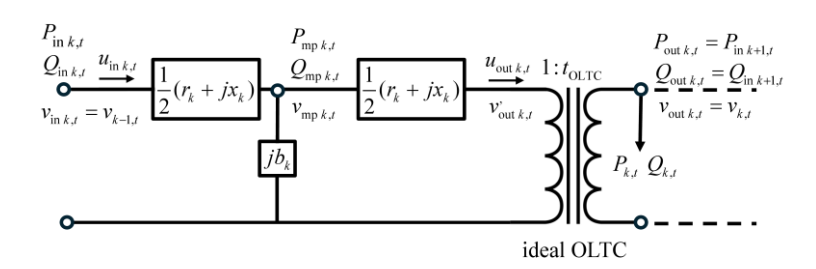


Figure 25 Generic T-model equivalent circuit

The model adopts the DistFlow approach [33], which uses the square rms values of the input and output currents $u_{ink,t}$ and $u_{outk,t}$, respectively, and the square rms values of the bus voltages, $v_{k,t}$. The nonnegative violations are:

$$\Delta u_{\text{ink,t}} \ge u_{\text{ink,t}} - I_{\text{max}k}^{2}, \ \Delta u_{\text{outk,t}} \ge u_{\text{outk,t}} - I_{\text{max}k}^{2}$$

$$\Delta v_{\text{mink,t}} \ge V_{\text{mink}}^{2} - v_{k,t}, \ \Delta v_{\text{max}k,t} \ge v_{k,t} - V_{\text{max}k}^{2}$$
(3.29)

By defining $\Delta u_t = \sum_{k=1}^{N} (\Delta u_{\text{ink,t}} + \Delta u_{\text{outk,t}})$ and $\Delta v_t = \sum_{k=1}^{N} (\Delta v_{\text{mink,t}} + \Delta v_{\text{maxk,t}})$, the DSO problem minimizes the summation of the violations:

$$OF^{DSO} = \sum_{t \in T} (\Delta u_t + M \, \Delta v_t)$$
(3.30)

where M differentiates the maximum branch current violations from the bus voltage violations. The application of the balanced DistFlow linearization presented in [49] to the T-model equations described in [50] yields, for each branch k, the relationships that relate the square rms values of the voltages with the power flows are:

$$v_{\text{mpk,t}} = v_{\text{ink,t}} - r_k P_{\text{ink,t}} - x_i Q_{\text{ink,t}} + \frac{1}{4} (r_k^2 + x_k^2) u_{\text{ink,t}}$$

$$v_{\text{ink,t}} - v'_{\text{outk,t}} = 2r_k P_{\text{ink,t}} + 2x_k Q_{\text{ink,t}} + x_k b_k v_{\text{mpk,t}} - \frac{3}{4} (r_k^2 + x_k^2) u_{\text{ink,t}} - \frac{1}{4} (r_k^2 + x_k^2) u_{\text{outk,t}}$$
(3.31)

where

$$P_{\text{ink,t}} = P_{\text{outk,t}} + P_{\text{userk,t}} + \frac{1}{2} r_k u_{\text{ink,t}} + \frac{1}{2} r_k u_{\text{outk,t}},$$

$$Q_{\text{ink,t}} = Q_{\text{outk,t}} + Q_{\text{userk,t}} - b_k v_{\text{mpk,t}} + \frac{1}{2} x_k u_{\text{ink,t}} + \frac{1}{2} x_k u_{\text{outk,t}}$$
(3.32)

The linear representation of the branch currents is:

$$u_{\text{in}k,t} = 2P_{\text{ini}k,t}^{0} P_{\text{ini},t} + 2Q_{\text{ini}k,t}^{0} Q_{\text{ini}k,t} - \left[(P_{\text{ini}k,t}^{0})^{2} + (Q_{\text{ini}k,t}^{0})^{2} \right]$$

$$u_{\text{out}k,t} = 2P_{\text{mp}k,t}^{0} P_{\text{mp}i,t} + 2Q_{\text{mp}k,t}^{0} Q_{\text{mp}k,t} - \left[(P_{\text{mp}k,t}^{0})^{2} + (Q_{\text{mp}k,t}^{0})^{2} \right]$$
(3.33)

that uses the power flow estimate marked with superscript 0, calculated by building the set of all buses that each branch feeds and then by adding the corresponding bus power, assuming bus voltages equal to 1 pu, as well as neglecting the control of on-load tap changers (OLTC), batteries, capacitor banks, and dispatchable generators. The substation transformers have $v_{\text{ink,t}} = V_0^2$, assumed to be

known and constant throughout the day. They are OLTC equipped with a tap ratio in the range $[t_{\min}, t_{\max}]$, continuous for simplicity, so that:

$$v_{\text{outk,t}} \le t_{\text{min}}^2 v_{\text{outk,t}}' \quad \text{and} \quad v_{\text{outk,t}} \ge t_{\text{min}}^2 v_{\text{outk,t}}'$$
 (3.34)

For all the branches that do not represent an OLTC transformer $v_{\text{outk,t}} = v'_{\text{outk,t}}$. Generalizing to the case of multiple branches originating and terminating on the same bus, the node equilibrium constraints are:

$$v_{\text{out}k \in \Omega_{j}^{\text{out}}, t} = v_{\text{in}k \in \Omega_{j}^{\text{in}}, t} = v_{k,t}$$

$$\sum_{k \in \Omega_{j}^{\text{out}}} P_{\text{out}k, t} = \sum_{k \in \Omega_{j}^{\text{in}}} P_{\text{in}k, t}$$

$$\sum_{k \in \Omega_{j}^{\text{out}}} Q_{\text{out}k, t} = \sum_{k \in \Omega_{j}^{\text{in}}} Q_{\text{in}k, t}$$
(3.35)

The values of the power at each bus are given by the solution of the optimization problem for each community and the users outside the community, as defined (3.21). The summation gives the total power at each bus of the network:

$$P_{k,t} = \sum_{c} P_{k,t}^{c} : \mu_{k,t}^{P} \quad | \quad Q_{k,t} = \sum_{c} Q_{k,t}^{c} : \mu_{k,t}^{Q}$$
(3.36)

These constraints are associated with the shadow prices that are used to update the multipliers of (3.20) as described below.

3.2.5. Multiplier Update

In each iteration, at first the models of the communities and the noEC users are solved, then the DSO model is solved. Finally, the λ multipliers of the previous iteration, indicated by an upper bar, are updated based on the values of the shadow prices from (3.36) and the violations from (3.29):

$$\lambda_{k,t}^{\mathrm{uP}} = \overline{\lambda}_{k,t}^{\mathrm{uP}} + \hat{\mu}_{k,t}^{\mathrm{uP}} \Delta u_t \quad \lambda_{k,t}^{\mathrm{vP}} = \overline{\lambda}_{k,t}^{\mathrm{vP}} + \hat{\mu}_{k,t}^{\mathrm{vP}} \Delta v_t$$
(3.37)

and analogously for $\lambda_{k,t}^{\mathrm{uQ}}$,and $\lambda_{k,t}^{\mathrm{vQ}}$.

The shadow prices relevant to current and voltage violations are distinguished in $\mu_{k,t}^{uP}$, $\mu_{k,t}^{uQ}$ and $\mu_{k,t}^{vP}$, $\mu_{k,t}^{uQ}$ respectively, by comparison with a threshold value set according to the M value introduced in (3.30). These values are also normalized (indicated by the hat) with respect to the norm of the corresponding prices for all branches and buses.

3.2.6. Case study and test results

A. Feeders and user characteristics

The case study includes 5 real MV feeders (here referred to as A to E) connected to a 132/15 kV substation, located in Modena, Italy Figure 26. The substation is equipped with a 50 MVA transformer (T1) and two 25 MVA transformers (T2 and T3), all with OLTCs. The system includes 134 buses and branches: 4 in feeder A connected to transformer T2, 27 in feeder B connected to transformer T1, 22 in feeder C connected to transformer T1, 26 in feeder D connected to transformer T1, and 55 in feeder E connected to transformer T3.

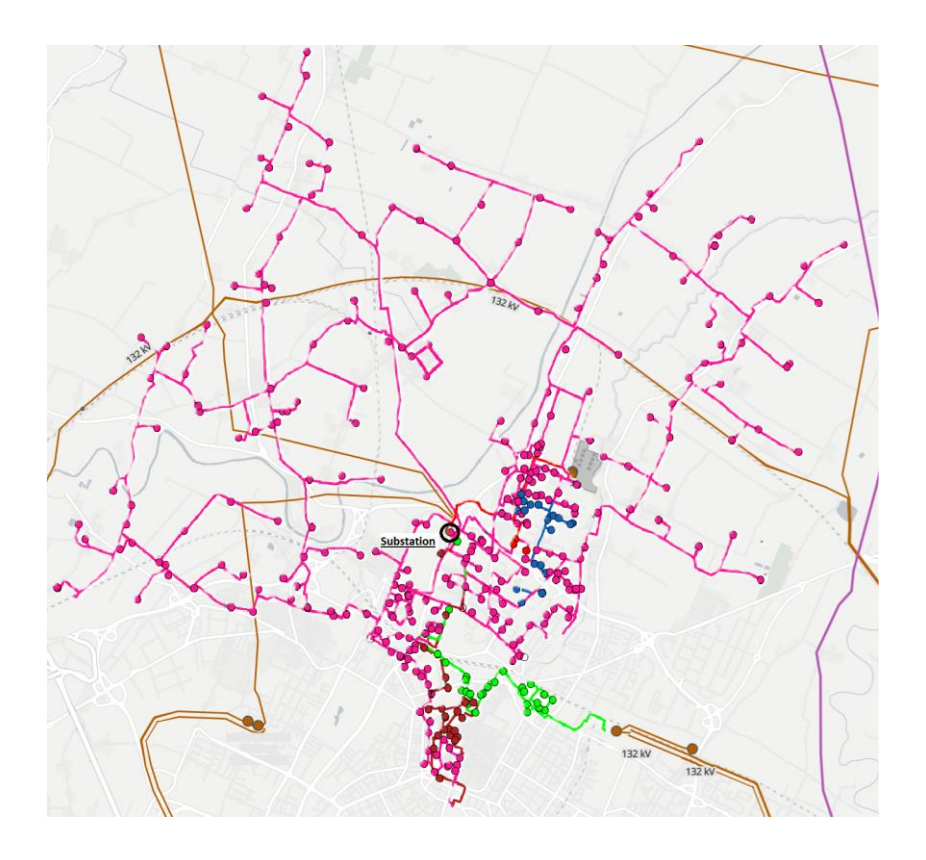


Figure 26 Layout of the real MV test network. The HV/MV substation is indicated by a circle and, the five feeders considered are distinguished by different colors.

Three electricity retailers (Pr1, Pr2, and Pr3) with different price profiles are considered: one (with minimum and maximum values equal to $0.093 \in \text{KWh}$ and $0.33 \in \text{KWh}$, respectively) follows the typical wholesale market price behavior with two peaks in the morning (9-11 am) and in the evening (6-9 pm), the second profile (with the same maximum and minimum values) has a low price during the night and a higher price during the day, the third is a 10% discount with respect to the second one. The π_{sell} profiles follow similar patterns, but with values halved.

For illustrative purposes, μ_{PF} is assumed to be equal to $5 \in \text{kvarh}$. The requested pf_{min} value is assumed to be 0.9. The bus voltage values are constrained to be within the interval 0.9 pu - 1.1 pu.

The load and generation profiles are obtained from the DSO records at each 15-minute interval, separately for each MV node, for three days in January and in July 2023. The weather data are summarized in Table 6 [51].

Table 6 weather data

		Winter			Summer	
Property	17	18	19	18	19	20
Cloud Coverage (%)	88.1	84.1	85.5	11	25.2	34.1
Solar Radiation (W/m²)	8	40	13	296	264	303
Temperature (°C)	4.1	3.8	2.6	30.2	30.2	27.4
Wind Speed (km/h)	37.1	13.2	17.1	14.8	18.4	20.5
Precipitations (mm)	3.1	0.2	3.2	0	0	2.6

The data of daily load consumption, PV generation and the generation from synchronous machines are summarized in Table 7. The voltage dependence of the loads is neglected. The users have batteries with a total capacity of 675 kWh.

Table 7 Energy Consumption and Generation Data

Property		Winter		Su	mmer (Ju	ıly)
Troperty	17	18	19	18	19	20
Load Consumption (MWh)	267.9	277.6	269.1	327.8	333.0	320.5
PV Generation (MWh)	5.8	6.2	6.0	11.0	10.6	11.0
in % wrt to Consumption	2.16	2.23	2.22	3.35	3.18	3.43
Sync. Generation (MWh)	11.4	11.4	10.6	11.5	11.5	11.5

Each user is randomly assigned to one of the three retailers. Similarly, users are randomly grouped, with equal probability, into three communities (EC1, EC2, EC3), or are not included in any community (noEC set). For the sake of simplicity, all the users connected to the same MV node are considered to be aggregated, and thus to belong to the same community or to the noEC set. Table 8 shows the allocation of the total energy demand during the three days, the corresponding PV generation, and the total installed storage capacity.

The test case data is available in an Excel file at: [52] https://www.doi.org/10.17632/8vzjxbxnnh\

The next subsection presents the results for the three-community configuration described above, referred to as the base case. Then, the results are compared with the cases where $Q_{\rm LEC}$ and also $P_{\rm LEC}$ transactions are forbidden, and with cases characterized by different numbers of communities. All the

results are obtained by implementing the optimization procedure in AIMMS with the Gurobi solver. The total computational time for each case is less than 2 minutes (CPU: Intel core i7, 12700H 5.2Ghz, RAM: 32GB).

Table 8 Allocation of the demand, PV generation, and battery storage as percentage of the total three-day values for the communities and the NoEC set

Group	Dema	and (%)	Genera	tion (%)	Installed BES (%)
Group	Winter	Summer	Winter	Summer	Instance DES (70)
EC1	26.3	27.2	37.2	33.6	14.8
EC2	15.5	14.1	5.4	14.2	44.4
EC3	25.3	27.0	17.2	11.5	14.8
noEC	32.9	31.7	40.2	40.7	26.0

B. Base Case Solution

Table 9 shows the cost of the energy provided by the retailers (P_{grid} cost) and the cost due to the internal transactions P_{LEC} (negative values indicate revenues) for the three days in winter and summer for the three communities EC and the three retailers P_{r} .

Table 9 Base case: energy costs in thousands of euros for each community considering the three different retailers on winter (W) and summer (S) days

		E	EC1		EC2		EC3	
Pr/EC	Cost	W	S	W	S	W	S	
Pr1	$P_{ m grid}$	26.56	31.83	17.62	17.10	30.27	29.63	
111	$P_{ m LEC}$	-1.77	0.16	-0.94	-1.12	-1.72	-0.67	
Pr2	P_{grid}	22.93	29.72	10.19	8.21	48.72	71.19	
112	$P_{ m LEC}$	2.83	-0.12	1.05	2.02	1.79	0.67	
Pr3	$P_{ m grid}$	37.98	43.99	26.97	28.46	11.50	13.82	
113	$P_{ m LEC}$	-1.07	-0.04	-0.11	-0.90	-0.06	0	

Table 10 shows the percentage cost reductions in the base case with respect to the case where both $P_{\rm LEC}$ and $Q_{\rm LEC}$ are prohibited and to the case where only $Q_{\rm LEC}$ transactions are prohibited. The energy costs include both the costs/revenues related to the exchanges with the retailers ($P_{\rm grid}$) and those related to the exchanges with other community participants ($P_{\rm LEC}$). The table shows that there are more reductions on winter days than in summer days. In summer, EC2 members also benefit from

community participation due to the presence of larger battery storage. Often, users having contracts with Pr1 and Pr2 benefit more from community participation than those with contracts with Pr3, which is the cheapest retailer. The difference between the results obtained in the reference case and those where only $Q_{\rm LEC}$ transactions are prohibited is very small, since the energy costs depend on the active power exchanges.

Table 10 Base case energy cost reductions in % with respect to the case where $P_{\rm LEC}$ and $Q_{\rm LEC}$ or only $Q_{\rm LEC}$ exchanges are forbidden

D/E/C	Forbidden	E	C1	E	C 2	EC	C 3
Pr/EC	rorbiaden	W	S	W	S	W	S
	$P_{ m LEC}$ / $Q_{ m LEC}$	5.09	0	2.62	5.22	4.28	1.15
Pr1	$Q_{ m LEC}$	0	0	0.01	0.05	-0.02	0.22
	$P_{ m LEC}$ / $Q_{ m LEC}$	3.34	2.97	0.01	0.04	0	0
Pr2	$Q_{ m LEC}$	0	0	0	-0.13	0	0
	$P_{ m LEC}$ / $Q_{ m LEC}$	1.43	-0.02	0.22	1.24	0.3	0
Pr3	$Q_{ m LEC}$	0.04	-0.09	0	0.02	0	0

Table 11 shows the costs due to minimum PF noncompliance. They are mainly on summer days. The availability of $Q_{\rm LEC}$ transactions is very effective in reducing these costs, as shown by comparing the base case results with those cases where these transactions are forbidden.

Table 11 Noncompliance costs (in euro) in the base case and when $P_{\rm LEC}$ and $Q_{\rm LEC}$ exchanges are forbidden

]	EC1	E	C 2		EC3
	W	S	W	S	W	S
Base case	0	12009.2	0.1	0	0	187.5
w/o $Q_{\scriptscriptstyle LEC}$	13.6	33886.7	9.9	5334.8	11.2	15761.6
w/o P_{LEC} / Q_{LEC}	19.5	33886.7	9.9	5334.8	11.2	15761.6

The goal of reducing the high noncompliance costs may also affect the $P_{\rm LEC}$ transactions. In general, this justifies the reduced benefit on summer days, when the $P_{\rm LEC}$ transactions are limited to reduce noncompliance costs. This also justifies the small negative values in Table 10. If $Q_{\rm LEC}$ are forbidden, then the noncompliance cost is high. If $P_{\rm LEC}$ transactions are allowed, the optimization also uses $P_{\rm LEC}$ transactions to reduce the noncompliance cost, and the energy cost may increase slightly compared to the case where transactions are not allowed.

The energy cost values (in thousands of euros) for the users in the noEC group are: in winter days, 19.26, 37.73, 59.15, for the users with contracts with Pr1, Pr2, and Pr3, respectively (total energy cost

116.13); in summer days, 21.54, 40.45, 69.52, for the users with contracts with Pr1, Pr2, and Pr3, respectively (total energy cost 131.52).

For the noEC group, in winter days, the noncompliance cost is $125.1 \in$; in summer days, it is $6110.1 \in$.

C. Different Number of Communities

For different numbers of communities, Figure 27 shows the percentage difference in energy procurement and noncompliance costs for users who belong to a community (i.e., those who do not belong to the noEC set in the base case) with respect to the case where $P_{\rm LEC}$ and $Q_{\rm LEC}$ transactions are prohibited. The graphs refer to the three-day costs and penalties, in winter and summer. Without $P_{\rm LEC}$ and $Q_{\rm LEC}$ transactions, the energy procurement and noncompliance costs (in thousands of euros) are 237.3 and 0.034 for winter days, and 276.3 and 55.0 for summer days, respectively.

The figure shows that as the number of communities increase, the percentage reductions decrease, meaning that both costs and penalties approach the values of the case without $P_{\rm LEC}$ and $Q_{\rm LEC}$ transactions.

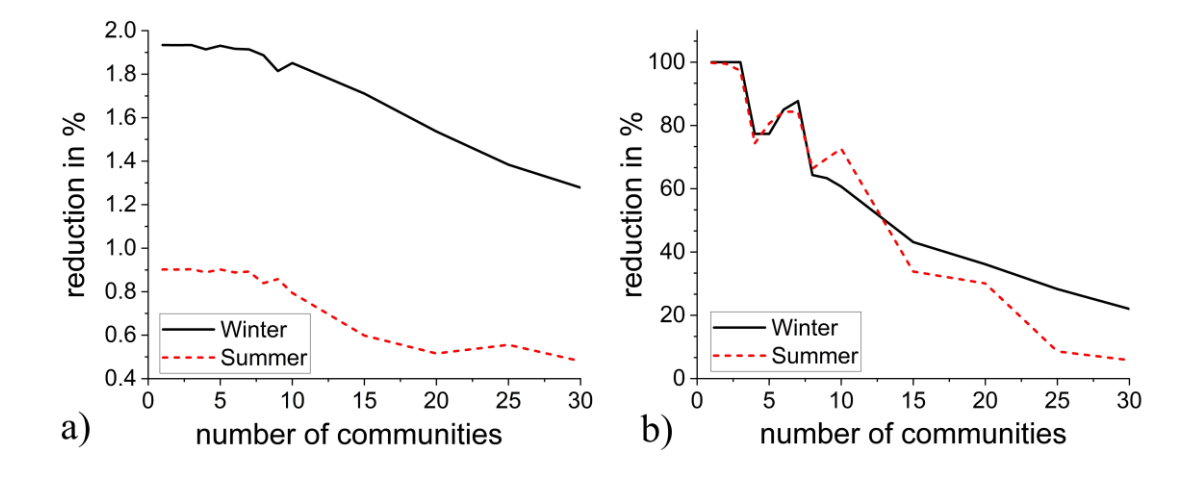


Figure 27 Percentage reduction of a) energy procurement cost and b) noncompliance penalties, varying the number of communities, with respect to the case in which P_{LEC} and Q_{LEC} transactions are forbidden.

3.3. Conclusion

Chapter 3 presents a day-ahead scheduling procedure for the case of multiple energy communities in the grid. Each user is free to join a community or not. Moreover, each user can choose a different energy provider.

The results obtained for the IEEE 123-bus test feeder show that each community reduces its procurement costs with respect to the case in which direct transactions are not allowed. Assuming the

presence of 2 providers characterized by different price profiles, the procedure correctly prefers to allocate the internal production to the consumers with higher tariff when the community globally imports power and prefers to use internally the generation of the producers with lower selling tariff when the community globally exports power.

The procedure defines the prices of the transactions among the users of the same community by using the shadow prices of the relevant balancing constraints. The increase of the number of communities results in the increase of the procurement costs also due to the reduction of the members with which each participant can transact. The procedure can also be used to analyze the effects of further installation of production and storage units. The calculation effort is reasonably limited.

The second part of chapter 3 presents a framework for analyzing the effects of multiple energy communities in the same distribution network, while preserving the user's free decision to join or not to join and its autonomous choice of electricity retailer. The presented day-ahead optimization procedure takes into account the network constraints and provides the prices of the internal transactions as the shadow prices of the power balancing constraints for each user. In addition, the procedure also allows reactive power exchanges between members of the same community other than active power. These reactive power transactions are performed to reduce the costs for low PF operation. The procedure is applied to a real MV distribution network, considering the consumption and generation profiles of three days in winter and summer. The results show the effectiveness in reducing both energy procurement costs and noncompliance costs for each community. The sensitivity analysis on the number of ECs shows that as the number of ECs increases, cost reductions and penalties decrease, approaching the case without internal transactions within ECs.

The scheme also appears to be suitable for investigating the provision of flexibility services to the DSO, e.g., for congestion management in the network, as well as the interaction between ECs and transmission network, the effects of the presence ECs on the energy market behavior, and the socioeconomic implications for different stakeholders. These aspects are not covered in this chapter as they deserve further investigation.

Chapter 4. Reactive power services from communities

4.1. Introduction

This chapter focuses presents a procedure for the optimal operation of a community of prosumers connected to a medium voltage distribution network equipped with generation and storage units that considers the penalization for low power factor operation, the exploitation of direct exchanges of both active and reactive power between the prosumers and the provision of reactive power services by the community to the local distribution system operator and the transmission system operator. The proposed procedure calculates the maximum and minimum reactive power deviations that each community participant can provide with respect to the reference profile.

4.2. Motivations and literature review

The regulatory framework on energy communities is in evolution to include different perspectives of the transition to a low carbon society other than the technical aspects of power system operation, such as environmental issues, eradicating energy poverty, sustainable development (e.g., [53] and references therein). The integration of distributed generation may lead to a decrease in power factor for individual sites [54]. Moreover, energy communities are expected to provide services (such as active and reactive power balancing) to the distribution and transmission networks to which they are connected. Emerging regulations are fostering the participation of final users, single or aggregated collectives, in both the energy market and the ancillary services markets. These services for the distribution network operation are expected to be provided by microgrids and energy communities, with the use of qualified generating and storage units, reactive power compensation devices, and the implementation of demand response techniques.

This chapter focuses on the provision of reactive power compensation services by a local energy community of prosumers connected to the same medium voltage (MV) distribution network. There is a growing literature on this specific topic both for separately managed final users or prosumers and for communities. In these studies, reactive and active compliant and non-compliant zones of operation are often considered, including penalties for non-compliant absorption of reactive power. Indeed, when a photovoltaic (PV) system, installed in a final user site, is operated at unitary power factor, it decreases the local active power demand with a corresponding worsening of the power factor of the site. The presence of penalties for non-compliant absorption of reactive power is indeed an issue There are several studies relevant to the reactive power control of distributed generators, with specific reference to PV systems, e.g. [55], [56], [57], [58], [59] that consider also the relationship with active

power curtailments and transformer control. Among the auxiliary services for distribution network operation, the provision of reactive power flexibility is one of the most important as it can be used to obtain improved voltage profiles, avoiding or postponing the need of expensive voltage control devices by the DSO (such as static var compensators and voltage regulators). The changes of the user reactive power injections or absorptions need to be coordinated with the control of the transformers equipped with on-load tap changers (OLTC) [60]. Optimization approaches have been developed for the reactive power management in grids with renewables [61], which need to consider both P-Q inverter capability curves and compliant regions (that may also involve the voltage value at the connection bus) defined in various countries [62],[63],[64].

The preliminary calculation of the maximum deviations with respect to a reference value [65],[66] are useful for DSO and TSO decisions relevant to the provision of ancillary services. In [67], the limitations of traditional reactive power compensation methods, particularly for distributed generation (DG), are addressed by a distribution level reactive power market that offers variable payments to units equipped with smart inverters. In the context of energy communities equipped with energy storage systems and aggregated distributed energy resources, [68] and [69] focus on active load flexibility, storage capacity sharing, and voltage ancillary services, using phasor measurement units for control coordination.

4.3. Contributions and chapter organization

This work presents an optimization model for the scheduling of the community resources that considers both active and reactive power direct exchanges among the community participants. Active power exchanges allow to reduce the energy procurement costs of the community with respect to the case in which the users can only transact with an external energy provider; reactive power exchanges are aimed at reducing the noncompliance penalties associated with low power factor operation.

A day-ahead scheduling problem of a community connected to a MV distribution network is considered. It is assumed that network users are members of the same community and have a common provider (identified for simplicity with the utility). The transactions among different users of the low voltage network connected to the same node of the MV network are aggregated without effects on the results. Daily profiles of the price of the energy bought from the utility, price profiles recognized for the energy sold to the utility, and penalizations for energy exchanges with low power factor are predefined. Direct exchanges of both active and reactive power are allowed among the community participants. The proposed optimization procedure of the community calculates the scheduling of these exchanges through the MV network and the prices of the transactions. The objective of the procedure minimizes the energy procurement costs of the community for the next day together with

the penalizations for low power factor operation. Moreover, specific optimization procedures are used to assess the maximum up and down reactive power variations that can be offered as a flexibility service by the community to the utility for the following day, being the flexibility reward tariffs predefined. The utility can use the reactive power flexibility service offered by the community for the online reactive power/voltage control in the network during the day. As these optimization procedures calculate the maximum reactive power increase and decrease at each node and at the substation that connects the distribution network with the transmission network, these flexibility capabilities can be exploited for both the distribution operation (by the DSO) and for the transmission system at the DSO/TSO interface. In any case, the community is rewarded by the variation of the reactive power at the connection points of the participants.

The developed model considers voltage control devices, such as transformers equipped with OLTC, capacitor banks or static var compensators, as well as the reactive power injection or absorption by distributed generators and storage units.

The effectiveness of the approach is demonstrated by applying it to a set of real MV test feeders supplied by the same HV/MV substation, under various operating conditions. The consumption and production profiles have a 15-minute resolution and follow actual recordings for three consecutive days, in winter and in summer. There are several connected users equipped with renewable energy units, mainly PV units, heat, and power generators (CHP), and small hydro power (SHP) units. In addition, some battery energy storage systems are introduced.

The procedure is implemented in a computer code and applied specifically to a real 15 kV power distribution network in Italy, and IEEE 14 and 123 bus system.

The results highlight the benefits of the energy community compared to independent users' operation, in terms of reducing energy procurement costs. This is achieved through an improved coordination between the scheduling of dispatchable distributed generation and storage units. Additionally, the analysis demonstrates the advantages of direct reactive power transactions in reducing penalties for low power factor operation. Coordination among distributed resources can also improve the community capability to provide reactive power flexibility services.

4.4. Structure of the chapter

Section 0 is devoted to the description of the optimization model and main assumptions. Section 4.6 focuses on the calculation of the reactive power flexibility limits. Section 4.17 describes the real case study and relevant available data. Section 4.20 presents the results of the analysis. Section 0 concludes the chapter 4.

4.5. Structure of the optimization procedures

In this chapter we consider a deterministic day-ahead scheduling problem, i.e., the optimization of the energy resources and control means for the 24 hours of the next day with 15 minutes resolution, assuming the forecast of load and photovoltaic production known without uncertainties. The optimization models can be adopted in scenario-based stochastic approaches and intraday rolling-horizon procedure (as described in e.g., [34]) able to cope with uncertainties. The formulation of the optimization problems and the solution computational requirements are suitable for the inclusion in a stochastic approach, although this is beyond the scope of the chapter.

The considered scheme includes the following steps.

- 1- Reference optimization: calculation of the scheduling of both active and reactive power resources that minimize the energy procurement costs of the entire community assuming known tariffs for the active power exchanges with the external provider and considering the penalties for the participants that operate with power factor lower than a predefined limit;
- 2- Qdown optimization: calculation of the maximum decrease of reactive power absorption or maximum increase of reactive power injection at the terminals of each community participant that minimizes the energy procurement costs considering the revenues (with predefined €/kvarh price) from the provision of a reactive power flexibility service consisting in the decrease with respect to the reactive power profile (assumed positive when power is absorbed) calculated in the reference step, according to DSO/TSO requests.
- 3- Qup optimization: calculation of the maximum increase of reactive power absorption or maximum decrease of reactive power injection at the terminals of each community participant that minimizes the energy procurement costs considering the revenues from the reactive power increase with respect to the reference profile.

Qdown and Qup optimizations are considered independent due to the lack of constraints relevant to reactive power compensation decisions taken in different times.

Following the typical local energy community scheme, participants are allowed to provide active power to other participants. The role of provider and consumer can vary at each period according to the generation and load levels inside each participant. The proposed optimization model provides the fair price for each transaction as the value of the shadows price of equilibrium constraints.

In the reference optimization, also reactive power exchanges among the participants in the community can be allowed, i.e., a participant that absorbs too much reactive power with the respect to active one (as it operates at low power factor), can reduce the penalty by the help of the reactive power injections of other participants. The model is conceived so that also these internal reactive power exchanges among the community participants are balanced to avoid excessive reactive power exchanges with the grid, both positive and negative. Section 4.20 will show the results obtained with and without reactive power compensations between community participants for the considered test cases.

The optimization models consider the typical operating constraints of the distribution network: maximum bus voltage deviations with respect to the reference value, maximum current limits in the branches, limitation in the OLTC of transformers and voltage regulators, maximum reactive power of variable capacitor banks.

In Qdown and Qup optimizations, the voltage control and reactive power compensation means of the distribution network (i.e., OLTCs and variable capacitor banks) can be operated to maximize the rewards (this can describe the case of an energy community that also acts as the operator for the relevant part of the distribution system) or can be operated to maintain the voltage profile close to the rated value (as in the typical case of a separate DSO from the community). Section 4.20 compares the results obtained for the two different ways of OLTCs and capacitor banks operation.

For the power flow representation, we have chosen the convex relaxation approach described in e.g., [31],[32], based on the DistFlow method [71], considering an equivalent single-phase representation of the three-phase network assumed as balanced.

Although some downsides (analyzed in e.g., [72],[73]) and the need of a careful model formulation to guarantee that the solution will meet the equality of the relaxed constraints, this approach appears suitable for a first implementation and comparison of novel objectives and strategies, to explore the new scenario characterized by the presence of communities, direct energy transaction among prosumers, and their participation to local and global ancillary service markets.

The relationship between load modelling and volt-var optimization can be significant, as shown in e.g., [74] and references therein. Since the study is focused on reactive power provision services, the proposed model includes the voltage dependence of active and reactive power loads represented by the ZIP model (i.e., combination of constant impedance, constant current, and constant power loads), other than transformers equipped with OLTCs, capacitor banks, and the representation of the charging current of the branch lines (i.e., the line shunt capacitance).

The linear representation of the ZIP model presented in [75] has been suitably adapted to be included in the DistFlow method. Moreover, to increase the accuracy of the solution and to avoid any link between loads and branch currents, the optimization is included in an iterative procedure in which, at

the first calculation, the ZIP models are evaluated at the voltage of the secondary side of the feeding OLTC transformers, and in the following iterations, loads are represented as constant power calculated at the bus voltage value of the previous iteration. The optimization model of the following iterations is simpler than that of the first iteration, as described in Section 4.16, so to significantly speed up the calculation. The iterative procedure stops when the maximum difference between the voltage values in consecutive iterations is smaller than a predefined tolerance.

The structure of the entire procedure is illustrated in Figure 28. The figure indicates the type of implemented optimization problems: MIQCP refers to mixed-integer quadratically constrained programming and QCP refers to quadratically constrained programming (without binary variables).

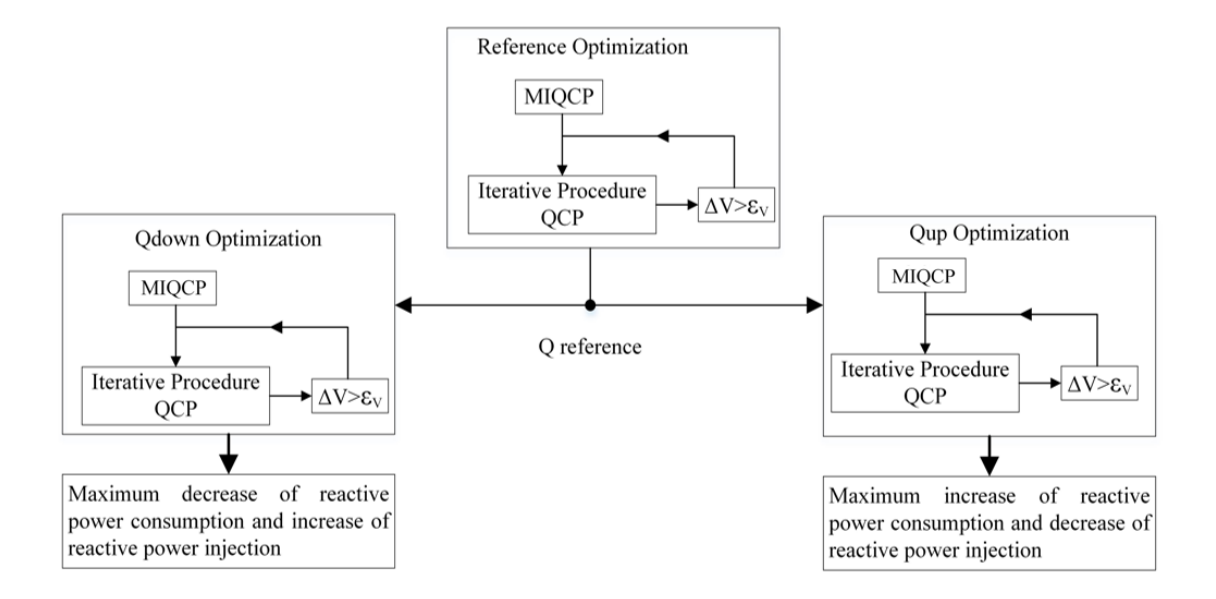


Figure 28 Scheme of the procedure.

The next two sections describe the optimization model adopted in this chapter for the scheduling of the community resources together with the calculation of the reference reactive power profiles and the models for the calculation of the maximum reactive power deviations, respectively.

4.6. Reference optimization model of the distribution network with the presence of a local energy community

The T equivalent circuit is adopted as line model, which may be advantageous with respect to the Π line model, adopted in other DistFlow-based optimization models as in, e.g. [76], for the easier calculation of the currents at the line ends. The network is assumed to be radial. The number of buses (excluding the connection to the transmission network) and branches is the same. The set of the bus and branches is denoted by Ω . For simplicity, a reference direction is assumed for the power flow along the lines from the external grid to the terminal buses. Each branch is denoted by the index i of

the sending bus. Each time interval Δt of the considered optimization horizon T is equal to 15 minutes. According to the DistFlow method, each generic branch of the network is represented by the line model connected to the input terminal or receiving bus, a transformer, a load and a shunt capacitance connected to the output terminal or receiving bus, as shown in Figure 29. $v_{\rm in}$, $v_{\rm out}$ denote the squared rms values of the voltages at the receiving and sending bus, respectively, while $v_{\rm mp}$ and $v'_{\rm out}$ refer to the internal and the sending bus of the T-model. $u_{\rm in}$, $u_{\rm out}$ are the squared rms values of the line currents in the two terminals of the T-model. $z=r+{\rm j}x$ is the line series impedance and ${\rm j}b$ is the line shunt admittance.

The transformer can be present or not. If present, a transformer ratio t_{OLTC} different than 1 is considered while the short circuit impedance and the magnetizing inductance are modelled by using the T equivalent circuit.

The community participants can transact with the external energy provider and among themselves, at prices taken equal to the marginal costs calculated as shadow prices of specific equality constraints (described in Section 4.14), under the assumption that the participants of the community are not in competition. Extending the approach presented in [35], the exchanges between participant i and any other participant in time t are represented by variables $P_{\text{LEC}\,i,t}$, $Q_{\text{LEC}\,i,t}$, for active and reactive power, respectively. Analogously, the exchanges with the external provider, which for simplicity we identify with the utility, are described by variables $P_{\text{grid}\,i,t}$ $Q_{\text{grid}\,i,t}$. The local active and reactive power $P_{\text{user}\,i,t}$, $Q_{\text{user}\,i,t}$, measured by the meter at the participant connection, should be equal to the sum of the transaction with the grid with the community. For each participant, the signs of the two exchanges with the grid and with the other participants are constrained to be the same, to avoid reselling. Variables $P_{\text{LEC}\,\text{in}\,i,t}$, $Q_{\text{LEC}\,\text{in}\,i,t}$ and $P_{\text{LEC}\,\text{out}\,i,t}$, $Q_{\text{LEC}\,\text{out}\,i,t}$, allow to represent the power flows associated with power generated and consumed in the same t inside the community.

At its point of connection, each community participant absorbs active and reactive power (nonnegative $P_{\mathrm{L}\,i,t}$, $Q_{\mathrm{L}\,i,t}$), injects active and reactive power by local generator ($P_{\mathrm{G}\,i,t}$, $Q_{\mathrm{G}\,i,t}$), BES unit ($P_{\mathrm{BES}\,i,t}$, $Q_{\mathrm{BES}\,i,t}$), and capacitor bank (nonnegative $Q_{\mathrm{C}\,i,t}$).

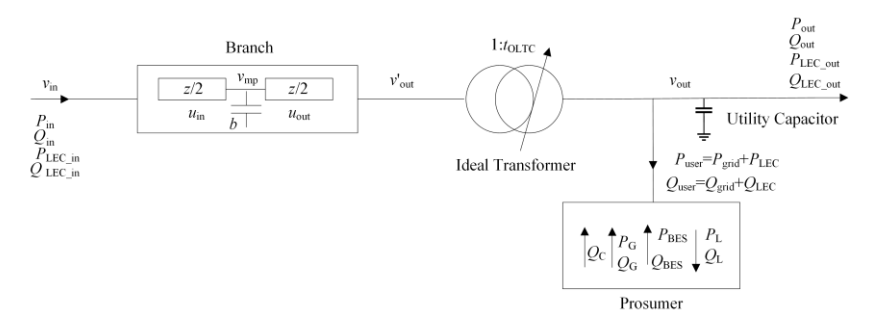


Figure 29 Scheme of the model of a generic branch with the connection point of a user.

4.7. Objective function

The considered objective minimizes the objective function *OF* as described in section 3.2.3 (3.20).

As the number and characteristics of the installed components are fixed in the considered day-ahead scheduling problem, as well as the community composition, only the costs that depend on the decision variables (i.e., the active and reactive power outputs of the controllable energy resources that are already available in the system, the transactions among the community participants, and the OLTC positions) are included. The objective function does not include generation costs since we assume here that all the local generation is provided by PV systems. If generation costs vary with production, they affect the optimal prices of the transactions among the community participants as shown in [27] where the presence of biogas units is considered.

As the price $\pi_{\text{buy},t}$ for buying energy from the utility is higher than the price $\pi_{\text{sell},t}$ recognized when the community participants sell energy to the utility at each time t, the feasible region of cost $C_{\text{grid}\,i,t}$ is defined by the minimization of following convex epigraph as described in 3.2.3 in equation (3.2).

4.8. Penalization of low power factor operation

 pf_{\min} The complies with is illustrated in Figure 30, where $\hat{Q}_{i,t} = Q_{Gi,t} + Q_{Ci,t} + Q_{BESi,t} + Q_{LECi,t}$ is the sum of reactive power decision variables, i.e. controllable reactive power resources $(Q_{G_{i,t}}, Q_{C_{i,t}}, Q_{BES_{i,t}})$ and reactive power exchanges among the users $Q_{LEC_{i,t}}$. According to section 3.2.3 in equation (3.20), when the operating point is outside the compliance area, a penalty is applied proportional to the noncompliance amount $Q_{\mathrm{PF}\,i,t}$. In some regulatory framework, for small active power consumption or production a fixed reactive power exchange is allowed without penalization, as illustrated in [60], [64] with reference to Swiss and Belgian regulation. For simplicity, these peculiarities are not included in the implementation of the model presented in this chapter, as customer penalizations for bus voltage violations.

 Q_G , Q_{BES} are constrained by the minimum power factor of the local generator and BES. Q_C is fixed or limited by the maximum output of the switchable capacitor bank (for simplicity, discrete switching is not represented).

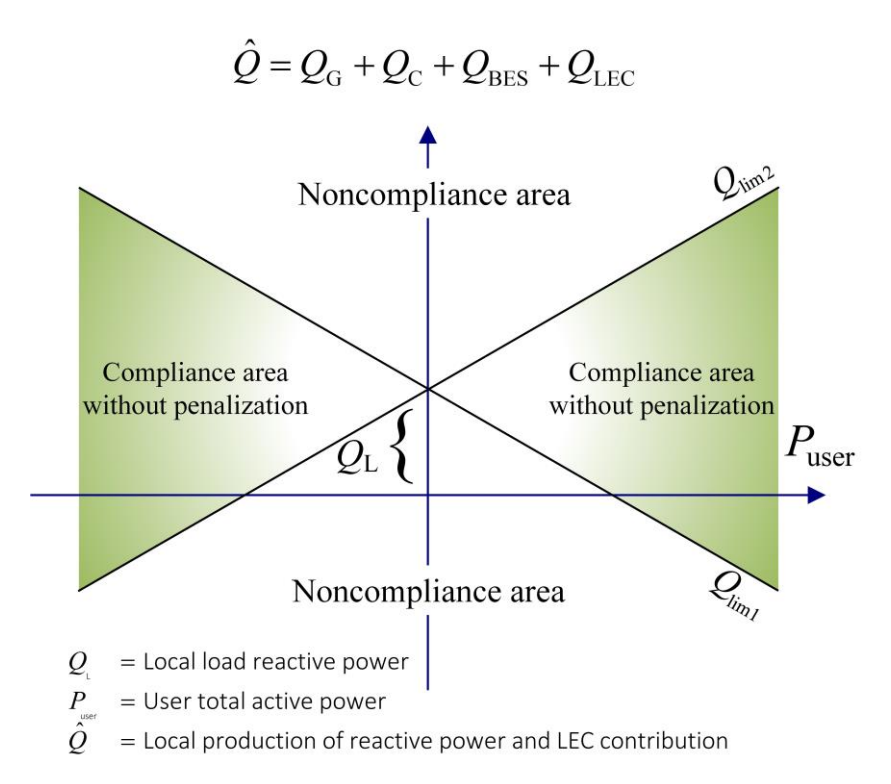


Figure 30 Operating region that complies with the minimum power factor

The noncompliance $Q_{\text{PF}\,i,t}$ is a nonnegative variable under the assumption that there is no reward for operating inside the compliance area. As the compliance area shown in Figure 30 is nonconvex, the representation of $Q_{\text{PF}\,i,t}$ includes a condition on the sign of $P_{\text{user}\,i,t}$ (dealt with the inclusion of binary variables), as described in section 3.2.3, in equation (3.20).

Joule power loss $\ell_{i,t}$ in each branch is illustrated in section 3.1.3 in equation (3.3).

Power losses associated with BES discharging and charging (corresponding to P_{BES} positive and negative) are as described in section 3.2.3, in equation (3.26).

where $\eta_{\text{dicharge }i}$ and $\eta_{\text{charge }i}$ are efficiency factors lower than one. P_{BES} is constrained by the maximum power limit of the battery.

Nonnegative variable \hat{P}_{LEC} is defined by

$$\hat{P}_{LEC\,i,t} \ge \begin{cases} P_{LEC\,i,t} \\ -P_{LEC\,i,t} \end{cases} \tag{4.1}$$

4.9. Coupling constraints

Values of $v_{\text{out }i,t}$, $P_{\text{out }i,t}$, $Q_{\text{out }i,t}$, $Q_{\text{LEC_out }i,t}$, $Q_{\text{LEC_out }i,t}$ should be equal to the values of $v_{\text{in }i+1,t}$, $P_{\text{in }i+1,t}$, $Q_{\text{in }i+1,t}$, $Q_{\text{LEC_in }i+1,t}$, considering i as the upstream branch and i+1 the downstream one. Generalizing to the case of multiple branches terminating and originating from the same bus as illustrated in section in 3.1.5 equations (3.11), (3.12) and (3.13) and for $Q_{\text{LEC out }i,t}$ and $Q_{\text{out }i,t}$:

$$\sum_{i \in \Omega_j^r} Q_{\text{out } i,t} = \sum_{i \in \Omega_j^s} Q_{\text{in } i,t}$$
(4.2)

$$\sum_{i \in \Omega_j^r} Q_{\text{LEC_out } i,t} = \sum_{i \in \Omega_j^s} Q_{\text{LEC_in } i,t}$$
(4.3)

where $v_{j,t}$ is the squared voltage of bus j and Ω_j^r , Ω_j^s denote the sets of branches connected to bus j as the sending and receiving end, respectively. The squared voltage V_0^2 at the connection point to the transmission network (slack bus 0) is assumed to be known and, for simplicity, is here assumed constant during the day.

Transactions between the participants of the community do not cause any power flow exchange with the utility, i.e.,

$$\sum_{i \in \Omega_0} P_{\text{LEC_in } i,t} = 0 \tag{4.4}$$

$$\sum_{i \in \Omega_0} Q_{\text{LEC_in } i, t} = 0 \tag{4.5}$$

4.10. Branch constraints

According to the DistFlow method, for each branch i and time interval t, the relationships between the voltages at the terminals and the power flows are given by the following relationships as described in section 3.1.4 in equation (3.6) and (3.7).

being $Q_{\text{cap }i,t}$ the reactive power injection of the utility capacitor bank connected at bus i (as shown in Figure 29) if present.

Nonnegative variable $u_{\text{in }i,t}$, $u_{\text{out }i,t}$ are constrained to be lower than the square of the maximum branch current limit ($I_{\text{max }i}^2$) and nonnegative variables $v_{\text{in }i,t}$, $v_{\text{out }i,t}$ are constrained between the square of the minimum and maximum bus voltage limits ($V_{\text{min }i}^2$, $V_{\text{max }i}^2$).

4.11. Cone constraints

As usually done to represent the DistFlow model as a quadratically constraint problem, the apparent power equalities are relaxed as shown in section 3.1.4 in equations (3.9) and (3.10).

In a feasible solution, all (3.9) should be verified as equalities, as well as one of (3.4). A specific check is automatically performed in the procedure and if the mismatch is greater than a predefined small tolerance the optimization is repeated as described in subsection 4.15.

4.12. OLTC and capacitor constraints

For the branches relevant to OLTC transformers, the constraints are

$$t_{\min}^2 v'_{\text{out } i,t} \le v_{\text{out } i,t} \le t_{\max}^2 v'_{\text{out } i,t}$$
 (4.6)

where t_{max} and t_{min} are the upper and lower bounds of t_{OLTC} (for the branches that describes a line $t_{\text{max}} = t_{\text{min}} = 1$). This formulation, for simplicity, does not explicitly represent discrete steps. A refined result that considers the discrete steps is obtained by the iterative optimization procedure described in section 4.16.

We consider two ways to operate the OLTC:

- a) the OLTC ratio is optimized, together with the other decision variables, to minimize the objective function or
- b) the OLTC tap is chosen to control the voltage by the two linearized constraints (by neglecting $\Delta V_{i,t}^2$ in the first constraint and assuming v_{out} close to 1 pu in the second one)

$$v_{\text{out }i,t} = V_{\text{r}i}^2 + 2 V_{\text{r}i} \Delta V_{i,t}$$

$$\Delta V_{i,t} = s_R P'_{\text{out }i,t} + s_X Q'_{\text{out }i,t}$$
(4.7)

where V_r is the rated voltage at the secondary side of the transformer, s_R and s_X are positive parameters that represent the regulator compensation settings. To consider t_{max} and t_{min} , (4.7) is conditioned by (4.6) with the inclusion of three binary variables (each corresponding to

 $v_{\text{out }i,t} = t_{\text{max}}^2 v'_{\text{out }i,t}$, $v_{\text{out }i,t} = t_{\text{min}}^2 v'_{\text{out }i,t}$, and $v_{\text{out }i,t}$ between $t_{\text{min}}^2 v'_{\text{out }i,t}$ and $t_{\text{max}}^2 v'_{\text{out }i,t}$) whose sum must be 1.

In a) the community also operates as a DSO for the network to which the participants are connected, in b) DSO and community are separated so the DSO operates the transformers to control the voltage near to the rated value.

Analogously, also the variable capacitor bank can be considered belonging to the community participant connected to the same bus or to the utility network. In both cases the nonnegative variable relevant reactive power injection $Q_{Ci,t}$ limited by maximum value $Q_{C\max i}$. If the capacitor bank belongs to the community participant, the capacitor reactive power injection is included in the evaluation of Q_{user} as shown in Figure 29.

4.13. User plant constraints

The net power for each user is given by as described in section 3.2.3 in equation (3.24).

The adopted simple model of the BES unit is represented by as described in section 3.2.3 in equation (3.26).

where $E_{i,t}$ is the energy content constrained by the minimum and maximum energy levels $E_{\min i}$, $E_{\max i}$. In the numerical tests, $E_{i,t}$ is assumed equal to $E_{\max i}$ at beginning and the end of the optimization horizon (t=1 and t=96, respectively).

The linearized ZIP model of the load (written in pu) described in section 3.1.6 in equation (3.17).

where $P_{\rm Z}$ and $Q_{\rm Z}$ represent the consumption at the rated voltage of the constant impedance component, $P_{\rm I}$ and $Q_{\rm I}$ represent the consumption at the rated voltage of the constant current component, $P_{\rm P}$ and $Q_{\rm P}$ represent the consumption of the constant power component, and $\Delta P_{{\rm I}i,t}$, $\Delta Q_{ii,t}$ (different from zero only when $P_{{\rm I}i,t}$ and $Q_{{\rm I}i,t}$ are not null) represent the linearized voltage dependence of the constant current component consumption described in (3.18) in section 3.1.6.

4.14. Active and reactive power exchanges among the community participants

As mentioned, each community participant can exchange active and reactive power with other participants ($P_{\text{LEC }i,t}$, $Q_{\text{LEC }i,t}$) and with the utility ($P_{\text{grid }i,t}$ $Q_{\text{grid }i,t}$). The balance described in section 3.2.3 in equation (3.22) and (3.19).

The representation of Q_{LEC} exchanges includes a condition on the sign of $Q_{\mathrm{LEC}\,i,t}$ (dealt with the inclusion of binary variables), in order to avoid that one participant may absorb reactive power from the utility to provide Q_{LEC} to other participants who need it to reduce the noncompliance penalty Q_{PF}

Since it is in general avoided to inject reactive power to the grid, if not requested, $Q_{\text{grid }i,t}$ is constrained by

$$Q_{\text{grid }i,t} \ge 0 \tag{4.8}$$

The $P_{\text{LEC }i,t}$ and $Q_{\text{LEC }i,t}$ flows in the network are represented by

$$P_{\text{LEC}\,i,t} = P_{\text{LEC}\,\text{in}\,i,t} - P_{\text{LEC}\,\text{out}\,i,t} \tag{4.9}$$

$$Q_{\text{LEC }i,t} = Q_{\text{LEC_in }i,t} - Q_{\text{LEC_out }i,t}$$
(4.10)

The shadow prices associated with the active power constraints (3.8) are used to define the prices of the transactions among the participants of the community. In summary, the objective function of the MIQCP reference problem is given by (3.20) with constraints (4.9), (4.10), and (3.2) and the lower and upper limits of the variables.

4.15. Repeated optimization to achieve a feasible solution

The model described in the previous subsections includes the two following relaxations:

- a) the convex representation of the losses in the battery (3.25).
- b) the conic model of power flows represented by (3.9).

Relaxation (a) is valid when the solution reaches an equality conditions for at least one constraint of (3.25). This condition is facilitated by the minimization of the summation of $\ell_{\text{BES}\,i,t}$, explicitly considered in the objective function. However, since the compliance reactive power limits Q_{lim1} and Q_{lim2} depends on the active power consumption P_{user} , as shown by (3.28), and due to the relationship between P_{user} and ℓ_{BES} shown by (3.24), in some cases, the lowest value of the objective function is achieved without reaching the minimum BES losses condition, if $\mu_{\text{BES}\,i,t}$ are not increased so much that the BES power loss minimization term becomes prevalent. To avoid this issue, in constraint (3.28) the calculation of P_{user} does not include ℓ_{BES} .

Relaxation (b) is valid when the solution reaches the equality conditions for all constraints in (3.9). The achievement of this solution is facilitated by the minimization of the branch power losses explicitly considered in the objective function. However, due to the voltage dependence model of the loads (3.17), (3.18) and the relationship between bus voltages and branch currents (3.6), in some cases, the lowest value of the objective function is achieved without reaching the minimum power losses condition, if $\mu_{loss\,i,t}$ are not increased so much that the power loss minimization term becomes prevalent. In order to overcome this condition, in the first optimization (MIQCP), the load consumption is made independent from the branch currents: in (3.17) and (3.18) $v_{out\,i,t}$ is replaced by variable $v_{load\,i,t}$ that is equal to the voltage at the secondary side of the feeding OLTC transformer or to V_0^2 if there are no OLTC transformers between bus i and slack bus 0. Analogously, to make the voltage at the secondary side of OLTC transformers independent from branch currents, in (4.6) $v'_{out\,i,t}$ is replaced by V_0^2 or, if there is another upstreaming OLTC, by its secondary side voltage v_{out} .

If at the end of an optimization neither of the two constraints (3.25) is satisfied as equality for some of the BES units, despite the described countermeasure, the optimization is repeated with the inclusion of an additional nonnegative penalization in (3.20), greater than the difference between ℓ_{BES} and the maximum of the right side terms of (3.25) calculated by using the $P_{\text{BES}\,i,t}$ values provided by the previous solution.

Analogously if at the end of an optimization, constraints (3.9) are not satisfied as equality for some branches, the optimization is repeated by adding a penalization in , greater than the difference between $u_{\rm in}$, $u_{\rm out}$ and the maximum values of $\left(P_{\rm in}^2+Q_{\rm in}^2\right)\!/v_{\rm in}$, $\left(P_{\rm mp}^2+Q_{\rm mp}^{\prime 2}\right/v_{\rm mp}\right)$ and $\left(P_{\rm mp}^2+Q_{\rm mp}^2\right)\!/v_{\rm mp}$, $\left(P_{\rm out}^{\prime 2}+Q_{\rm out}^{\prime 2}\right)\!/v_{\rm out}$, respectively, evaluated according to the previous solution.

4.16. Iterative procedure to obtain a refined solution

The iterative procedure mentioned in Figure 28 improves the accuracy of the results. The model (3.20) and (4.10) is iteratively solved again with these changes:

- a) the voltage at the secondary side of OLTC transformers are fixed in agreement of the step nearest to the previously calculated value,
- b) the sign of P_{user} and the sign of Q_{LEC} at each bus are fixed as previously calculated,
- c) the total power of each load is recalculated by using the bus voltage value obtained in the previous iteration and all load types are transformed in constant P.

The iterative procedure ends when the difference between the bus voltage values in two subsequent iterations becomes lower than a predefined tolerance. As the binary variable are fixed the model (3.20) and (4.10)becomes a quadratically constrained problem (QCP).

At the end of this procedure, the reference profile $Q_{\text{ref }i,t}$ for each participant is defined equal to the calculated $Q_{\text{user }i,t}$. The same reference profile is used in both the Qdown and Qup procedures described in the next sections.

4.17. Calculation of the maximum and minimum reactive power deviations

To exploit the community willingness to provide a variation of the reactive power consumptions or injections with respect to the reference profile, DSO and TSO needs to know the maximum amount of the reactive power flexibility.

These flexibility limits are calculated by two distinct optimization models, one (Qdown) provides the maximum value of reactive power consumption decrease or of reactive power injection increase for each t and i; the other (Qup) provides the maximum value of reactive power consumption increase or of reactive power injection decrease for each t and i.

In both optimizations, the objective functions the revenues for the provision of the flexibilities replace the penalizations for the noncompliance of the minimum power factor.

4.18. Maximum increase of reactive power injection or decrease of reactive power absorption

The considered objective function of the Qdown problem is

$$OF_{\mathbf{Q}_{\text{down}}} = \sum_{i \in \Omega} \sum_{t \in T} \left(C_{\text{grid } i, t} - \pi_{\text{down}} Q_{\text{down } i, t} + \mu_{\text{loss } i, t} \ell_{i, t} + \mu_{\text{BES } i, t} \ell_{\text{BES } i, t} \right) \Delta t$$

$$(4.11)$$

where π_{down} is the amount of money that DSO/TSO gives to the community for each kvarh of consumption decrease or injection increase, Q_{down} is the variation of the reactive power at each t and i with respect to the reference value Q_{ref} calculated by the reference optimization procedure, i.e.:

$$Q_{\text{down } i,t} = Q_{\text{ref } i,t} - Q_{\text{user } i,t}$$

$$\tag{4.12}$$

Function (4.11) is conceived under two assumptions:

a) reactive power decisions in one period do not have significant relationship with the reactive power decisions taken in previous periods,

b) the inclusion of the reward term does not significantly affect costs C_{grid} (i.e., active power decisions).

Indeed, as shown in the test cases, in general, the replacement of noncompliance penalization with the flexibility reward does not significantly modify the value of C_{grid} . In cases this is not true (i.e., when reactive power compensation or voltage control do affect active power outputs or consumptions), it might be appropriate to include the expected probability ϕ_t that DSO/TSO will require the activation of the reactive power flexibility at period t of the next day in the objective function. With this change, the flexibility reward is weighted by ϕ_t and the objective function also includes the noncompliance penalization weighted by $(1-\phi_t)$. For simplicity, the consideration of this aspect is not addressed in the chapter.

Problem Q_{down} includes constraints (3.2), (3.3), (4.3), (3.6), (4.4), (3.19), (4.9), (4.12). If the OLTC transformers are operated according to (4.7), the model is still MIQCP although binary variables are limited to those relevant to such a constraint. If (4.7) is not included (i.e., OLTCs are optimized to minimize the objective function), the model does not include binary variables and it is classified as QCP.

The same repeated solutions and iterative procedures describe in sections 04.15 and 04.16 are also applied in the Qdown procedure, to achieve a feasible and accurate solution.

4.19. Maximum decrease of reactive power injection or increase of reactive power absorption.

Analogously, the objective function of Qup procedure is

$$OF_{Q_{\text{up}}} = \sum_{i \in \Omega} \sum_{t \in T} \left(C_{\text{grid } i, t} - \pi_{\text{up}} Q_{\text{up } i, t} + \mu_{\text{loss } i, t} \ell_{i, t} + \mu_{\text{BES } i, t} \ell_{\text{BES } i, t} \right) \Delta t$$

$$(4.13)$$

where π_{up} is the amount of money that DSO/TSO gives to the community for each kvarh of consumption increase or injection decrease, Q_{up} is the variation of the reactive power at each t and i with respect to the reference value Q_{ref} calculated by the reference optimization procedure, i.e.:

$$Q_{\mathrm{up}\,i,t} = Q_{\mathrm{user}\,i,t} - Q_{\mathrm{ref}\,i,t} \tag{4.14}$$

Problem Q_{up} includes constraints (3.2), (3.3), (4.3), (3.6), (3.19), (4.4), (4.9),(4.14). It is a MIQCP or QCP model if (4.7) is included or not. The repeated solutions and iterative procedures of sections 0 and 0 are applied to achieve a feasible and accurate solution.

4.20. Model implementation, test cases description and results

The complete procedure of Figure 28, which illustrates all the described optimization models, has been implemented in AIMMS Developer modelling environment [37], using Gurobi 9.5 solvers (MIQCP for the first reference optimization and QCP for Q_{down} , Q_{up} and iterative solutions respectively). The results have been obtained by using a computer equipped with an Intel-i7 and 32 GB of RAM, running 64-bit Windows 10.

The numerical tests included in this chapter consider three different test cases. The complete set of data of the 3 test cases is included in the Excel file available at https://ldrv.ms/x/s!Anog_gEaBkch0OIAi2WcvHrg-zBdNQ?e=yrdktC (it will be posted in a public domain data repository). The file contains also the schemes of the networks, the 96 period per unit load profiles used in all the test cases obtained by the CREST tool [36] using different numbers of dwellings, the daily profiles of π_{buy} and π_{sell} , and the daily profile of the ratio between power output and panel surface, assumed the same for all PV units.

Each prosumer may be equipped with a PV system, a load, and a BES unit. All the prosumers belong to the same energy community. All the calculations refer to a time window of one day, divided into 96 periods of 15 minutes each. Noncompliance penalty tariff μ_{PF} is equal to 5 ϵ /kvarh, flexibility reward tariffs π_{down} and π_{up} are equal to 3 ϵ /kvarh, in agreement with [64]. The minimum power factor value that complies with the requirements is assumed equal to 0.9. The bus voltages values are constrained to be inside of the 0.9 pu, 1.1 pu interval.

Regarding the iterations needed to obtain feasible (section 3.8) and accurate (section 3.9) solutions, a predefined tolerance of 1% is adopted for both the branch maximum current limit and the difference between the bus voltage values in two subsequent iterations. A 1% value is also set for the mixed integer relative optimality tolerance of the global optimum gap in the MIQCP solver.

A. Test case A

The test system, adapted from [77], is a 14-bus network, in which three feeders are connected to the same substation bus. All the BES units can inject or absorb reactive power as determined by the optimization procedure. The minimum and maximum reactive power limits are ±48.43% (0.9 power factor) of the rated value. All PV units operate at unitary power factor. The forecasted total energy demand during the day is 349.4 MWh, the PV energy generation is 52.4 MWh (15% of the load), the total storage capacity installed is equal to 5.5 MWh (10.5% of the daily PV generation). For the provision of reactive power, All the BES units can inject or absorb reactive power as determined by

the optimization procedure. The minimum and maximum reactive power limits are $\pm 48.43\%$ (0.9 power factor) of the rated value. All PV units operate at unitary power factor.

Assuming that all variable capacitor banks belong to community participants and reactive power exchanges between participants are allowed, Figure 31 shows the profiles of $P_{\rm LEC}$ and $Q_{\rm LEC}$ during the day. Figure 32 shows the bus voltages, Figure 33 compares the profile of the average price of the internal transactions $\pi_{\rm LEC}$ with $\pi_{\rm buy}$ and $\pi_{\rm sell}$, i.e. the prices of the transaction with the external energy provider. Figure 33 also shows the profile $P_{\rm grid}$ tot, i.e., the sum of $P_{\rm grid}$, i. As expected, the prices of the internal transactions are close to $\pi_{\rm buy}$ as $P_{\rm grid}$ tot always positive during the day. It has been verified that the both sum of all $P_{\rm LEC}$ and $Q_{\rm LEC}$ in each period are null and that the voltage profiles (and the relevant power flows in the network) corresponds to those provided by Matpower [78]. The same tests have been carried out for all the other test cases.

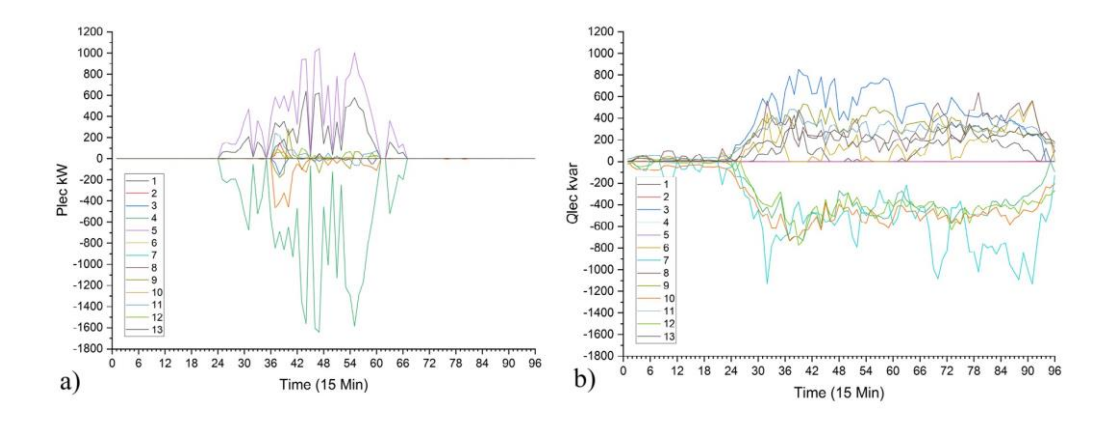


Figure 31 Profiles of the a) active and b) reactive power exchanges between community participants. Test case A.

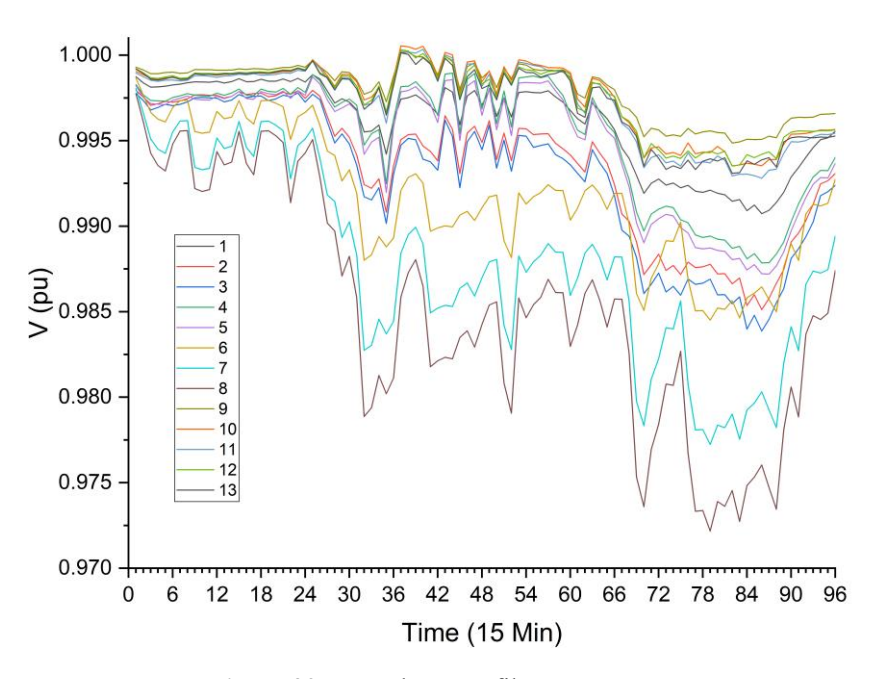


Figure 32 Bus voltage profiles. Test case A.

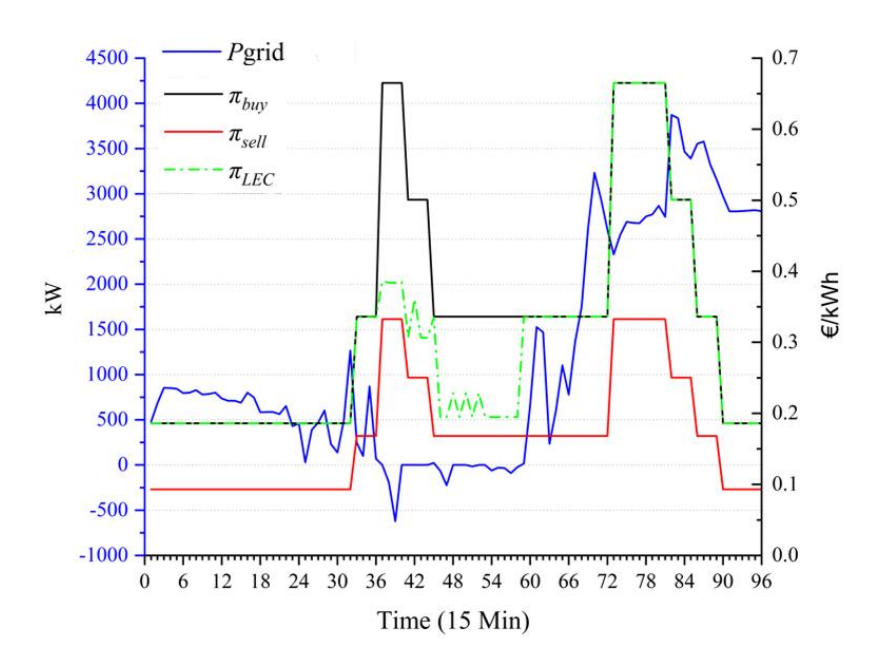


Figure 33 Prices of the internal transactions, prices of the transactions with the external energy provider, cumulative value of the power exchanged with the energy provider. Test case A.

The calculations are repeated for 4 scenarios that differentiate for the type of operation of the capacitor banks and whether $Q_{\rm LEC}$ exchanges are allowed (scenario 0 is without community, i.e., without $P_{\rm LEC}$; in all the other scenarios $P_{\rm LEC}$ transactions are allowed):

scenario 0 - all capacitors belong to the utility without community;

scenario 1 – all capacitors belong to the prosumers without Q_{LEC} exchanges;

scenario 2 – all capacitors belong to prosumers and Q_{LEC} exchanges are allowed;

scenario 3 – all capacitors belong to the utility and $Q_{\rm LEC}$ exchanges are allowed;

scenario 4 – all capacitors belong to the utility without Q_{LEC} exchanges.

Table 12, provides the values of the objective function, of the total daily costs of the exchanges with the energy provider and the daily value of the power factor noncompliance penalty obtained by the first (MIQCP) and the final of the iterative solutions (QCP), for the 4 scenarios.

Table 13 and

Table 14 provide the solution results for the Qdown and Qup procedures where the rewards corresponding to the provision of reactive power change with respect to the reference value replace the noncompliance penalties.

For all the calculations, the computer time is indicated. The final solutions (denoted in

Table 13 and

TABLE **14** as final iter.) are achieved with a single iteration. Figure 34 compares the profiles of the sum of the $Q_{\text{user }i}$ values calculated by the reference, Q_{down} , and Q_{up} procedures for the considered scenarios, showing the margins for each period that can be used as provision of the reactive power flexibility service by the community. In Table 12, the comparison between scenarios 1 and 2 and between scenarios 3 and 4 show the capability of QLEC exchanges to significantly reduce the noncompliance penalties.

In this case, the optimization of the available capacitor banks by the prosumers (scenarios 1 and 2) provides a significant advantage only for the provision of the Qdown reserve, whilst the penalty in the reference case is not reduced, as shown by the comparison between scenarios 1 and 4.

In all the scenarios, the energy procurement costs due to the transactions with the external energy provider are similar, being higher for scenario 0 (without community) especially for the reference case in which the voltages are kept high to increase the active power consumption by the voltage dependent loads and reduce the noncompliance penalties.

The comparison between scenarios 0 and 4 for the reference case shows that, in this test case, the decrease of energy procurement costs by the participation in the community leads to a slightly increase of the noncompliance penalties.

Table 12 Summary of the results for the reference optimization of case study A.

		Objective function	Cost of exchanges with the energy provider (k€)	Noncompliance penalty (k€)	CPU time (s)
Samuel 0	1st solution	$230.5 \ 10^3$	114.8	115.6	9.0
Scenario 0	final iter.	$228.9 \ 10^3$	114.1	114.7	4.9
G	1st solution	$229.5 \ 10^3$	113.0	116.4	3.2
Scenario 1	final iter.	$227.5 \ 10^3$	112.2	115.2	2.6
Samuel 2	1st solution	$112.4\ 10^3$	112.2	0	3.2
Scenario 2	final iter.	$111.6\ 10^3$	111.5	0	2.4
G 2	1st solution	$159.2 \ 10^3$	113.1	45.9	14.7
Scenario 3	final iter.	$157.7 \ 10^3$	112.5	45.1	2.2
Samuel A	1st solution	$229.4\ 10^3$	113.0	116.3	3.0
Scenario 4	final iter.	$227.8 \ 10^3$	112.3	115.4	3.0

Table 13 Summary of the results for the Qdown optimization of case study A

		Objective function	Cost of exchanges with the energy provider (k€)	Reward (k€)	CPU time (s)
Scenario 0	1st solution	22.9	113.7	90.9	3.4
Scenario u	final iter.	19.4	113.0	93.8	3.7
Scenario 1	1st solution	$-278.7\ 10^3$	112.2	391.0	3.2
Scenario 1	final iter.	$-281.7\ 10^3$	111.6	393.5	1.9
Scenario 2	1st solution	$-175.3 \ 10^3$	112.2	287.7	3.2
Scenario 2	final iter.	$-178.3 \ 10^3$	111.6	290.1	1.9
Carraria 2	1st solution	$89.6\ 10^3$	112.2	22.8	1.4
Scenario 3	final iter.	$86.1\ 10^3$	111.5	25.6	1.8
Carraria A	1st solution	$21.9 \ 10^3$	112.2	90.4	1.4
Scenario 4	final iter.	$18.4\ 10^3$	111.5	93.3	1.9

Table 14 Summary of the results for the Qup optimization of case study A

		Objective function	Cost of exchanges with the energy provider (k€)	Reward (k€)	CPU time (s)
Scenario 0	1st solution	$-178.8 \ 10^3$	113.7	292.6	3.4
Scenario o	final iter.	$-176.1\ 10^3$	112.9	289.1	3.9
Scenario 1	1 st solution	$-211.4\ 10^3$	112.2	323.8	5.9
Scenario 1	final iter.	$-207.9\ 10^3$	111.2	319.3	2.1
g	1st solution	$-314.7\ 10^3$	112.2	427.1	6.0
Scenario 2	final iter.	$-311.3 \ 10^3$	111.2	422.7	2.1
G 2	1st solution	$-248.5\ 10^3$	112.2	360.8	6.6
Scenario 3	final iter.	$-245.8\ 10^3$	111.4	357.3	1.9
G 4	1st solution	$-180.8 \ 10^3$	112.2	293.2	6.7
Scenario 4	final iter.	$-178.1\ 10^3$	111.4	289.6	2.0

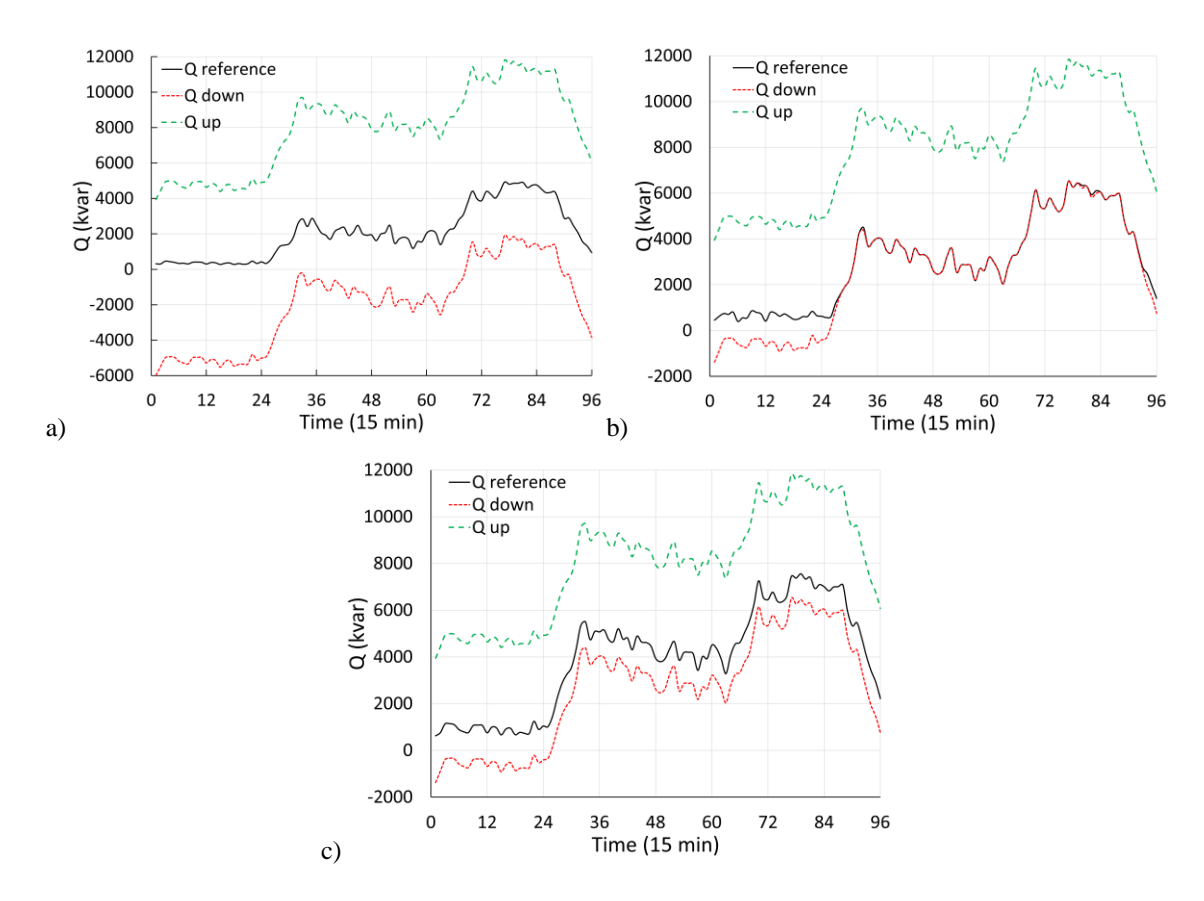


Figure 34 Profiles of the cumulative value of the community reactive power calculated by the reference, Qup and Qdown procedures for scenarios: a) 2 (like 1 not shown), b) 3, c) 4 (like 0 not shown). Test case A.

For this test case A, as well as for test case B and C, it has been verified that participating in the community does not disadvantage any of the prosumers.

In the case the variable capacitor banks belong to the utility, if QLEC exchanges are allowed, all the capability of providing reactive power by the participants is already used in the reference optimization to reduce noncompliance penalties. Therefore, the margin allowed for the provision of Qdown services is almost zero for large part of the day as shown in Figure 34) and the low value of the corresponding reward in

Table 13.

In order to show the sensitivity of the results for different values of noncompliance penalty and flexibility reward tariffs, Table 15 reports the summaries for scenario 3 with $\mu_{PF} = 0.1$ €/kvarh and $\mu_{PF} = 2.5$ €/kvarh (other than 5 €/kvarh as in the previous results), $\pi_{down} = \pi_{up} = 1.5$ €/kvarh (other than 3 €/kvarh as in the previous results). The results show that, as expected, decreasing the value of μ_{PF} decreases the noncompliance penalty, whereas lowering $\pi_{down/up}$ reduces the flexibility rewards. No effect is observed on the overall cost of exchanges with the energy provider.

Table 15 Summary of the results for case study A Scenario 3 with different values of reactive power penalty and flexibility reward (in parentesis, percentage variations with respect to Tables 1, 2, and 3)

	Refere	ence	Qdow	n	Qu	ıp
$\mu_{ ext{PF},} \ \pi_{ ext{down/up}} \ (ext{ϵ/kvarh})$	Cost of exchanges with the energy provider (k€)	Noncompliance penalty (k€)	Cost of exchanges with the energy provider (k€)	Reward (k€)	Cost of exchanges with the energy provider (k€)	Reward (k€)
0.1, 3	111.6 (-0.8)	1.1 (-97.6)	111.5 (0)	26.3 (2.7)	111.4 (0)	356.6 (-0.2)
2.5, 3	112.5 (0)	22.7 (-49.7)	111.5 (0)	25.1 (-2.0)	111.4 (0)	357.7 (0.1)
0.1, 1.5	111.6 (-0.8)	1.1 (-97.6)	111.5 (0)	13.1 (-48.8)	111.4 (0)	178.3 (-50.1)
2.5, 1.5	112.5 (0)	22.7 (-49.7)	111.5 (0)	12.6 (-50.8)	111.4 (0)	178.9 (-49.9)
5, 1.5	112.5 (0)	45.1 (0)	111.5 (0)	12.8 (-50.0)	111.4(0)	178.7(-50.0)

B. Test case B

Test case B is based on 13-bus IEEE feeder [22]. All the branches are considered symmetrical by averaging the non-zero values of the diagonal and off diagonal elements of the impedance and shunt admittance matrices and using the positive sequence values. The loads are assumed balanced too, increasing the original load values indicated in [22].

All the BES units can operate and can inject or absorb reactive power with minimum and maximum limits equal to ±48.43% of the rated value. All PV units operates at unitary power factor. The forecasted total energy demand during the day is 52.5 MWh, the PV energy generation is 24.5 MWh (46.7% of the load), the total storage capacity installed is equal to 1.7 MWh (6.9% of the daily PV generation). Both transformers at the substation and the one feeding a low voltage bus are considered equipped with OLTCs, between 0.9 pu and 1.1 pu.

Assuming that OLTCs and variable capacitor banks as operated by the community with $Q_{\rm LEC}$ exchanges allowed, Figure 35 compares the profile of the average price profile of the internal transactions π_{LFC} with the profile of $P_{grid tot}$. As expected, the prices of the internal transactions are bounded between π_{buy} and π_{sell} , close to π_{buy} when $P_{\text{grid tot}}$ is positive and close to π_{sell} when $P_{\text{grid tot}}$ is negative.

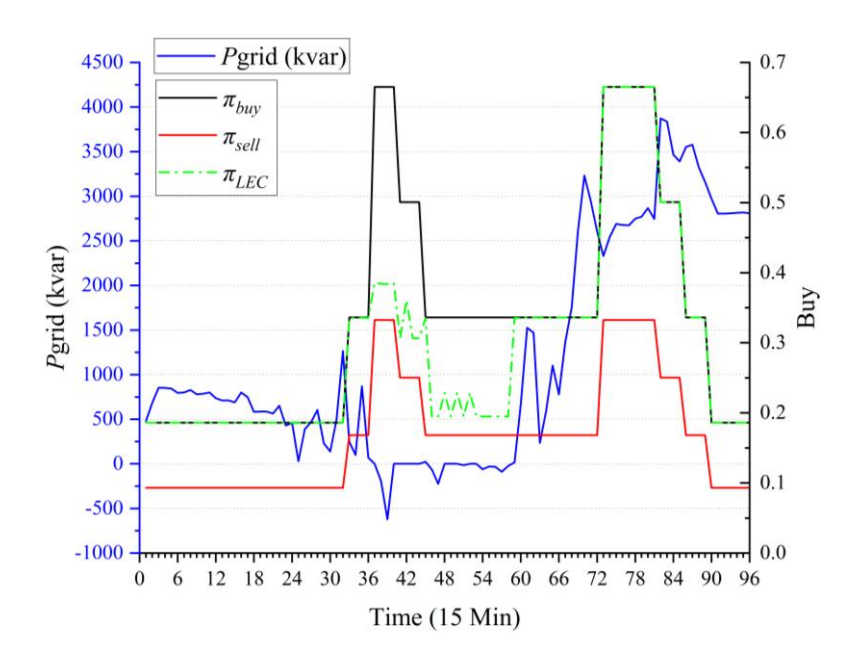


Figure 35 Comparison between the prices of the internal transactions and the prices of the transactions with the external energy provider. Cumulative value of the power exchanged with the energy provider. Test case B.

The calculations are repeated for 9 scenarios that differentiate for the type of operation of the OLTC

transformers, of the capacitor banks, and whether $Q_{\rm LEC}$ exchanges are allowed (scenario 0 is without community, all the other scenarios are with $P_{\rm LEC}$): scenario 0 - OLTCs operated by the utility, all capacitors belong to the utility without community; scenario 1 - OLTCs operated by the utility, all capacitors belong to the utility without $Q_{\rm LEC}$; scenario 2 - OLTCs operated by the community, all capacitors belong to the utility without $Q_{\rm LEC}$; scenario 3 - OLTCs operated by the utility, all capacitors belong to the prosumers with $Q_{\rm LEC}$; scenario 4 - OLTCs operated by the community, all capacitors belong to the prosumers with $Q_{\rm LEC}$; scenario 5 - OLTCs operated by the community, all capacitors belong to the utility with $Q_{\rm LEC}$; scenario 6 - OLTCs operated by the community, all capacitors belong to prosumers without $Q_{\rm LEC}$; scenario 7 - OLTCs operated by the utility, all capacitors belong to the utility with $Q_{\rm LEC}$; scenario 8 - OLTCs operated by the utility, all capacitors belong to prosumers without $Q_{\rm LEC}$;

Table 16 Summary of the results for the reference, Qup and Qdown optimizations of case study B. C_{ep} indicates the cost of the exchanges with the energy provider, P_{NC} indicates the noncompliance penalty, R indicates the reward.

	·	CEP (k€)	D (10)				
		CEP (KC)	<i>P</i> _{NC} (k€)	<i>C</i> _{EP} (k€)	<i>R</i> (k€)	<i>C</i> ep (k€)	<i>R</i> (k€)
2	Scenario 0	12.4	45.5	12.0	20.0	11.9	98.0
5	Scenario 1	10.8	45.5	10.6	20.5	10.6	97.4
9	Scenario 2	9.5	40.0	9.4	21.0	12.1	115.1
5	Scenario 3	10.6	0	10.7	48.0	10.5	131.4
\$	Scenario 4	9.4	0	9.3	35.0	12.0	163.0
\$	Scenario 5	9.5	22.1	9.4	8.7	12.1	127.5
\$	Scenario 6	9.6	39.9	9.4	80.1	12.0	118.0
S	Scenario 7	10.8	28.0	10.6	7.7	10.5	110.3
9	Scenario 8	10.7	45.1	10.7	78.1	10.5	101.3
(1000 -		36 48 60 Time (15 min)	72 84	0 -1000 -2000 b)	0 12	24 36 48 Time (15	60 72 min)
4000 3000 2000 (lask) 1000 O	-Q reference -Q down -Q up			4000 3000 2000 (xear) 1000 0	—Q referenc —Q down —Q up	e	
-1000				-2000			

Figure 36 Profiles of the cumulative value of the reactive powers of the community participants calculated by the reference, Qup and Qdown procedures for scenarios: a) 1 (like 0 and 2 not shown), b) 4 (like 3 not shown), c) 6 (like 8 not shown), d) 7 (like 5 not

Table 16 shows the summary of the values of energy procurement cost from the external provider, noncompliance penalty or reactive power service reward obtained at the last iteration of the reference, Qdown, and Qup procedures, respectively. The average (maximum) computational times in s are: 20.5 (44.4) for reference optimization, 3.3 (5.6) for Qdown, 3.1 (5.4) for Qup. The final solutions are achieved with 1 or 2 iterations.

Figure 36 compares the profiles of the sum of the $Q_{user\,i}$ values calculated by the reference, Q_{down} , and Q_{up} procedures for the considered scenarios.

The results of Table 16 show that minimum values of the noncompliance penalties are achieved when Q_{LEC} transactions are allowed (scenarios 3, 4, 5, and 7), reaching the complete compensation when the capacitor banks belong to the participants (scenarios 3 and 4).

The effects of the different way of operation of the OLTC transformers are quite negligible for both the reference and the Qdown optimizations.

Higher rewards in the Qup optimization are obtained when the OLTC transformers are operated by the community (scenario 2 compared to 1, scenario 4 compared to 3, scenario 5 compared to 7, and scenario 6 compared to 8). In the Qup optimization of these scenarios however, there is also a slight increase of the costs C_{EP} relevant to the transactions with the external energy provider the Qup optimization (from around 10.5 in scenarios 1,3,7,8 to around 12 in scenarios 2,4,5,6). When Q_{LEC} transactions are allowed and the capacitor banks belong to the utility (scenarios 5 and 7), the reduction margin available is negligible, resulting in very low rewards in the Qdown solution, as also illustrated by Figure 36d). As expected, other conditions equal, the highest value of the energy procurement costs from the external provider are those without community (scenario 0).

C. Test case C

Test case C is based on 123-bus IEEE feeder [22]. All the lines are considered balanced with positive sequence parameters obtained by averaging self and mutual impedances and admittances given in [22]. The loads are assumed balanced too, by averaging the single-phase loads. 49 PV units are added at load buses, with peak power taken equal to the load power multiplied by a randomly generated factor with a uniform distribution between 0 and 2, provided the production/consumption ratio is greater than 0.9, otherwise taken as zero. The apparent rated power of the PV inverters is increased by 10% respect to the PV rated powers. The BES units operate at unitary power factor, while the PV units may exchange the reactive power determined by the optimization procedure. With reference to the rated power of the inverter, the minimum and maximum reactive power limits are \pm 48.43% if the produced active power is larger than 10%, \pm 4.84% otherwise.

The forecasted total energy demand during the day is 13.0 MWh, the PV energy generation is 7.3 MWh (56.2% of the load), the total storage capacity installed is equal to 68 kWh (0.9% of the daily PV generation). The substation transformer and the voltage regulators feeding buses 14, 26, and 67 are considered equipped with OLTCs, between 0.9 pu and 1.1 pu. Variable capacitor banks are

connected to buses 83, 88, 90, 92 (with maximum power equal to the average values indicated in [22] for the three phases).

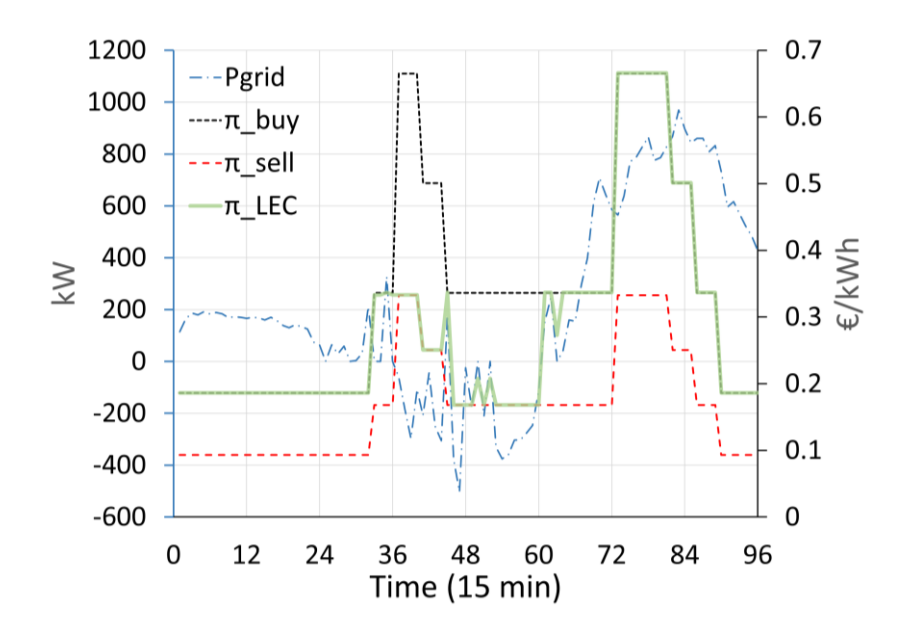


Figure 37 Comparison between the prices of the internal transactions and the prices of the transactions with the external energy provider. Cumulative value of the power exchanged with the energy provider. Test case C.

Assuming that OLTCs and variable capacitor banks are operated by the community with $Q_{\rm LEC}$ exchanges allowed, Figure 37 compares the average price profile of the internal transactions $\pi_{\rm LEC}$ with the profile of $P_{\rm grid\ tot}$ and, as in previous test cases, the prices of the internal transactions are bounded between $\pi_{\rm buy}$ and $\pi_{\rm sell}$, quite closely following the sign of $P_{\rm grid\ tot}$. The calculations are repeated for 5 scenarios that differentiate whether $Q_{\rm LEC}$ exchanges are allowed and how the OLTC and capacitor banks are operated (scenario 0 is without community, all the other scenarios are with $P_{\rm LEC}$):

scenario 0 – OLTCs and capacitors operated by the utility, without community;

scenario 1 – OLTCs and capacitors operated by the utility, without $Q_{\rm LEC}$;

scenario 2 – OLTCs and capacitors operated by the utility, with $Q_{\rm LEC}$;

scenario 3 – OLTCs and capacitors operated by the community, without $Q_{\rm LEC}$;

scenario 4 – OLTCs and capacitors operated by the community, with $Q_{\rm LEC}$;

Table 17 Summary of the results for the reference, Qup and Qdown optimizations of case study B. C_{ep} indicates the cost of the exchanges with the energy provider, P_{NC} indicates the noncompliance penalty, R indicates the reward, cpu indicates the total computational time

	Reference				Qdown			Qup		
	C _{EP} (k€)	P _{NC} (k€)	CPU (s)	C _{EP} (k€)	<i>R</i> (k€)	CPU (s)	C _{EP} (k€)	<i>R</i> (k€)	CPU (s)	
Scenario 0	2.9	3.0	135.2	2.9	10.0	43.6	2.9	32.9	43.5	
Scenario 1	2.5	3.0	141.3	2.5	9.9	47.4	2.5	33.0	53.2	
Scenario 2	2.5	1.7	464.2	2.5	9.5	48.7	2.5	33.5	52.5	
Scenario 3	2.4	2.9	153.3	2.4	9.9	54.8	2.6	34.5	49.1	
Scenario 4	2.4	1.6	127.7	2.4	8.8	50.8	2.6	35.5	49.2	

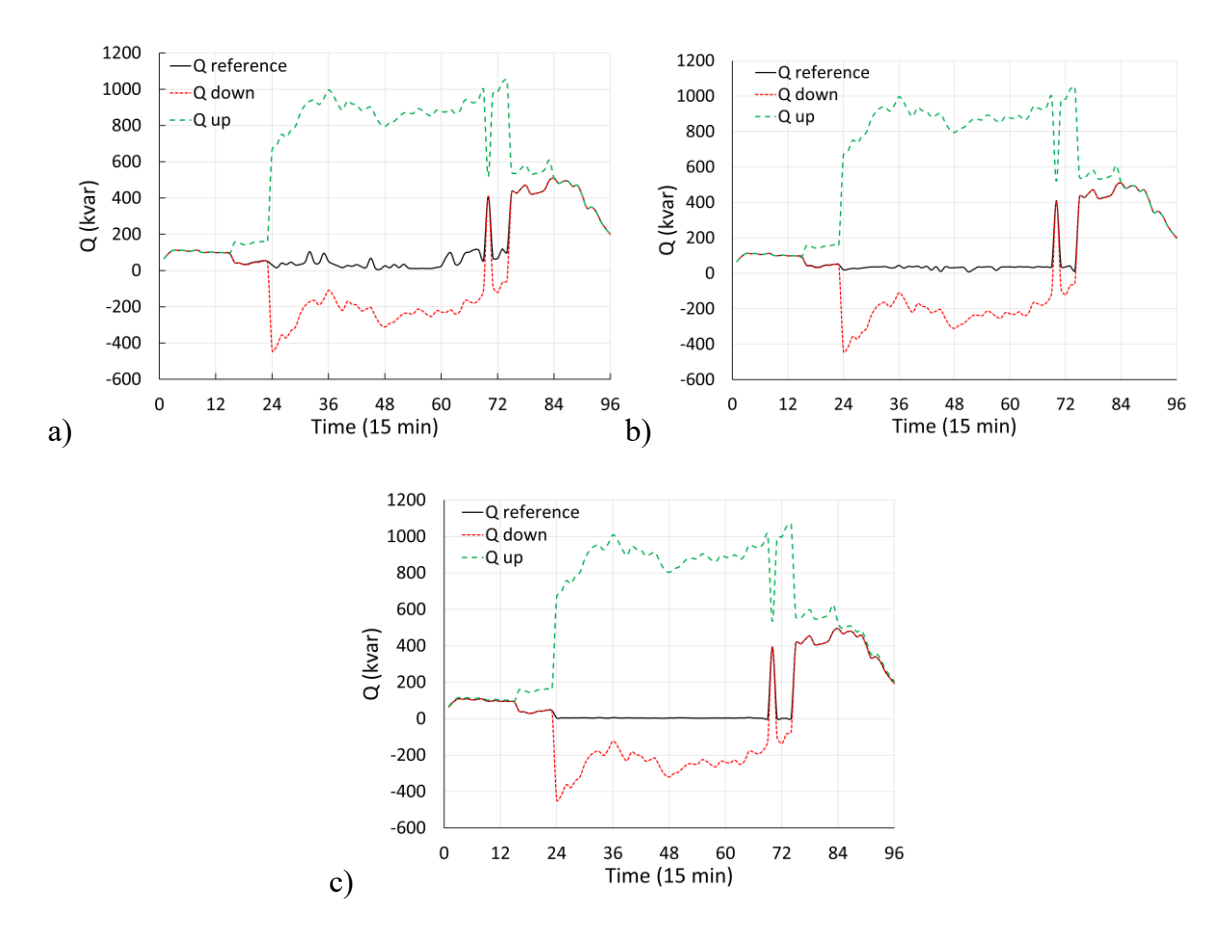


Figure 38 Profiles of the cumulative value of the reactive powers of the community participants calculated by the reference, Qup and Qdown procedures for scenarios: a) 1 (like 0 and 3 not shown), b) 2, c) 4. Test case B.

Table 17 shows the summary of the values of energy procurement cost from the external provider, noncompliance penalty or reactive power service reward obtained at the last iteration of the reference, Qdown, and Qup procedures, respectively, as well as the total computation time for of the three optimizations. Figure 38 compares the profiles of the sum of the $Q_{\text{user }i}$ values calculated by the reference, Q_{down} , and Q_{up} procedures for the considered scenarios. The final solutions are achieved with 4 or 5 iterations.

The results show that in this case considering the capacitor banks as included in the prosumers does not provide significant advantages due to the limited number and size of the banks. The operation as a community reduces the energy procurement costs ($C_{\rm EP}$ values of scenario 0 are the highest). The possibility to exchange reactive power among the community participants significantly reduces the noncompliance penalties (the $P_{\rm NC}$ values of scenarios 2 and 4 are the lowest). The values of the energy procurement cost, associated with the active power exchanges with the external provider, are almost the same in the different reactive power optimizations (there is only a slight increase for the Qup optimization, when OLTCs and capacitor banks are operated by the community, i.e., in scenarios 3 and 4).

D. Real case study and available data (Test case D)

The case study refers to five MV feeders (here named with letters from A to E) connected to a 132/15 kV substation, located in Modena, Italy, already described in section 3.2.6. We refer here to the profiles relevant to three days in January 17 and 19, 2023.

The considered π_{buy} profile is described in Table 18. The π_{sell} follows a similar pattern, but with halved values.

Table 18 Assumed daily profile of the prices π_{buy} in ϵ /kWh

until 8	8-9	9-10	10-11	11 – 18	18 – 20:15	20:15 - 21:15	21:15 - 22:15	after 22:15
0.186	0.336	0.665	0.5	0.336	0.665	0.5	0.336	0.186

For illustrative purposes, noncompliance penalty tariff μ_{PF} is assumed equal to 5 ϵ /kvarh, flexibility reward tariffs π_{down} and π_{up} are assumed equal to 3 ϵ /kvarh, following [64]. The minimum power factor value that complies with the requirements is assumed equal to 0.9. The bus voltage values are constrained to be within the interval 0.9 pu – 1.1 pu.

The forecasted total energy demands for the three days are 267.9 MWh (129.7 Mvarh), 277.6 MWh (134.5 Mvarh), and 269.1 MWh (130.4 Mvarh), respectively. The PV energy generation in the three days is 5.8, 6.2, and 6 MWh, while the energy generation from synchronous machines is 11.4, 11.4, and 10.6 MWh, respectively. For simplicity, all costumers connected to the same MV node are aggregated into a single user. The voltage dependence of the loads is neglected.

The complete data set of the test case is available in [22].

The calculations are performed for each day and for three different scenarios, each one can allow active power P_{LEC} and reactive power Q_{LEC} or not:

scenario 0- with community including all users and with $Q_{\rm LEC}$;

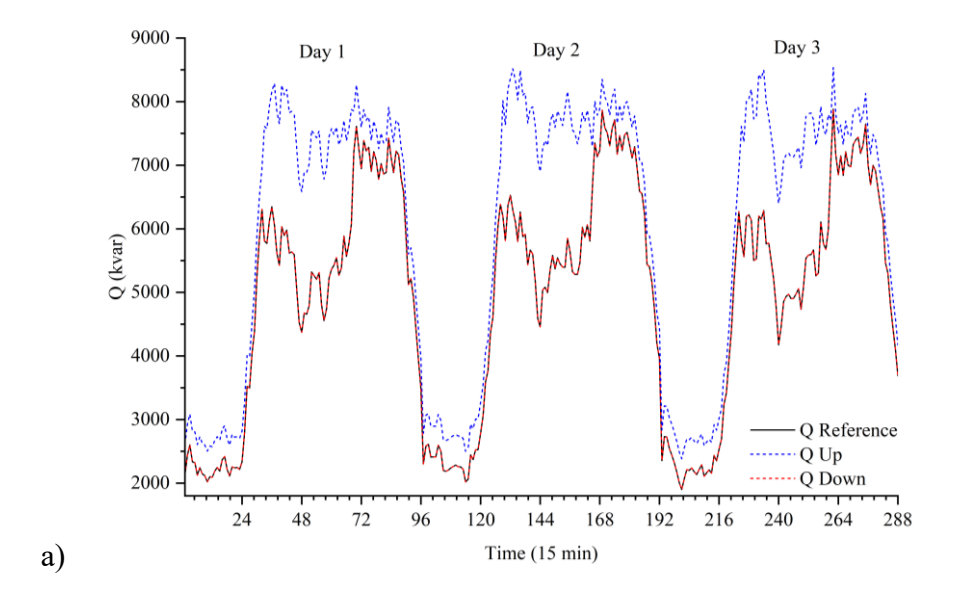
scenario 1 – with community including all users but without $Q_{\rm LEC}$;

scenario 2 – without community.

In these calculations, all the users connected to the feeders are members of the community. Additionally, both PV inverters and synchronous generators are assumed to be controllable, allowing them to supply or absorb reactive power, with a minimum power factor of 0.9.

For the three days, Figure 39 compares the profiles of the total reactive power consumed by the community members (obtained by the reference, Qdown and Qup calculations) in scenario 0 and scenario 1. Table 19 shows the total cost of the exchanges with the utility, the penalty for power factor noncompliance (reference calculation) and the rewards for reactive power changes (in the Qdown and Qup calculations), in the three scenarios. The values of the rewards correspond to a case where the flexibility service is required throughout the day and are therefore significantly higher than typical situations.

In scenario 0, the reactive power exchange completely avoids the low power factor penalties, but the resources used for this purpose are not available to the Qdown flexibility service. Scenario 1 results show that blocking Q_{LEC} exchanges allows for Qdown changes. Qup offers are lower in scenario 1 because the absence of Q_{LEC} increases the Q_{ref} profile. Scenario 2 shows the overall benefits of community participation, ensuring no disadvantages for members as transaction prices, calculated as shadow prices of Figure 37, closely matching the π_{buy} or π_{sell} profiles during power import (as always happens in the considered case) or export, respectively.



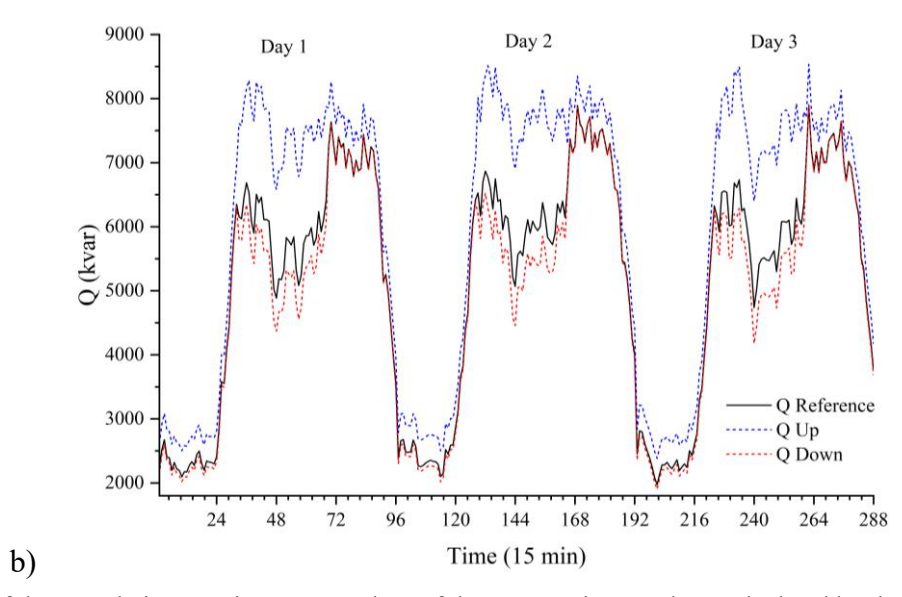


Figure 39 Profiles of the cumulative reactive power values of the community members calculated by the reference, Qup and Qdown procedures for the scenarios: a) 0, b) 1.

Table 19 Summary of the results for the reference, Qup and Qdown optimizations in the first three scenarios. C_{grid} is the cost of the exchanges with the energy provider, P_{NC} is the noncompliance penalty, R is the reward.

	Reference		Qdov	wn	Qup	
	C _{grid} (k€)	P _{NC} (k€)	C _{grid} (k€)	<i>R</i> (k€)	C _{grid} (k€)	<i>R</i> (k€)
Scenario 0	287.82	0	287.82	0	287.82	240.27
Scenario 1	287.82	0.16	287.82	45.15	287.82	195.13
Scenario 2	289.75	0.16	289.75	45.15	289.75	195.13

Figure 40 shows that the reactive power flow through the transformers at the substation, resulting from the five feeders, is lower in scenario 0 than in scenario 2 (with a similar profile to scenario 1). This confirms that allowing direct reactive power exchange between community members reduces the need for reactive power compensation of the entire network.

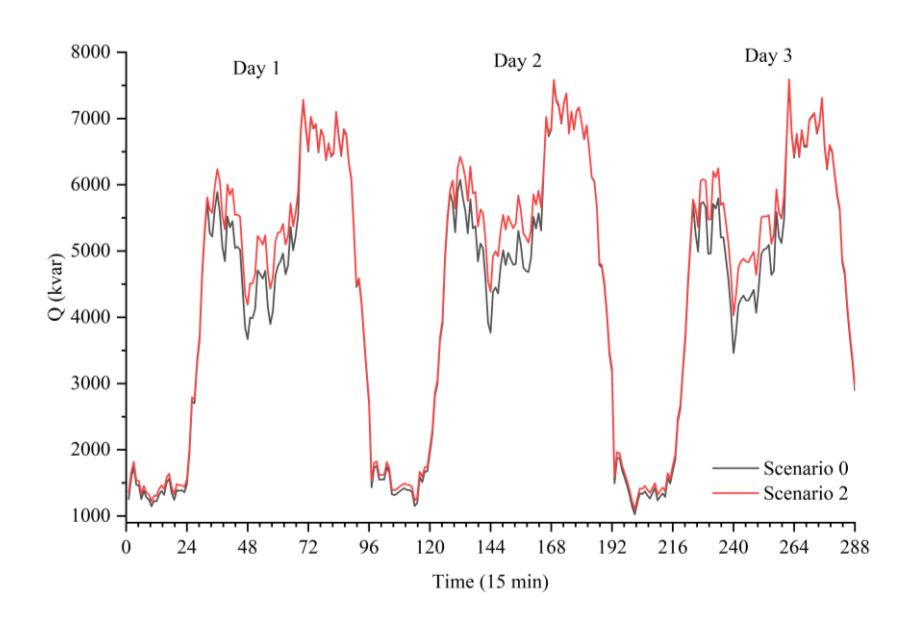


Figure 40 Comparison of the reactive power reference profiles through the HV/MV transformers at the substation due to the five feeders in scenario 0 and scenario 2.

Obviously, the results vary depending on the season and weather conditions. For example, Table 20 shows results analogous to Table 19 for three summer days (July 18-20, 2023), when the load consumption was 327.8 MWh, 333.0 MWh, and 320.5 MWh, respectively, the PV energy generation was 11.0, 10.6, and 11.0 MWh, and the energy generation from synchronous machines was 11.5 MWh for each of the three days. The summer days (maximum solar elevation 66.4°) were little cloudy, no precipitation in the first two days and little precipitation in the early morning of the third day, with average solar radiation of 296, 264, and 303 W/m², average temperature of 30.2, 30.2, 27.4 °C, and average wind speed of 14.8, 18.4, 20.5 km/h, respectively.

Table 20 Summary of analogous results of Table 19 for three summer days.

	Reference		Qdov	wn	Qup	
	$C_{\mathrm{grid}}\left(\mathbf{k}\mathbf{\in}\right)$	$P_{\mathrm{NC}}\left(\mathbf{k}\mathbf{\in}\right)$	$C_{grid}\left(\mathbf{k}\mathbf{\in}\right)$	<i>R</i> (k€)	$C_{\mathrm{grid}}\left(\mathbf{k}\mathbf{\in}\right)$	<i>R</i> (k€)
Scenario 0	323.9	16.8	323.9	0.7	323.9	311.8
Scenario 1	323.9	71.4	323.9	50.1	323.9	262.4
Scenario 2	324.9	86.8	324.9	35.1	324.9	207.5

The comparison between Table 20 and Table 19 shows that, during summer days, the noncompliance penalties for low power factor operation increase with the increase in PV production. However, the $Q_{\rm LEC}$ exchanges allow a penalty reduction of more than 76%. While in Table 19 the results of scenarios 1 and 2 are similar (with an increase only in $C_{\rm grid}$), the corresponding results in Table 20

show the importance of P_{LEC} exchanges also for the penalty reduction and the increase of Qdown and Qup revenues.

Considering scenario 0 of the winter days as reference, the following modified scenarios are also analyzed to show the impact of the reactive power contribution of the PV units, the increased production of the PV units, the partial user participation of the users in the community, and the benefits due to the inclusion of battery storage systems, which were absent in the previous scenarios:

Scenario 3 – PV units without reactive power control (power factor fixed at 1);

Scenario 4 – PV production increased by 50% (with reactive power control);

Scenario 5 – only some nodes in the community (randomly selected);

Scenario 6 – with three additional batteries (without reactive power control).

In scenario 5, the nodes within the community account for 45.16%, 45.29%, and 45.06% of the system consumption over the three days, respectively. The daily PV production of the restricted community represents 75.73%, 75.88%, and 75.75% of the total PV production, respectively. The share of the generation from synchronous machines is 31.29% in the first two days and increases to 33.69% in the last day.

In scenario 6, the three batteries are assumed to be connected to feeder B, feeder C, and feeder E, with maximum power of 75 kW, 75 kW, and 20 kW, respectively. The energy capacity in kWh is numerically equal to the maximum power. The charging and discharging efficiencies are set to 90%. The procedure optimizes the active power output of the batteries (with a minimum state of charge set at 20%) while maintaining a unitary power factor.

Table 21 Summary of the results for the reference, Qup and Qdown optimizations in four variations of scenario 0.

	Reference		Qdo	wn	Qup		
	C _{grid} (k€)	P _{NC} (k€)	C _{grid} (k€)	<i>R</i> (k€)	C _{grid} (k€)	<i>R</i> (k€)	
Scenario 3	287.82	18.41	287.82	0	287.82	103.64	
Scenario 4	284.34	0	284.34	0	284.34	240.28	
Scenario 5	288.31	0.14	288.31	8.72	288.31	231.56	
Scenario 6	287.60	0.01	287.60	0	287.60	240.28	

In Table 21, the results of scenario 3 in the reference calculation show the importance of reactive power compensation from PV units as $P_{\rm NC}$ penalties increase significantly compared to scenario 0 when enforcing unitary power factor. Scenario 4 results confirm the expected reduction in energy procurement costs due to increased PV production. Scenario 5 results show that smaller communities

are less capable to reduce energy prosumer costs and compensate for $P_{\rm NC}$ penalties in the reference case. The Qup and Qdown calculations assume that flexibility services are also provided by users outside the community, so that the unused reactive power margin for $P_{\rm NC}$ reduction is available for the Qdown service. Finally, scenario 6 demonstrates the effectiveness of batteries in reducing energy procurement costs.

The computation time is in the order of a few minutes for all cases considered, running on a CPU Intel core i7, 12700H, 5.2Ghz (during all simulations less than 3.8 Ghz was used), with 32 GB RAM.

4.21. Conclusions

This chapter has presented a procedure for the day-ahead scheduling of an energy community in which direct exchanges of both active and reactive power among the participants are allowed. Direct transactions of active powers allow to decrease the total costs due to energy procurement from the external provider with respect to the case in which each prosumer can only transact with the energy provider, under the (usual) assumption that the purchase tariffs are higher than sale rates. The procedure calculates the scheduling of the energy resources and the fair prices of the internal transactions among the community participants as the shadow prices of the balance constraints. As these prices stay between the purchase and sale rates fixed by the external provider, none of the prosumers suffer an economic disadvantage in participating in the community. The reactive power exchanges allow to reduce the noncompliance penalties that each prosumer would pay whenever it operates at a power factor lower than the minimum value fixed by the energy authority or the utility. The issue of low power factor operation is of increasing importance with the diffuse installations of PV units that significantly reduce, during the central hours of the day, the active power consumption. The optimization procedure calculates the scheduling of the available reactive power compensation resources, coordinated with the voltage control means of the network. For this purpose, the voltage dependence of the loads is considered.

The procedure is completed by the calculation of the maximum and minimum reactive power deviations that can be provided by the community, following a DSO/TSO request, for each period of the following day. In these calculations, the noncompliance penalties are replaced by the revenues provided by the reactive power flexibility assuming a predefined tariff. The results obtained for three test cases and a real case show that the different scheduling of the reactive power compensation resources has a limited impact on the community energy procurement costs, making the procedures economically advantageous. This conclusion also applies for lower values of the noncompliance penalties and reactive power remuneration than those assumed in the calculations, as they would result in smaller reactive power compensation actions by the community participants. For this reason, and

due to the lack of intertemporal coupling constraints in the reactive power decisions, the assumption of neglecting the probability that the flexibility service will be requested during the day appears reasonable.

The computation times are reasonably low for all the calculations. This makes the proposed deterministic models suitable to be included in stochastic procedures that consider the uncertainties related to the PV production and load consumption profiles, other than the already mentioned probability that DSO/TSO can require a reactive power reduction or increase during the day.

In this section of thesis, all the users of the network participate in the same community and share the same energy provider (or at least the same $\pi_{\text{buy},t}$ and $\pi_{\text{sell},t}$ profiles). Although beyond the scope of this chapter, the presented modelling approach can be applied for the analysis of systems where the users belong to different communities or do not participate in any community, with the presence of multiple energy providers.

Chapter 5. Conclusions

This thesis deals with the following main topics: flexibility exploitation with the model of the EV parking lot and its use for voltage optimization, model of the energy communities with the pricing of the internal transactions, and the provision of reactive power services from communities.

5.1. Flexibility exploitation of EV parking lots

For the flexibility exploitation, the model of the parking lot and its application for voltage optimization, described in Chapter 2, outlines a method to characterize the flexibility offered by parking lots with EV charging stations. This flexibility can assist distribution system operators in addressing challenges such as voltage regulation and congestion. The method focuses on calculating the reference demand profile and the flexibility margins for each time period of the following day, taking into account predefined incentives for adjusting loads.

The approach uses a multistage stochastic procedure that adapts to real-time conditions and vehicle connections to the charging stations. The stochastic optimization scenarios are generated based on forecasts of EV arrivals and departures, accounting for factors like battery size, EVs penetration in the model, and maximum charging power. Clustering similar scenarios utilizing the *k*-medoid method reduces computational complexity though maintaining scenario feasibility.

The optimization model aggregates EV battery behavior and formulates the problem as a linear one, making it computationally efficient even for large parking lots. The optimization model is formulated as a linear programming problem, computationally efficient even for large scale parking lots. It makes possible to represent losses associated with grid charging and vehicle-to-vehicle energy exchanges allowed by the use of the bidirectional technology in the charging stations.

For increasing the flexibility of the EV parking lots, power reduction and increases are regarded in sequential periods, ensuring schedule feasibility, by including a recovery after the interval when the flexibility is requested.

Numerical tests in different scale of EV parking lots show the performance and capability of the method. In total, this model ensures that charging requirements are met.

The second part of the chapter presents a method to characterize and use the flexibility provided by parking lots equipped with EV charging stations for the optimization of the voltage profile in distribution networks. The flexibility margins calculated by the EV charging stations aggregators are incorporated as a control resource in the voltage optimization procedure of the distribution system operator. The procedure is applied to the 123-bus test feeder, including a parking lot with several

charging stations. The results show the effectiveness of the flexibility services for the optimization of the voltage profile.

5.2. Model and analysis of the energy communities

The model of the energy communities in Chapter 3 presents a day-ahead scheduling procedure for the case of multiple energy communities in the grid. Each user is free to join a community or not. Moreover, each user can choose a different energy provider.

The optimization model procedure considers the price of the transaction community among the users of the same community calculated by the shadow prices of the relevant balancing constraints. The increase of the number of communities results in the increase of the procurement costs also due to the reduction of the members with which each participant can transact. Considered optimization procedure could analyze the changes of further installation of production and storage units. The calculation effort is reasonably limited.

The results in IEEE 123-bus test feeder case study illustrate procurement costs of each community have decreases beside the cases that direct transactions are forbidden. The model presents two unique providers with a different price profile and consider high rate cost for internal production when the community generally import power, in addition the model set lowest rate tariff in total when the community export power.

The second part of chapter 3 presents the distributed optimization model and the application to a real MV distribution network, considering the consumption and generation profiles of three days in winter and summer. The day-ahead optimization procedure takes into account the network constraints and provides the prices of the internal transactions as the shadow prices of the power balancing constraints for each user. In addition, the optimization model considered reactive power exchanges between community users in the same community beside active power. Reactive power transactions support the cost reduction for low PF operation.

The real MV case study includes the supply/demand profiles of three days in winter and summer. The results illustrate the improvements in reducing both energy procurement costs and noncompliance costs for each community. The analysis on the number of ECs shows that as the number of ECs increases, the reductions of the costs and penalties decrease, approaching the case without internal transactions within ECs.

The optimization model can represent the provision of flexibility services to the DSO. The reactive power services from communities are dealt with in Chapter 4. The reactive power exchanges help

reduce penalties for prosumers who operate below the minimum power factor set by the energy authority. This issue is growing with the increased installation of PV units, which lower active power consumption during midday hours. The optimization procedure schedules reactive power compensation resources, coordinated with the network's voltage control, considering load voltage dependence. It also calculates the maximum and minimum reactive power deviations that the community can provide on request from the DSO/TSO for each day. These deviations replace penalties with revenue from reactive power flexibility at a predefined tariff. Results from three test cases and a real case show that different scheduling of reactive power resources has minimal impact on energy procurement costs, making the procedure economically advantageous.

5.3. Future work

Future activities can deal with the refinement of the adopted models, with specific reference to the implementation of network constraints able to represent unbalanced conditions. Moreover, the approach can be applied to the analysis of the advantages of using different types of storage units, such as small-pumped hydro stations in rural areas. In the context of the application of communities in the cities, the flexibility associated with the district heating systems equipped with heat pumps appears to deserve a specific analysis.

References

- [1] C. Xu *et al.*, "Electric vehicle batteries alone could satisfy short-term grid storage demand by as early as 2030," *Nat. Commun.*, vol. 14, no. 1, 2023, doi: 10.1038/s41467-022-35393-0.
- [2] Y. Li, S. He, Y. Li, L. Ge, S. Lou, and Z. Zeng, "Probabilistic Charging Power Forecast of EVCS: Reinforcement Learning Assisted Deep Learning Approach," *IEEE Trans. Intell. Veh.*, vol. 8, no. 1, pp. 344–357, 2023, doi: 10.1109/TIV.2022.3168577.
- [3] M. Ahrabi, M. Abedi, H. Nafisi, M. A. Mirzaei, B. Mohammadi-Ivatloo, and M. Marzband, "Evaluating the effect of electric vehicle parking lots in transmission-constrained AC unit commitment under a hybrid IGDT-stochastic approach," *Int. J. Electr. Power Energy Syst.*, vol. 125, no. August 2020, p. 106546, 2021, doi: 10.1016/j.ijepes.2020.106546.
- [4] A. Pirouzi, J. Aghaei, S. Pirouzi, V. Vahidinasab, and A. R. Jordehi, "Exploring potential storage-based flexibility gains of electric vehicles in smart distribution grids," *J. Energy Storage*, vol. 52, no. PC, p. 105056, 2022, doi: 10.1016/j.est.2022.105056.
- [5] R. Deng *et al.*, "Exploring flexibility of electric vehicle aggregators as energy reserve," *Electr. Power Syst. Res.*, vol. 184, no. February, 2020, doi: 10.1016/j.epsr.2020.106305.
- [6] I. Sengor, O. Erdinc, B. Yener, A. Tascikaraoglu, and J. P. S. Catalao, "Optimal energy management of EV parking lots under peak load reduction based DR programs considering uncertainty," *IEEE Trans. Sustain. Energy*, vol. 10, no. 3, pp. 1034–1043, 2019, doi: 10.1109/TSTE.2018.2859186.
- [7] M. De Santis, A. R. Di Fazio, M. Russo, T. Harighi, and A. Borghetti, "Voltage Optimization in Distribution Networks using EV Parking Lots and PV systems as flexibility options," *Proc. 2023 IEEE Int. Conf. Environ. Electr. Eng. 2023 IEEE Ind. Commer. Power Syst. Eur. EEEIC / I CPS Eur. 2023*, pp. 1–6, 2023, doi: 10.1109/EEEIC/ICPSEurope57605.2023.10194708.
- [8] M. P. Evans, S. H. Tindemans, and D. Angeli, "Flexibility Framework with Recovery Guarantees for Aggregated Energy Storage Devices," *IEEE Trans. Smart Grid*, vol. 13, no. 5, pp. 3519–3531, 2022, doi: 10.1109/TSG.2022.3173900.
- [9] Y. Li, M. Han, Z. Yang, and G. Li, "Coordinating flexible demand response and renewable uncertainties for scheduling of community integrated energy systems with an electric vehicle charging station: A Bi-level approach," *IEEE Trans. Sustain. Energy*, vol. 12, no. 4, pp. 2321–2331, 2021, doi: 10.1109/TSTE.2021.3090463.

- [10] G. Piazza, S. Bracco, F. Delfino, and S. Siri, "Optimal design of electric mobility services for a Local Energy Community," *Sustain. Energy, Grids Networks*, vol. 26, p. 100440, 2021, doi: 10.1016/j.segan.2021.100440.
- [11] D. Falabretti, F. Gulotta, and D. Siface, "Scheduling and operation of RES-based virtual power plants with e-mobility: A novel integrated stochastic model," *Int. J. Electr. Power Energy Syst.*, vol. 144, no. September 2022, p. 108604, 2023, doi: 10.1016/j.ijepes.2022.108604.
- [12] S. R. Dabbagh, M. K. Sheikh-El-Eslami, and A. Borghetti, "Optimal operation of vehicle-to-grid and grid-to-vehicle systems integrated with renewables," *19th Power Syst. Comput. Conf. PSCC 2016*, pp. 1–7, 2016, doi: 10.1109/PSCC.2016.7540933.
- [13] C. Orozco, A. Borghetti, F. Napolitano, and F. Tossani, "Day-ahead Multistage Stochastic Optimization of a Group of Electric Vehicle Charging Stations," 2021 IEEE 15th Int. Conf. Compat. Power Electron. Power Eng. CPE-POWERENG 2021, pp. 1–8, 2021, doi: 10.1109/CPE-POWERENG50821.2021.9501228.
- [14] Z. Wang, P. Jochem, and W. Fichtner, "A scenario-based stochastic optimization model for charging scheduling of electric vehicles under uncertainties of vehicle availability and charging demand," *J. Clean. Prod.*, vol. 254, p. 119886, 2020, doi: 10.1016/j.jclepro.2019.119886.
- [15] H. S. Park and C. H. Jun, "A simple and fast algorithm for K-medoids clustering," *Expert Syst. Appl.*, vol. 36, no. 2 PART 2, pp. 3336–3341, 2009, doi: 10.1016/j.eswa.2008.01.039.
- [16] M. R. M. Cruz, D. Z. Fitiwi, S. F. Santos, and J. P. S. Catalão, "A comprehensive survey of flexibility options for supporting the low-carbon energy future," *Renew. Sustain. Energy Rev.*, vol. 97, no. September, pp. 338–353, 2018, doi: 10.1016/j.rser.2018.08.028.
- [17] G. R. Bharati and S. Paudyal, "Coordinated control of distribution grid and electric vehicle loads," *Electr. Power Syst. Res.*, vol. 140, pp. 761–768, 2016, doi: 10.1016/j.epsr.2016.05.031.
- [18] F. Marasciuolo, C. Orozco, M. Dicorato, A. Borghetti, and G. Forte, "Two-stage Scheduling of Electrical Vehicle Charging Station Clusters in a Community of DC Microgrids," 21st IEEE Int. Conf. Environ. Electr. Eng. 2021 5th IEEE Ind. Commer. Power Syst. Eur. EEEIC / I CPS Eur. 2021 Proc., no. 876868, pp. 1–6, 2021, doi: 10.1109/EEEIC/ICPSEurope51590.2021.9584584.
- [19] A. R. Di Fazio, M. Russo, S. Valeri, and M. De Santis, "Linear method for steady-state analysis of radial distribution systems," *Int. J. Electr. Power Energy Syst.*, vol. 99, no. February, pp. 744–755, 2018, doi: 10.1016/j.ijepes.2018.02.001.

- [20] A. R. DI Fazio, C. Risi, M. Russo, and M. De Santis, "Coordinated Optimization for Zone-Based Voltage Control in Distribution Grids," *IEEE Trans. Ind. Appl.*, vol. 58, no. 1, pp. 173–184, 2022, doi: 10.1109/TIA.2021.3129731.
- [21] F. Varshosaz, M. Moazzami, B. Fani, and P. Siano, "Day-Ahead Capacity Estimation and Power Management of a Charging Station Based on Queuing Theory," *IEEE Trans. Ind. Informatics*, vol. 15, no. 10, pp. 5561–5574, 2019, doi: 10.1109/TII.2019.2906650.
- [22] "IEEE PES Test Feeder." 1992. [Online]. Available: https://cmte.ieee.org/pestestfeeders/resources/
- [23] H. Xu, A. D. Dominguez-Garcia, V. V. Veeravalli, and P. W. Sauer, "Data-Driven Voltage Regulation in Radial Power Distribution Systems," *IEEE Trans. Power Syst.*, vol. 35, no. 3, pp. 2133–2143, 2020, doi: 10.1109/TPWRS.2019.2948138.
- [24] "Github." https://github.com/mdesantis2601/Simulation
- [25] European Union, Models of Local Energy Ownership and the Role of Local Energy Communities in Energy Transition in Europe. 2018. doi: 10.2863/603673.
- [26] C. Inês, P. L. Guilherme, M. G. Esther, G. Swantje, H. Stephen, and H. Lars, "Regulatory challenges and opportunities for collective renewable energy prosumers in the EU," *Energy Policy*, vol. 138, no. December 2019, 2020, doi: 10.1016/j.enpol.2019.111212.
- [27] G. Pulazza, C. Orozco, A. Borghetti, F. Tossani, and F. Napolitano, "Procurement Cost Minimization of an Energy Community with Biogas, Photovoltaic and Storage Units," 2021 IEEE Madrid PowerTech, PowerTech 2021 Conf. Proc., 2021, doi: 10.1109/PowerTech46648.2021.9494878.
- [28] F. Moret and P. Pinson, "Energy collectives: a community and fairness based approach to future electricity markets," *IEEE Trans. Power Syst.*, vol. 34, no. 5, pp. 3994–4004, 2019, doi: 10.1109/TPWRS.2018.2808961.
- [29] W. Tushar, T. K. Saha, C. Yuen, D. Smith, and H. V. Poor, "Peer-to-Peer Trading in Electricity Networks: An Overview," *IEEE Trans. Smart Grid*, vol. 11, no. 4, pp. 3185–3200, 2020, doi: 10.1109/TSG.2020.2969657.
- [30] Z. Siqin, D. X. Niu, M. Y. Li, T. Gao, Y. Lu, and X. Xu, "Distributionally robust dispatching of multi-community integrated energy system considering energy sharing and profit allocation," *Appl. Energy*, vol. 321, no. June, p. 119202, 2022, doi:

- 10.1016/j.apenergy.2022.119202.
- [31] R. A. Jabr, "Radial distribution load flow using conic programming," *IEEE Trans. Power Syst.*, vol. 21, no. 3, pp. 1458–1459, 2006, doi: 10.1109/TPWRS.2006.879234.
- [32] S. H. Low, "Convex relaxation of optimal power flow Part i: Formulations and equivalence," *IEEE Trans. Control Netw. Syst.*, vol. 1, no. 1, pp. 15–27, 2014, doi: 10.1109/TCNS.2014.2309732.
- [33] Mesut Baran; Felix F. Wu, "Network reconfiguration in distribution systems for loss reduction and load balancing," *IEEE Trans. Power Deliv.*, vol. 4, no. 2, pp. 1401–1407, 1989.
- [34] C. Orozco, A. Borghetti, B. De Schutter, F. Napolitano, G. Pulazza, and F. Tossani, "Intra-day scheduling of a local energy community coordinated with day-ahead multistage decisions," *Sustain. Energy, Grids Networks*, vol. 29, p. 100573, 2022, doi: 10.1016/j.segan.2021.100573.
- [35] M. M. Gambini, C. Orozco, A. Borghetti, and F. Tossani, "Power loss reduction in the energy resource scheduling of a local energy community," *SEST 2020 3rd Int. Conf. Smart Energy Syst. Technol.*, vol. 675318, no. 675318, 2020, doi: 10.1109/SEST48500.2020.9203444.
- [36] E. McKenna, M. Thomson, and J. Barton, "CREST Demand Model. Loughborough University. Dataset." 2015. [Online]. Available: https://doi.org/10.17028/rd.lboro.2001129.v8
- [37] M. Roelofs and J. Bisschop, "AIMMS User's Guide." Paragon Decision Technology B.V., 2011.
- [38] M. Gancheva, S. O'Brien, N. Crook, and C. Monteiro, *Models of local energy ownership and the role of local energy communities in energy transition in Europe*. European Committee of the Regions, 2018.
- [39] C. Inês, P. L. Guilherme, M. G. Esther, G. Swantje, H. Stephen, and H. Lars, "Regulatory challenges and opportunities for collective renewable energy prosumers in the EU," *Energy Policy*, vol. 138, no. April 2019, 2020, doi: 10.1016/j.enpol.2019.111212.
- [40] J. Guerrero, A. C. Chapman, and G. Verbič, "Decentralized P2P Energy Trading Under Network Constraints in a Low-Voltage Network," *IEEE Trans. Smart Grid*, vol. 10, no. 5, pp. 5163–5173, 2019, doi: 10.1109/TSG.2018.2878445.
- [41] A. Dimovski, M. Moncecchi, and M. Merlo, "Impact of energy communities on the distribution network: An Italian case study," *Sustain. Energy, Grids Networks*, vol. 35, p. 101148, 2023, doi: https://doi.org/10.1016/j.segan.2023.101148.

- [42] J. Kim and Y. Dvorkin, "A P2P-Dominant Distribution System Architecture," *IEEE Trans. Power Syst.*, vol. 35, no. 4, pp. 2716–2725, 2020, doi: 10.1109/TPWRS.2019.2961330.
- [43] R. Rana, K. Berg, M. Z. Degefa, and M. Löschenbrand, "Modelling and Simulation Approaches for Local Energy Community Integrated Distribution Networks," *IEEE Access*, vol. 10, pp. 3775–3789, 2022, doi: 10.1109/ACCESS.2022.3140237.
- [44] M. Tostado-Véliz, Y. Liang, A. Rezaee Jordehi, S. A. Mansouri, and F. Jurado, "An intervalbased bi-level day-ahead scheduling strategy for active distribution networks in the presence of energy communities," *Sustain. Energy, Grids Networks*, vol. 35, p. 101088, 2023, doi: https://doi.org/10.1016/j.segan.2023.101088.
- [45] L. He and J. Zhang, "Energy Trading in Local Electricity Markets With Behind-the-Meter Solar and Energy Storage," *IEEE Trans. Energy Mark. Policy Regul.*, vol. 1, no. 2, pp. 107–117, 2023, doi: 10.1109/TEMPR.2023.3250948.
- [46] T. Harighi, A. Borghetti, F. Napolitano, and F. Tossani, "Optimization Model for the Analysis of Multiple Energy Communities in the Same Distribution Network with Different Providers," 2023 IEEE Belgrade PowerTech, pp. 1–6, 2023, doi: 10.1109/PowerTech55446.2023.10202985.
- [47] D. P. Bertsekas and J. N. Tsitsiklis, "Parallel and Distributed Computation: Numerical Methods," *Parallel and Distributed Computation Numerical Methods*, vol. 23. p. 715, 1989.
- [48] J. Peschon, D. S. Piercy, W. F. Tinney, and O. J. Tveit, "Sensitivity in Power Systems," *IEEE Trans. Power Appar. Syst.*, vol. PAS-87, no. 8, pp. 1687–1696, 1968, doi: 10.1109/TPAS.1968.292130.
- [49] B. A. Robbins, H. Zhu, and A. D. Domínguez-García, "Optimal Tap Setting of Voltage Regulation Transformers in Unbalanced Distribution Systems," *IEEE Trans. Power Syst.*, vol. 31, no. 1, pp. 256–267, 2016, doi: 10.1109/TPWRS.2015.2392693.
- [50] T. Harighi, A. Borghetti, F. Napolitano, and F. Tossani, "Provision of reactive power services by energy communities in MV distribution networks," *Sustain. Energy, Grids Networks*, vol. 34, p. 101038, 2023, doi: https://doi.org/10.1016/j.segan.2023.101038.
- [51] "Weather data." https://www.visualcrossing.com/
- [52] T. Harighi, "No Title."
- [53] F. Barroco Fontes Cunha, C. Carani, C. A. Nucci, C. Castro, M. Santana Silva, and E. Andrade

- Torres, "Transitioning to a low carbon society through energy communities: Lessons learned from Brazil and Italy," *Energy Res. Soc. Sci.*, vol. 75, no. March, p. 101994, 2021, doi: 10.1016/j.erss.2021.101994.
- [54] R. Passey, T. Spooner, I. MacGill, M. Watt, and K. Syngellakis, "The potential impacts of grid-connected distributed generation and how to address them: A review of technical and non-technical factors," *Energy Policy*, vol. 39, no. 10, pp. 6280–6290, 2011, doi: 10.1016/j.enpol.2011.07.027.
- [55] E. Demirok, P. C. González, K. H. B. Frederiksen, D. Sera, P. Rodriguez, and R. Teodorescu, "Local reactive power control methods for overvoltage prevention of distributed solar inverters in low-voltage grids," *IEEE J. Photovoltaics*, vol. 1, no. 2, pp. 174–182, 2011, doi: 10.1109/JPHOTOV.2011.2174821.
- [56] R. Kabiri, D. G. Holmes, B. P. McGrath, and L. G. Meegahapola, "LV Grid Voltage Regulation Using Transformer Electronic Tap Changing, with PV Inverter Reactive Power Injection," *IEEE J. Emerg. Sel. Top. Power Electron.*, vol. 3, no. 4, pp. 1182–1192, 2015, doi: 10.1109/JESTPE.2015.2443839.
- [57] X. Su, M. A. S. Masoum, and P. J. Wolfs, "Optimal PV inverter reactive power control and real power curtailment to improve performance of unbalanced four-wire LV distribution networks," *IEEE Trans. Sustain. Energy*, vol. 5, no. 3, pp. 967–977, 2014, doi: 10.1109/TSTE.2014.2313862.
- [58] A. Safayet, P. Fajri, and I. Husain, "Reactive Power Management for Overvoltage Prevention at High PV Penetration in a Low-Voltage Distribution System," *IEEE Trans. Ind. Appl.*, vol. 53, no. 6, pp. 5786–5794, 2017, doi: 10.1109/TIA.2017.2741925.
- [59] S. Lilla *et al.*, "Mixed integer programming model for the operation of an experimental low-voltage network," Jun. 2017. doi: 10.1109/PTC.2017.7981175.
- [60] G. Valverde, D. Shchetinin, and G. Hug-Glanzmann, "Coordination of distributed reactive power sources for voltage support of transmission networks," *IEEE Trans. Sustain. Energy*, vol. 10, no. 3, pp. 1544–1553, 2019, doi: 10.1109/TSTE.2019.2892671.
- [61] V. Kekatos, G. Wang, A. J. Conejo, and G. B. Giannakis, "Stochastic Reactive Power Management in Microgrids with Renewables," *IEEE Trans. Power Syst.*, vol. 30, no. 6, pp. 3386–3395, 2015, doi: 10.1109/TPWRS.2014.2369452.
- [62] D. A. Contreras and K. Rudion, "Improved assessment of the flexibility range of distribution

- grids using linear optimization," 20th Power Syst. Comput. Conf. PSCC 2018, 2018, doi: 10.23919/PSCC.2018.8442858.
- [63] S. Karagiannopoulos, C. Mylonas, P. Aristidou, and G. Hug, "Active Distribution Grids Providing Voltage Support: The Swiss Case," *IEEE Trans. Smart Grid*, vol. 12, no. 1, pp. 268–278, 2021, doi: 10.1109/TSG.2020.3010884.
- [64] I. I. Avramidis, F. Capitanescu, V. A. Evangelopoulos, P. S. Georgilakis, and G. Deconinck, "In Pursuit of New Real-Time Ancillary Services Providers: Hidden Opportunities in Low Voltage Networks and Sustainable Buildings," *IEEE Trans. Smart Grid*, vol. 13, no. 1, pp. 429–442, Jan. 2022, doi: 10.1109/TSG.2021.3112925.
- [65] F. Capitanescu, "TSO–DSO interaction: Active distribution network power chart for TSO ancillary services provision," *Electr. Power Syst. Res.*, vol. 163, pp. 226–230, Oct. 2018, doi: 10.1016/j.epsr.2018.06.009.
- [66] J. Silva *et al.*, "Estimating the Active and Reactive Power Flexibility Area at the TSO-DSO Interface," *IEEE Trans. Power Syst.*, vol. 33, no. 5, pp. 4741–4750, 2018, doi: 10.1109/TPWRS.2018.2805765.
- [67] A. Potter, R. Haider, G. Ferro, M. Robba, and A. M. Annaswamy, "A reactive power market for the future grid," *Adv. Appl. Energy*, vol. 9, no. September 2022, p. 100114, 2023, doi: 10.1016/j.adapen.2022.100114.
- [68] A. O. Rousis, D. Tzelepis, Y. Pipelzadeh, G. Strbac, C. D. Booth, and T. C. Green, "Provision of Voltage Ancillary Services through Enhanced TSO-DSO Interaction and Aggregated Distributed Energy Resources," *IEEE Trans. Sustain. Energy*, vol. 12, no. 2, pp. 897–908, Apr. 2021, doi: 10.1109/TSTE.2020.3024278.
- [69] H. Nagpal, I. I. Avramidis, F. Capitanescu, and A. G. Madureira, "Local Energy Communities in Service of Sustainability and Grid Flexibility Provision: Hierarchical Management of Shared Energy Storage," *IEEE Trans. Sustain. Energy*, pp. 1–13, 2022, doi: 10.1109/TSTE.2022.3157193.
- [70] T. Harighi, A. Borghetti, F. Napolitano, and F. Tossani, "Provision of reactive power services by energy communities in MV distribution networks," *Sustain. Energy, Grids Networks*, vol. 34, p. 101038, 2023, doi: 10.1016/j.segan.2023.101038.
- [71] M. E. Baran and F. F. Wu, "Network reconfiguration in distribution systems for loss reduction and load balancing," *IEEE Trans. Power Deliv.*, vol. 4, no. 2, pp. 1401–1407, 1989, doi:

- 10.1109/61.25627.
- [72] D. K. Molzahn and I. A. Hiskens, *A Survey of Relaxations and Approximations of the Power Flow Equations*. Now Foundations and Trends, 2019. doi: 10.1561/3100000012.
- [73] L. Bobo, A. Venzke, and S. Chatzivasileiadis, "Second-order cone relaxations of the optimal power flow for active distribution grids: Comparison of methods," *Int. J. Electr. Power Energy Syst.*, vol. 127, no. September 2020, p. 106625, 2021, doi: 10.1016/j.ijepes.2020.106625.
- [74] A. Li and J. Zhong, "Market-Based Volt-Var Optimization and Its Applications on Bottom-Up Load Modeling Method," *IEEE Trans. Power Syst.*, vol. 36, no. 3, pp. 2103–2113, 2021, doi: 10.1109/TPWRS.2020.3035465.
- [75] A. Borghetti, "A mixed-integer linear programming approach for the computation of the minimum-losses radial configuration of electrical distribution networks," *IEEE Trans. Power Syst.*, vol. 27, no. 3, pp. 1264–1273, 2012, doi: 10.1109/TPWRS.2012.2184306.
- [76] M. Nick, R. Cherkaoui, J. Y. Le Boudec, and M. Paolone, "An Exact Convex Formulation of the Optimal Power Flow in Radial Distribution Networks Including Transverse Components," *IEEE Trans. Automat. Contr.*, vol. 63, no. 3, pp. 682–697, 2018, doi: 10.1109/TAC.2017.2722100.
- [77] S. Civanlar, J. J. Grainger, H. Yin, and S. S. H. Lee, "Distribution feeder reconfiguration for loss reduction," *IEEE Trans. Power Deliv.*, vol. 3, no. 3, pp. 1217–1223, 1988, doi: 10.1109/61.193906.
- [78] R. D. Zimmerman, C. E. Murillo-sánchez, and R. J. Thomas, "MATPOWER: Steady-State Operations, Systems Research and Education," *IEEE Trans. Power Syst.*, vol. 26, no. 1, pp. 12–19, 2011.